Modelling, Simulation and Experimental Investigation of the Effects of Material Microstructure on the Micro-Endmilling Process

A thesis
Submitted to Cardiff University
For the degree of

Doctor of Philosophy

By

Ahmed Abd-Elrahman Elkaseer

Institute of Mechanical and Manufacturing Engineering
Cardiff School of Engineering
Cardiff University

Cardiff, Wales
United Kingdom

2011

ABSTRACT

Recently it has been revealed that workpiece microstructure has dominant effects on the performance of the micro-machining process. However, so far, there has been no detailed study of these effects on micro-endmilling. In this research, the influence of the microstructure on the matters such as cutting regime, tool wear and surface quality has been investigated.

Initially, an experimental investigation has been carried out to identify the machining response of materials metallurgically and mechanically modified at the micro-scale. Tests have been conducted that involved micro-milling slots in coarse-grained (CG) Cu99.9E with an average grain size of 30 μm and ultrafine-grained (UFG) Cu99.9E with an average grain size of 200 nm. Then, a method of assessing the homogeneity of the material microstructure has been proposed based on Atomic Force Microscope (AFM) measurements of the coefficient of friction at the atomic scale, enabling a comparative evaluation of the modified microstructures. The investigation has shown that, by refining the material microstructure, the minimum chip thickness can be reduced and a better surface finish can be achieved. Also, the homogeneity of the microstructure can be improved which in turn reduces surface defects.

Furthermore, a new model to simulate the surface generation process during micro-endmilling of dual-phase materials has been developed. The proposed model considers the effects of the following factors: the geometry of the cutting tool, the feed rate, and the workpiece microstructure. In particular, variations of the minimum chip thickness at phase boundaries are considered by feeding maps of the microstructure into the model. Thus, the model takes into account these variations that alter the machining mechanism from a proper cutting to ploughing and vice versa, and are the main cause of micro-burr formation. By applying the proposed model it is possible to estimate more accurately the resulting roughness owing to the dominance of the micro-burrs formation during the surface generation process in micro-milling of multi-phase materials. The model has been experimentally validated by machining two different samples of dual-phase steel, AISI 1040 and AISI 8620,

under a range of chip-loads. The results have shown that the proposed model accurately predicts the roughness of the machined surfaces with average errors of 14.5% and 17.4% for the AISI 1040 and AISI 8620 samples, respectively. The developed model successfully elucidates the mechanism of micro-burr formation at the phase boundaries, and quantitatively describes its contributions to the resulting surface roughness after micro-endmilling.

Moreover, a new generic method has been proposed to estimate the tool wear based on the average values of cutting edge radius and tool flute profile. To determine these two parameters a new experimental setup has been utilised to conduct a series of experiments on two materials with distinctive properties and thus to assess the validity of the method. Especially, the machining response of pearlite and ferrite phases in the materials were studied independently to identify differences in their cutting conditions, and thus to model their effects on the tool wear. Then, based on this experimental data two regression models have been created to estimate the increase of the cutting edge radius when machining single and dual-phase steels. To demonstrate their applicability and at the same time to validate them, the models have been tested at two different levels and under different conditions. There has been a good agreement between the estimated tool wear and the experimental results. In particular, the average error was 14.7% and 17.5% for AISI 1040 and AISI 8620, respectively, when the machining was conducted with 800 μm cutters and 20% and 19% when processing AISI 1040 with 600 μm and 400 μm tools.

Additionally, a simulation-based study of the surface generation process in micro-endmilling of dual-phase materials has been carried out. Initially, the generated roughness for AISI 1040 and AISI 8620 has been simulated under a wide range of cutting conditions with and without considering tool wear. Next, the workpiece material, AISI 1040, has been heat-treated aiming to achieve different morphological microstructures and thus to compare their machinability in terms of the achievable roughness. The results of the conducted simulations have been utilised to optimise the cutting process and identify processing windows, cutting conditions and material microstructure, which can reduce the resulting roughness while extending the tool life. Finally, using the surface roughness model, a three dimensional virtual environment of the micro-milling process has been created to simulate the surface generation process in micro-endmilling of dual-phase materials.

In The Name of Allah,

The Most Gracious, The Most Merciful

ACKNOWLEDGEMENTS

First, I would like to give thanks to **Allah** (My Lord) the almighty, the all great without whom I could not have completed this educational endeavour.

I wish to express my sincere thanks to Cardiff University, especially the Manufacturing Engineering Centre (MEC) for the use of the facilities to pursue this research.

I would like to extend special thanks and gratitude to my supervisor Professor D. T. Pham. Thanks for all the inspiring and wonderful discussions, encouragement and patience he provided throughout my stay at Cardiff University. Also, I am deeply grateful to my advisor Professor S. S. Dimov, for all his direction and expert insight which he has shared with me and supported me during my study.

In addition, I would like to express my gratitude to Dr K. B. Popov. I am deeply grateful to him for his consistent encouragement, invaluable guidance and strong support during the course of this study. Also, I am highly indebted to Dr E. Brousseau. I must appreciate his ever-ready helping attitude, which was a constant motivating factor for me to complete this thesis.

However, the support provided by my senior colleagues Dr Eldaw, Dr Afify, Dr Fahmy, Dr Minev, Mr Negm and Mr Scholz from the MEC is more than appreciated. I am also very grateful to all the members of the Manufacturing Engineering Centre for their friendship and help. Special thanks go to Dr Michael Packianather, Mrs Celia Rees, Mrs Rhian Williams, Miss Jeanette Whyte and Dr Chris Matthews for their sincere help and support.

Grateful acknowledgement of my funding and support must be made to my home country Egypt and the Egyptian Ministry of Higher Education. Also, my sincere thanks go to their representative in the UK, the Egyptian Educational and Cultural Bureau in London and all of its members for their advice, encouragement and support.

Thanks are also due to all the members of staff of the Production Engineering & Mechanical Design Department, Port-Said University, Port Said, Egypt, who taught me and gave me the scientific base to continue my postgraduate studies. Special thanks go to Professor Aly Eldomiaty, Dr Saleh Zoromba from Port Said University and to Professor Azza Barakt from Helwan University for their support during my former study.

My most sincere gratitude and appreciation go to my dear wife Mrs S. S. Ali for her patience, continuous encouragement and support over the past difficult years. Thanks as well to Allah for his gifts; my beloved kids “Abd-Elrahman” and “Marium”.

I am deeply indebted to my parents and all the members of my family who gave me continuous support and encouragement throughout my life.

DECLARATION

This work has not previously been accepted in substance for any degree and is not concurrently submitted in candidature for any degree.

Signed …… (candidate) Date ……

STATEMENT 1

This thesis is being submitted in partial fulfillment of the requirements for the degree of ……(insert MCh, MD, MPhil, PhD etc, as appropriate)

Signed …… (candidate) Date ……

STATEMENT 2

This thesis is the result of my own independent work/investigation, except where otherwise stated.

Other sources are acknowledged by explicit references.

Signed …… (candidate) Date ……

STATEMENT 3

I hereby give consent for my thesis, if accepted, to be available for photocopying and for inter-library loan, and for the title and summary to be made available to outside organisations.

Signed …… (candidate) Date ……

CONTENTS

LIST OF FIGURES

LIST OF TABLES

NOMENCLATURES

ΔW_1 absolute values of changes in the normal force when the sample is travelling forward along the direction of the cantilever length

ΔW_2 absolute values of changes in the normal force when the sample is travelling backward along the direction of the cantilever length

ECEA end cutting edge angle

f_t feed per tooth

L the length of the cantilever

l vertical distance between the tip of the cantilever and point P

$l^i_{\theta,j}$ horizontal coordinate of $p^i_{\theta,j}$ relative to the centre point of the tool edge corner

MR_n normalised material removal volume

n sensitivity factor of the surface roughness model

no number of measurements in the set of cutting edge radius measurement

N_p the number of the revolutions already completed

$p^{i-1}_{\theta,j}$ corresponding point to point $p^i_{\theta,j}$ for surface roughness calculation

$p^i_{\theta,j}$ current point under calculations

r cutting edge radius of the tool

R nominal cutting tool radius

r_c cutting tool corner radius of the tool

R_f percentage of ferrite phase in the dual-phase material

R_p percentage of pearlite phase in the dual-phase material

s estimated standard deviation of cutting edge radius measurement

Sa total surface roughness

t_c local chip thickness

t_{Cmin} minimum chip thickness

t_{cmin}^{f} minimum chip thickness for ferrite

t_{cmin}^{p} minimum chip thickness for pearlite

u standard uncertainty of cutting edge radius measurement

V cutting speed

W_o applied force between the tip and the sample; W ranges from 10 to 200 nN;

Xc the coordinate of the cutter centre point in **X** direction

X_f the coordinate of the centre point of the cutter edge corner in **X** direction

Yc the coordinates of the cutter centre point in **Y** direction

Y_f the coordinate of the centre point of the cutter edge corner in Y direction

$z^{i}_{\theta,j}$ vertical coordinate of $\boldsymbol{p}^{i}_{\theta,j}$ relative to the centre point of the tool corner radius

β friction angle between a tool and uncut workpiece

Δr increase of the edge radius

Δr_f tool wear when machining ferrite

Δr_p tool wear when machining pearlite

θ rotational angle of the cutter

λ_n normalised minimum chip thickness of any material

λ_{nf} normalised minimum chip thickness value for the ferrite phase

λ_{np} normalised minimum chip thickness value for the pearlite phase

μ coefficient of friction between a tool and workpiece

GLOSSARY OF TERMS

Burnishing plastic deformation of a machined surface due to sliding of the tool without removing material.

Chip-load thickness of the material to be removed in one machining path.

Dimple a severely strain-hardened piece of the workpiece material with a hooked edge which lies on the cutting plane. The surface of the dimple is initially below the cut surface and rises back up to the cutting plane.

Floor-burr a type of surface defect produced on the machined floor, particularly at the grain boundaries, due to the different responses to the cutting conditions of the phases, present within the microstructure.

Micro-crack a type of machined surface defect which usually occurs at ferrite–pearlite grain boundaries when machining dual-phase steel.

Micro-void a type of machined surface defect that results from extreme plastic deformation of a softer matrix material around a hard particle.

Minimum chip thickness the minimum undeformed thickness of chip removed from a work surface at a cutting edge under perfect performance of a metal cutting system.

Prow a severely strain-hardened piece of workpiece material that is hook-shaped and protrudes above the cutting plane and can have a hardness value 2 to 3 times greater than that of the original workpiece.

Smearing degrading of the machined surface due to the ploughing caused by the tool sliding without removing material.

CHAPTER 1

INTRODUCTION

1.1 Background and Motivation

The emergence of miniaturisation technologies is considered one of the key features of future interactions between people, machines and the physical world (Liu *et al.* 2004). However, a number of key phenomena that dominate the underlying mechanisms of miniaturisation technologies have emerged and their effects have not been fully examined yet (Liu *et al.* 2004 and Liu *et al.* 2007a). Thus, these factors have to be systematically studied and characterised to achieve successful development of such technologies. Among these technologies, mechanical micro-machining plays a significant role as a cost-effective technology to produce complex 3D features with tight tolerances and high accuracies (Uriarte *et al.* 2008 and Aramcharoen and Mativenga 2009). The main advantage of the micro-machining process is mainly due to its "direct write" capability. However, to some extent, the large body of cumulative knowledge and expertise that exist for macro-scale machining cannot be scaled-down and transferred directly to be applied at micro-scale (Dornfeld *et al.* 2006 and Miao *et al.* 2007). Size effects are considered the main cause of the distinguishing characteristics of micro-scale machining. In particular, performing machining on the micro-scale fundamentally changes cutting regimes, surface generation mechanisms, tool wear and cutting forces from those in macro-scale machining (Liu *et al.* 2004).

In the micro-endmilling process, the effect of the material microstructure on the process exemplifies one of its unique characteristics that need addressing. Especially, in micro-milling, chip-loads and machined features are comparable in size to the cutting edge radius of the tool, and also similar in scale to the grain sizes of the phases present within the microstructure. This phenomenon leads the cutting process sometimes to take place inside the individual grain itself. So, the assumption of homogeneity of workpiece material is no longer valid (Vogler *et al.* 2003; Liu *et al.* 2004; Dornfeld *et al.* 2006; Pham *et al.* 2008; Mian *et al.* 2009 and Mian *et al.* 2010). However, the effects of this heterogeneity of the processes microstructure have not been fully examined, especially on the quality of the machined part and the progression of tool wear.

The surface roughness achievable with a given machining process is always considered as one of its main characteristics. Taking into account the specific scale constraints in micro-milling the resulting surface roughness is even more important because it would be very difficult or even impossible to apply any follow-up processing, and thus to improve the surface quality (Dornfeld *et al.* 2006 and Pham *et al.* 2008). Moreover, the generated roughness in micro-scale machining cannot be fully explained using kinematic parameters only (Liu and Melkot 2006). This means that, the other factors which dominate the underlying cutting mechanism such as the cutting edge radius of the tool and the workpiece material have to be considered (Vogler *et al.* 2004a and Liu and Melkote 2006). Therefore, to achieve optimum machined surfaces, the selection of the workpiece material, especially multi-phase ones, and then the cutting conditions for their processing at micro-scale is one of the

challenging research issues that need addressing (Vogler *et al.* 2004a and Elkaseer *et al.,* 2010a).

In addition to the genrated surface roughness, cutting forces and tool wear are the main criteria that can be used for assessing the machinability of any material. Furthermore, the tool wear is associated with changes in the tool geometry, especially, cutting edge radius and cutting tool corner radius. This is mainly attributed to the significant increase of the friction between the tool and the workpiece associated with a thermal growth and wear (Chae *et al.* 2006), and also the small chip-load usually applied in micro-milling. Consequently, surface roughness is directly affected by such changes in the tool geometry, and ultimately the tool wear affects the quality and dimensional accuracy of the machined parts. Moreover, an increase in the cutting edge radius can alter the machining condition from cutting to ploughing and hence also leads to changes in cutting forces (Li *et al.* 2008). Therefore, one can advocate that getting a better understanding of the mechanism and progression of tool wear in micro-endmilling is very important for advancing this technology further. However, there are only few studies of tool wear at micro-scale machining reported due to some limitation of the available inspection technologies and difficulties in conducting empirical research (Jun *et al.* 2008 and Li *et al.* 2008).

For any machining process, optimisation is rightly claimed to be the most significant contribution distinguishing the modern approach in the field of industrial machinery research (Pham and Karaboga 1998). Mathematical models can act as fitness functions and they can be optimised to obtain the best results for a process. One example of that is optimising the surface roughness of the micro-machined parts. After successfully being able to find a reliable model of generated roughness for

multi-phase materials, cutting parameters and the materials microstructure are considered the variables of the optimisation problem while the final surface roughness acts as the objective of the same problem.

Furthermore, since reduction of energy and raw material consumption is the main goal of the miniaturisation philosophy (Ehmann 2007 and Mintegi 2007), the objective of future manufacturing is to produce parts virtually before manufacturing on the shop floor (Altintas and Merdol 2007). Such manufacturing scenarios need to be carried out in virtual environment, which can realistically simulate the machining process using mathematical-based models (Merdol and Altintas 2008). These models would also serve to provide a better physical understanding of cutter/workpiece interactions in micro-milling and aid in optimising the machining conditions.

In summary, the main barrier to further development of the micro-milling process is the lack of full scientific understanding of the process. In particular, the influence of the machined material microstructure on the cutting regime, generated surface and tool wear has not been fully examined yet. Therefore, there is a real need to examine some of the process conditions such as scaling issues, material microstructure behaviour and to address their influence on the process outcomes, and thus optimising the process to achieve the best possible performance.

1.2 Research Hypothesis and Objectives

The hypothesis followed in this research is that, in micro-endmilling, the effect of workpiece microstructure has a significant role in increasing the achievable

roughness compared to that obtained from conventional machining. In this context, the overall aim of this research was to obtain a deeper understanding of the influence of the workpiece microstructure on cutting regime, tool wear and surface quality when processing a part at micro-scale, and thus to optimise the cutting process.

To achieve the overall aim of the research, the following objectives were set:

- To investigate experimentally the machining response of modified materials at micro-scale in order to address the relationship between their microstructure in terms of grain sizes and the resultant surface quality.

- To introduce a new method for assessing the microstructure homogeneity of the processed microstructures and thus enabling a comparative evaluation of the modified morphology prior to the cutting process.

- To develop and validate a new model that can describe analytically the influence of the material microstructure on the surface generation process in micro-endmilling. This model should consider micro-burr formation and quantitatively model its effect on the total surface generated.

- To propose new ways, e.g. experimental setups, for characterising and monitoring tool wear in the micro-scale. Also, special attention of the effect of the material microstructure on the exhibited tool wear should be paid.

- To create models of tool wear based on the experimental data which can be used to estimate the increase of the cutting edge radius when machining single and dual-phase steels.

- To exercise the proposed models for surface generation and tool wear to develop a comprehensive optimisation model of the machining process, and thus to improve the surface roughness and reduce wear when machining materials with different microstructures.

- To create a virtual micro-milling environment that implements the developed surface generation and tool wear models. This model would provide a reliable tool for performing machining trials virtually without consuming energy and raw materials.

1.3 Thesis Organisation

The remainder of the thesis is organised as follows:

Chapter 2 contains a review and analysis of the current trends and recent developments of the micro-machining process. Special attention is given to the size effects and material microstructure on the process themes such as cutting mechanism, surface quality and tool wear due to its importance on the process feasibility. Then, some of the simulation studies that were developed recently for machining process are discussed. Finally, the chapter presents a number of virtual-simulation approaches in

the macro-scale machining in order to provide a foundation for similar applications in the micro-endmilling process.

Chapter 3 presents an experimental investigation of modified materials at the micro-scale to identify their machining response. First, the selected workpiece materials are described. Then, a method to assess microstructures based on AFM measurements is presented. Also, the selected machining conditions, in particular, the cutting tools and cutting parameters used in the trials, are defined and the rationale behind their selection is explained. Next, the results obtained are discussed, focusing on the effects of material microstructure on surface quality and cutting mechanisms. Measurements of the hardness of the machined surface are presented to support the discussion.

Chapter 4 describes a new model to simulate the surface generation process during micro-milling of dual-phase materials together with an experimental study to validate it. First, the chapter presents a multi-phase microstructure mapping procedure developed to incorporate the effect of the machined microstructure into the surface generation model. Then, modelling the cutting tool trajectory and the minimum chip thickness effect on the surface generation process are discussed. Next, an experimental study conducted on two different dual-phase steel samples to validate the proposed model is described. Finally, the comparison between simulation and experimental results is discussed.

Chapter 5 reports a new approach for modelling the tool wear when machining multi-phase materials at micro-scale followed by an evaluation of its effectiveness under different machining conditions. Initially, the most relevant research to the work

presented here is reviewed. After that, the proposed experimental setup is described. Then, the selected machining conditions, especially, workpiece materials, cutting tools and cutting parameters used in the trials are defined and the rational behind their selections is given. Next, the results are presented and discussed, especially focusing on the material effects on tool wear. This is followed by the creation of two regression models based on these trails. Then an experimental validation to demonstrate the applicability of the approach to predict tool wear when machining a wide range of multi-phase steels and iron is described.

Chapter 6 focuses on the simulation, optimisation and virtual modelling of the micro-endmilling of multi-phase materials. The chapter is organised as follows. First, the simulation of the generated roughness is presented followed by a discussion of the improvement made for the surface generation model through incorporating a tool wear model. Then, a modification of the investigated material microstructure is given. Next, an optimisation of the cutting conditions for the studied microstructures is discussed. Finally, a virtual environment that developed to conduct simulation trials of the micro-endmilling process is presented.

Finally, **chapter 7** summarises the contributions and conclusions of the thesis and proposes directions for further research.

Appendix A outlines of the Equal Channel Angular Pressing (**ECAP**) process that was used to produce Cu test parts for some of the experiments in this research.

Appendix B includes a VR simulation of micro-endmilling of dual-phase steel.

CHAPTER 2

MATERIAL MICROSTRUCTURE EFFECTS-BASED REVIEW OF THE MICRO-MACHINING PROCESS

2.1 Overview

In this chapter, a brief review and analysis of reported research relevant to the micro-machining process is presented in four sections followed by a summary. The chapter is organised as follows. First, reported work on cutting mechanisms of the micro-machining process is discussed. This section focuses on the size effect of the process, especially, effects of minimum chip thickness and cutting geometry on the cutting performance. In addition, special attention is given to the influence of material microstructure on the underlying mechanisms of the micro-machining process. Second, previous research covering the topic of surface generation in the micro-machining process is presented. Third, some of the research studying the tool wear in the micro-machining process is discussed. Fourth, prior work on the simulation of the machining process is summarised and particular emphasis is given to the virtual-modelling approaches. The virtual models reported herein chapter are generally relevant to macro-scale machining. However, such review provides a foundation for similar applications at micro-scale. Finally, the chapter is concluded with a summary of some of the key research issues in micro-milling research area.

2.2 Cutting Mechanisms of Micro-Machining

Mechanical micro-milling is becoming increasingly important for its capability of producing parts with complex three-dimensional features in a range of sub-millimetre for a wide range of materials (Uriarte *et al.* 2008). Apparently, micro-machining and conventional machining are kinematically similar, i.e., the material removal principles (Chae *et al.* 2006). However, there are a number of key differences between micro-scale and macro-scale machining which arise from changes in the underlying physical phenomena (Liu *et al.* 2004). These changes are mainly attributed to the size effects, e.g. applied chip-loads (Liu *et al.* 2004 and Pham *et al.* 2009), tool geometry and characteristics of the workpiece microstructure (Kim *et al.* 2002; Liu *et al.* 2004; Vogler *et al.* 2004a and Vogler *et al.* 2004b) in performing machining at micro-scale. In micro-endmilling, where chip-load varies between zero and the value set by the operator, the edge radius of the tool could be significantly larger than the applied chip-load (Filiz *et al.* 2007). Thus, transitional regime associated with intermittent cutting and ploughing becomes more dominant. Further, when the chip thickness is below a critical value of chip thickness, so-called minimum chip thickness, chips may not be formed during each tooth passing, instead, the workpiece material elastically deforms (Weule *et al.* 2001; Kim *et al.* 2002*,* vogler *et al.* 2004 and Arif *et al.,* 2011). As a result, higher cutting force, larger tool wear, micro-burr formation and subsequently degraded surfaces are produced (Liu *et al.* 2004 and Wang 2008).

In addition, the anisotropic behaviour of the material microstructure when processing at micro scale becomes an important factor that has to be considered throughout the machining process. This is especially the case when chip-loads and machined features are similar in

scale to the grain sizes of the phases present within the material microstructure (Liu *et al.* 2004; Pham *et al.* 2008; Pham *et al.* 2009; Mian *et al.* 2009 and Mian *et al.* 2010). Also, the varying crystallography of the processed microstructure could leads to noticeable variation in the cutting forces associated with vibration during the cutting process (Liu *et al.* 2004 and Wang 2008). However, because this vibration originates from the workpiece itself, it is difficult to be avoided by conventional ways, e.g., adopting process conditions or changing the machine tool design (Kata and Ozdoganlar 2010). Therefore, the nature of the workpiece is considered a salient factor for fabricating accurate micro-parts (Elkaseer *et al.,* 2009a).

To sum up, the process special characteristics, e.g., tool geometry effect, minimum chip thickness effect and influence of the processed microstructure, are considered significant issues that need addressing to achieve successful development of the process. This section discusses reported work related to these factors.

2.2.1 Size effects in micro-machining

As formerly mentioned, both the micro-machining and conventional cutting are kinematically similar. Especially, cutting tools are used to mechanically remove materials in the form of chips (Chae *et al.* 2006). However, unlike conventional macro-machining processes, the significant size reduction at micro-machining is associated with fundamentally different characteristics (Liu *et al.* 2004; Vogler *et al.* 2004a and Jina and Altintas, 2011).

The phenomenon of minimum chip thickness, which is mainly related to the applied chip-load and cutting edge radius of the tool in addition to the workpiece material, is

described by Chae *et al.* (2006), as shown in Fig. 2.1. In particular, when the undeformed chip thickness, $\boldsymbol{h}$, is less than a critical minimum chip thickness, $\boldsymbol{t_{cmin}}$, as shown in Fig. 2.1a, elastic deformation takes place and no chip is formed. However, with the increase of the chip-load to a value close the minimum chip thickness, the cutting mechanism becomes mixed, cutting and ploughing. In particular, shearing of the workpiece occurs and leads to chips formation, with some elastic deformation still occurring, as illustrated in Fig. 2.1b. Consequently, the generated surface is higher than the desired depth. However, when the undeformed chip thickness increases further than the minimum chip thickness, the elastic deformation decreases drastically and newly workpiece surface is formed close to the lowest point of the cutting edge, Fig. 2.1c (Chae *et al.* 2006).

In the light of the effect of the minimum chip thickness, the cutting regime is altering between chip removal and ploughing/rubbing mechanisms. As a result, higher cutting forces, larger tool wear, burr formation and rougher surface are expected (Liu *et al.* 2006). Thus, to eliminate this effect, minimum chip thickness has to be determined prior to the cutting process enabling the selection of appropriate machining conditions (Liu *et al.* 2006). The investigation of this size effect, especially minimum chip thickness and tool geometry, has had a great deal of interests (Liu *et al.* 2004; Chae *et al.* 2006; Dornfeld *et al.* 2006 and Gowri *et al.* 2007).

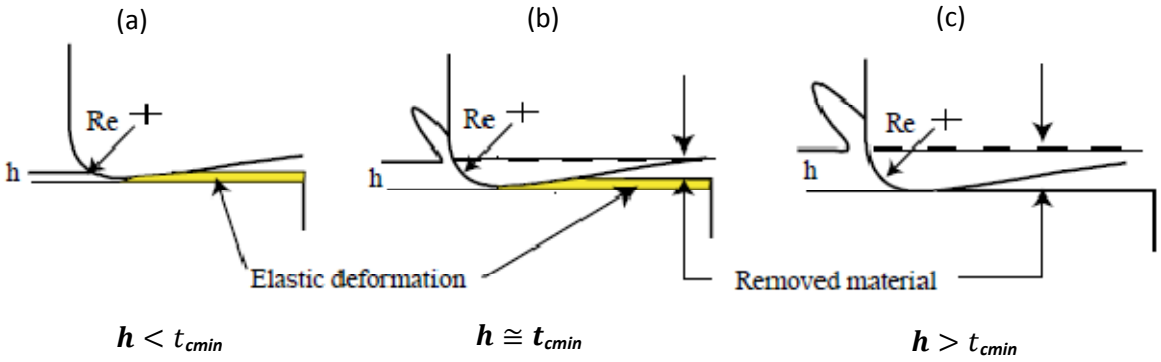

Fig. 2.1: Schematic of the effect of the minimum chip thickness (Re, radius of cutting tool; *h*, undeformed chip thickness; t_{cmin}, minimum chip thickness) (adopted: Chae *et al.* 2006).

The significance of the minimum chip thickness effect was investigated by Ikawa *et al.* (1992). The author defined the minimum thickness of cut (MTC) as "the minimum undeformed thickness of chip removed from a work surface at a cutting edge under perfect performance of a metal cutting system." The authors concluded that a well-defined diamond tool can be used to obtain a very fine chip with an undeformed thickness of the order of a nano-meter in face turning of electroplated copper. In particular, it is noted that the minimum thickness cut could be on the order of 1/10 of the cutting edge radius.

Yuan *et al.* (1996) performed an experimental study of the minimum chip thickness effect on the generated surface in diamond turning of Aluminium alloy. The results showed that larger cutting edge radius produced rougher surface which is explained by the minimum chip thickness effect. Moreover, minimum chip thickness was found in the range of 20-40% of the cutting edge radius..

Weule *et al.* (2001) examined the effect of minimum chip thickness on the generated roughness. The generated surface by micro-cutting of SAE1045 was assessed using laser-based topography measuring device. However, the saw-tooth-like profile, Fig. 2.2, was attributed to the effect of the minimum chip thickness. Also, the minimum chip thickness was determined experimentally to be 0. 293 of the cutting edge radius of the tool.

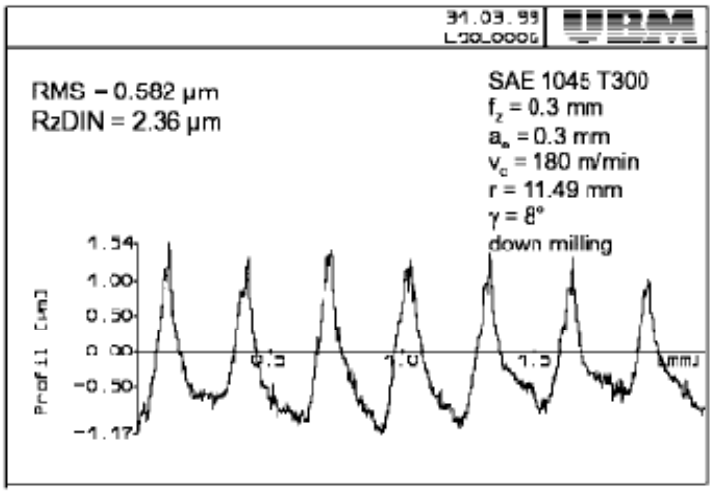

Fig. 2.2: Measured surface topography (Weule *et al.* 2001).

Kim *et al.* (2002) conducted experimental trials to study the effect of minimum chip thickness on the chip formation process in micro-milling of brass. The experiments were carried out under a range of feed rate from 0.188 μm to 6 μm with 635 μm tool. The authors found that, at very small chip-loads, a chip might not be formed during every tool pass. Moreover, the formed chips had larger volume than expected based on the volume of material removed throughout one tool pass. However, they attributed this observation to the comparable relationship in size between the cutting edge radius and the applied chip-load. As a result, it was concluded that no chip formation occurred unless the chip-loads reach a certain value, minimum chip thickness.

Vogler *et al.* (2003) developed finite Element model to determine the minimum chip thickness for ferrite and pearlite phases at micro-scale machining, as shown in Fig. 2.3a and Fig. 2.3b. Different edge radii, 2-7 μm, and a range of chip thicknesses, 0.1-3 μm, were used in the simulation study. The ratio of minimum chip thickness to edge radius of the tool was found to range between 0.14-0.25 and 0.29–0.43 for pearlite and ferrite, respectively.

Lai *et al.* (2008) studied the effect of the size effect in micro-milling of Oxygen Free High Conductivity (OFHC) copper. The author developed a finite Element (FE) model for orthogonal machining at micro-scale considering the material characteristics and cutting edge radius. The minimum chip thickness was determined to be 0.25 of the cutting edge radius for copper in case of 2 μm cutting edge radius and 10º rake angle. Also, the author explained the increase of the specific cutting energy at very small feed rate to the ploughing regime that dominating the underlying mechanism due to the minimum chip thickness effect and the accumulated chip thickness.

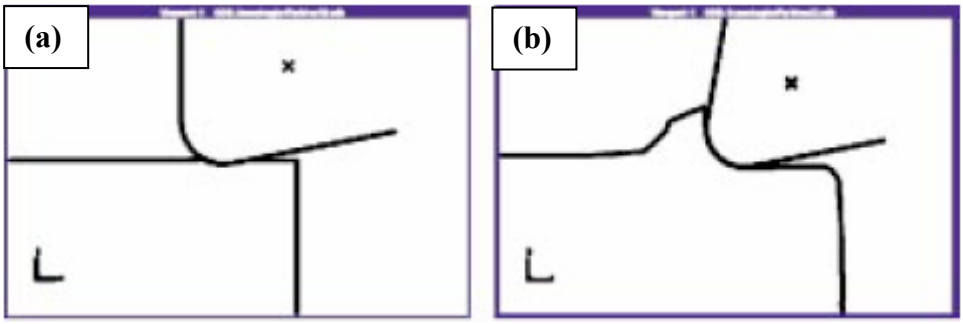

Fig. 2.3: FE simulation with different chip thicknesses (a) below minimum chip thickness and (b) above minimum chip thickness (Vogler *et al.* 2003).

Biermann and Kahnis (2010) studied the influence of the cutting edge radius on the process. The cutting edge radius of the tool was enlarged by abrasive water-jet blasting to achieve a range of cutting edge radii. It was revealed that lower surface quality and higher cutting forces were obtained by such larger cutting edge radius. However, less tool wear also achieved, Fig. 2.4. In addition, it was shown that with low undeformed chip thicknesses, the specific cutting forces and surface roughness increase, Fig. 2.5 and Fig. 2.6, and a significant higher burr formation occurs owing to the ploughing effects.

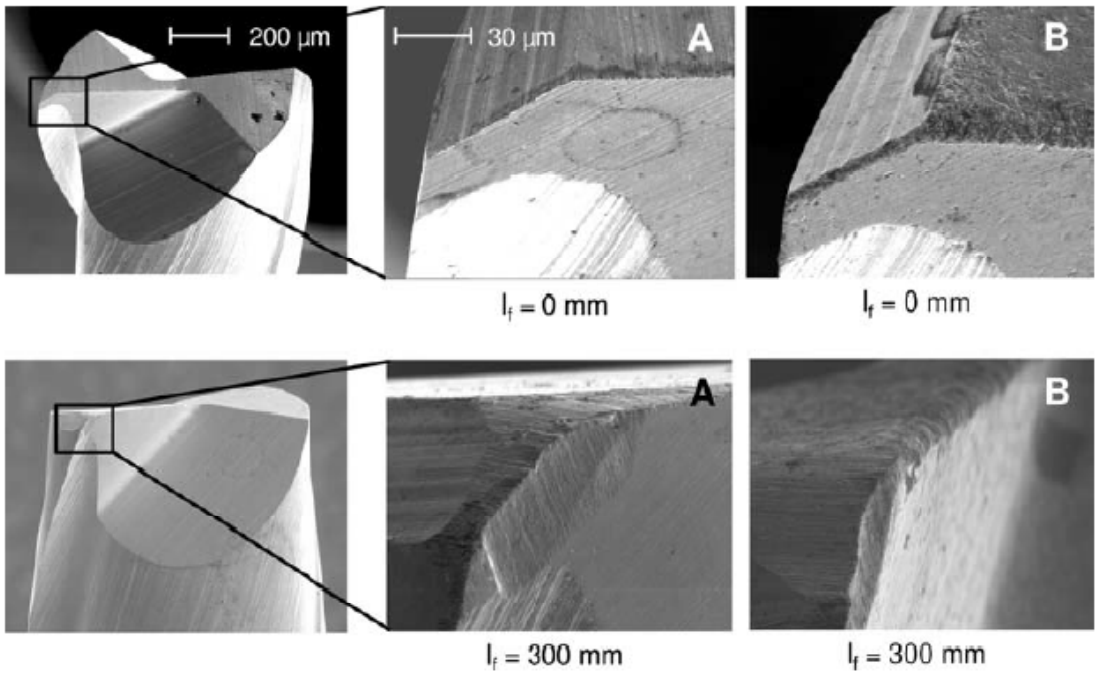

Fig. 2.4: Influence of a cutting edge rounding on the tool wear for tool with (A) small edge radius and (b) large edge radius (Biermann and Kahnis 2010).

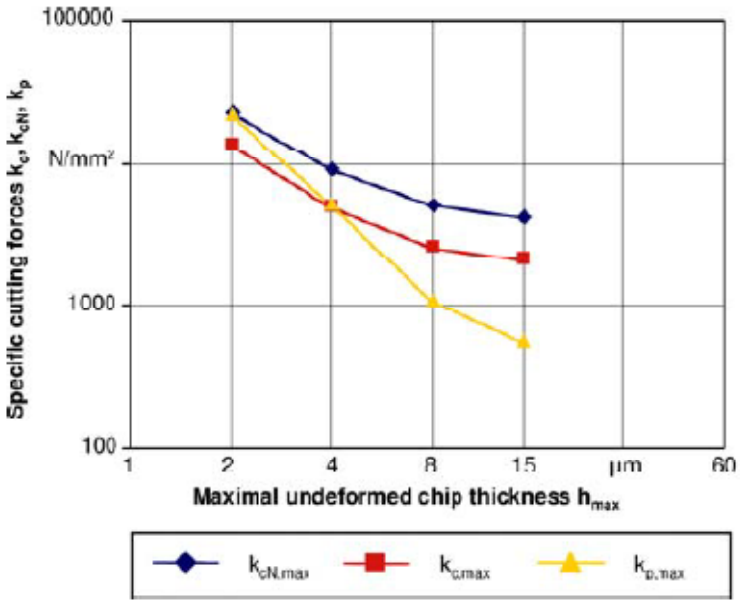

Fig. 2.5: Influence of the undeformed chip thickness on the specific cutting forces (Biermann and Kahnis 2010).

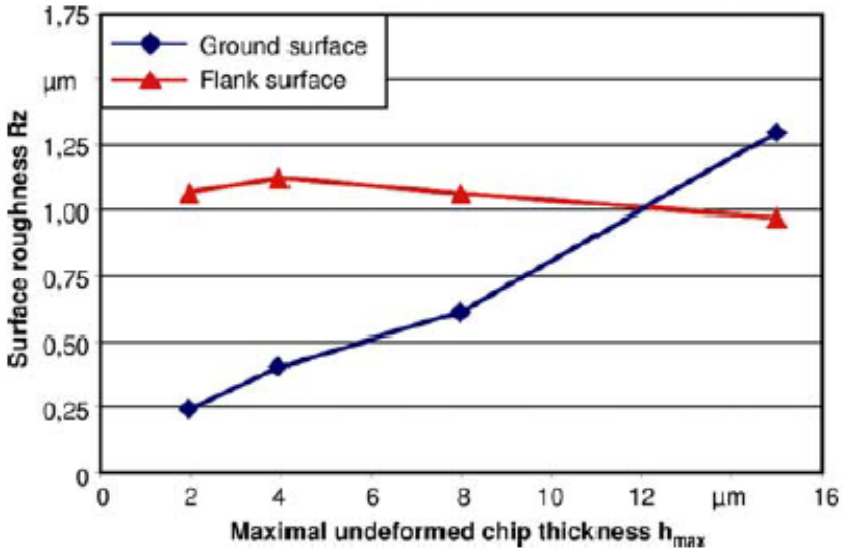

Fig. 2.6: Influence of the undeformed chip thickness on the surface roughness (Biermann and Kahnis 2010).

2.2.2 Material microstructure effect

There has been an increasing trend for products to be made smaller in many application areas, e.g. optics, electronics, medicine, biotechnology, communications, and avionics (Liu *et al.* 2004; Dornfeld *et al*. 2006; Chae *et al.* 2006; Ehmann 2007; Filiz *et al*. 2007; Gowri *et al.* 2007; Mintegi 2007; Dhanorkerand Özel 2008 and Pham *et al.* 2008). Due to the technical requirements of the wide variety of devices involved, they may have to be made from one or more of a broad range of engineering materials, such as aluminium alloys, stainless steel, titanium, copper, brass, plastics, ceramics, and composites (Liu *et al.* 2004). Therefore, there are stringent demands on both the micro fabrication processes and materials used owing to the need for dependable and robust micro components (Ng *et al.* 2006).

Because the grain sizes of most commonly used engineering materials, such as steel, copper and aluminium, and the feature sizes of micro-machined components or the edge radius of the cutting tool can be comparable in scale (Liu *et al.* 2004 and Gowri *et al.* 2007) as shown in Figure 2.7b, the material cannot be considered isotropic or fully homogeneous (Vogler *et al.* 2003; Liu *et al.* 2004 and Mian *et al.* 2010). As a result, it is necessary to perform sub-grain size (mechanical) processing (Taniguchi 1996). In addition, the crystalline texture of the material resulting from its processing could lead to variations in chip thickness and the removal process can be considered to some extent stochastic. Cutting takes place in the so-called dislocation micro-crack range with material removal units varying from 100 nm to 10 μm (Taniguchi 1996). In particular, the cutting process does not rely only on developing micro-cracks along the grain boundaries but also involves dislocation slips in the crystalline structure of the material. In addition, during cutting, the dislocation density increases due to dislocation multiplication and the formation of new dislocations. Thus,

material microstructure effects are significant in micro-machining (Vogler *et al.* 2003; Liu *et al.* 2004 and Mian *et al.* 2010), and the specific processing energy (Taniguchi 1996) required to initiate chip formation depends directly on the ability of a metal to produce dislocation slips.

Many researchers have investigated the effect of material microstructure on process conditions, such as cutting forces, chip formation, and surface roughness during micro-machining of multi-phase, polycrystalline and amorphous materials in the micro-machining processes (Dornfeld *et al.* 2006).

Furukawa and Moronuki (1988) reported different cutting mechanisms for polycrystalline, single crystal and amorphous materials, and also for brittle and ductile materials. They suggested that, by increasing the undeformed chip thickness to ten times the average grain size for a given material, it would be possible to avoid the negative crystallographic effects of the material microstructure.

Also, vibration caused by heterogeneous materials, especially, aluminium single crystal with (110) and (111) plane in precision machining was investigated by Lee et al. (1999 and 2002). It is concluded that shear angle and strength is influenced by changing crystallography and grain orientation of the machined material.

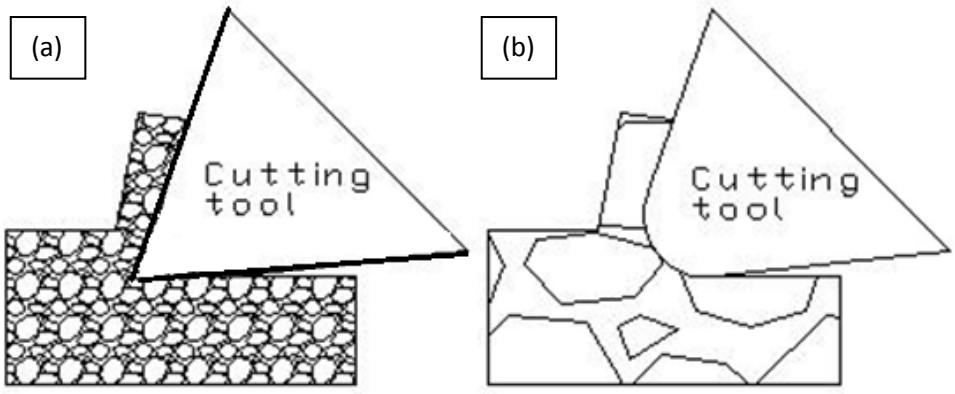

Fig. 2.7: Macro (a) and micro cutting (b).

Weule *et al.* (2001) studied the effect of the material microstructure of steel workpieces, SAE 1045, in precision fly cutting process. It was suggested that, for a good projection of the cutting tool into the workpiece, processed material should have only one phase, or its microstructure could be homogenised to reduce the grain diameter of the material when compared with cutting edge radius. However, a pre-heat treatment to the workpiece before micromachining is proposed to obtain a homogeneous workpiece. Also, relatively large feed rates were suggested to improve machined surface.

Grum *et al.* (2003) observed significant influence of the machined microstructure on the cutting force when different aluminium and silicon alloys were processed in hard turning process. Also, changes in cutting conditions which in turn lead to machining errors, vibration, or accelerated tool wear was detected when the cutting tool moves from one metallurgical phase to another.

Vogler *et al*. (2004b) conducted series of full-slot endmilling tests with two fluted carbide end-mills on single-phase ferrite and pearlite, and also on multi-phase iron. Low frequency cutting forces were observed in both, pure ferrite and pure pearlite. At the same time, high frequency forces appeared in the multi-phase iron, which was attributed to the heterogeneity of the workpiece microstructure. This in turn led to changes in cutting conditions causing a vibration increase and the occurrence of highly fragmented chips.

Uhlmann *et al*. (2005) reported an experimental study into micro-milling of sintered tungsten-copper (WCu) composite materials with different ratios of tungsten, W, and copper,

Cu, and with microstructures as shown in Fig. 2.8. They uncovered a strong relationship between surface quality and homogeneity of the material microstructure.

Simoneau *et al.* (2007a) performed micro-machining tests for normalised AISI1045 steel and a refined AISI1045 steel. A comparison of the experimental results demonstrated that by reducing the size of the material microstructure, the scale of cutting could be shifted. For the refined 1045 steel microstructure, the shift in grain size translated to a shift in the scale of cutting, the resulting chip morphology and the transition between macro-, meso- and micro-scale cutting occurred at a smaller uncut chip thickness as compared to the cutting of normalised 1045 steel. Also they developed a new heterogeneous FE model to model the multi phase microstructure materials (Simoneau *et al.* 2006a; Simoneau *et al.* 2006b; Simoneau *et al.* 2006c and Simoneau *et al.* 2007b).

Goo *et al.* (2010) carried out micro-milling tests to compare between plain polystyrene and Carbon Nano-Tube (CNT) composite polystyrene in terms of forces, acoustic emissions, and burr formations under a range of chip-loads. It is found that shearing regime was more dominant when machining CNT composite polystyrene compared with plain polystyrene. This was attributed to the decrease of the minimum chip thickness when plain Polystyrene modified to be reinforced composite with CNTs.

Kata and Ozdoganlar (2010) examined the effect of the crystallographic anisotropy of coarse grained aluminium on the cutting forces over different cutting conditions. Significant changes in machining forces were observed at different grains. In addition, the average

surface was found basically depend on particular grain orientation being cut. Specifically, based on the crystal orientation, the values of cutting force and surface roughness can vary up to 300% and 687% respectively, Fig. 2.9. The authors noticed that specific cutting energy can be reduced when uncut ship thickness increases and/or the cutting speed decreases. Also, the observed significant variation of the forces between two levels with consecutive cuts was attributed possibly to the effect of the sub-surface deformation.

Following a review of related work, the anisotropic behaviour of the microstructure when processing materials at micro scale becomes an important factor that has to be considered throughout the machining process. This is especially the case when chip-loads and machined features are comparable in size to the cutting edge radius of the tool, and also similar in scale to the grain sizes of the phases present within the material microstructure. Therefore, there is a real need to investigate the machining response of different materials at micro-scale in order to address the relationship between their microstructure and the process performance, especially quality of the resulting surface and exhibited tool wear.

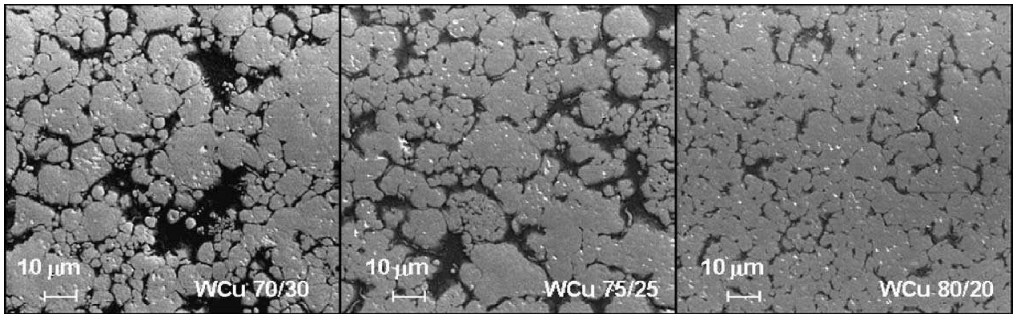

Fig. 2.8: Microstructure of WCu (Uhlmann et al. 2005).

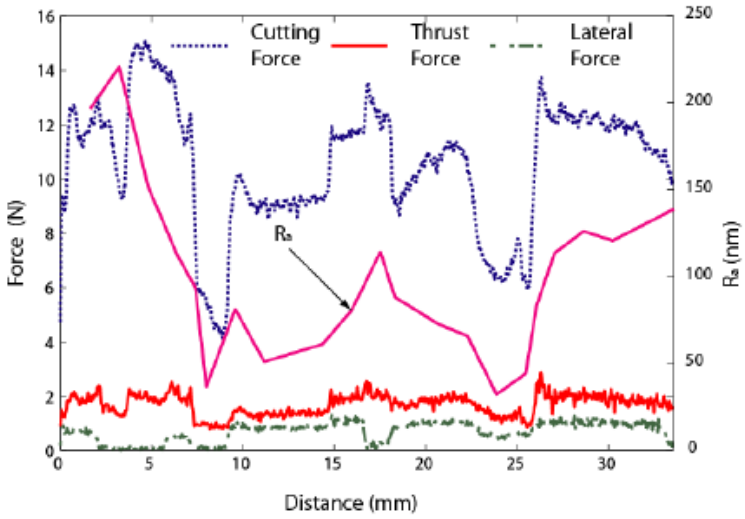

Fig. 2.9: Variations in surface roughness and forces (Kota and Ozdoganlar 2010).

2.3 Surface Generation in Micro-Machining Process

The surface achievable with a given machining process is always considered as one of its main characteristics. However, geometric parameters of the tool and process conditions have verified accurate prediction of the surface generation in conventional machining, this is not the case in micro-milling due to the specific scale constraints the process (Vogler *et al.* 2004a). In addition, taking into account the inverse relationship between surface-to-volume ratios and the size-scale of machining, more attention to surface generation mechanisms in micro-scale machining should be forthcoming (Liu *et al.* 2004). Therefore, it is not surprising that many researchers have investigated the mechanism and the factors affecting the surface generation during the micro-machining process. This section reviews work done in the area of surface generation in micro-machining process. In particular, generated surface roughness and surface defect are mainly covered herein section.

2.3.1 Surface roughness

Vogler *et al.* (2004) proposed a model to predict surface roughness considering the minimum chip thickness effect, Fig. 2.10. It is reported that the tool-edge radius and the feed rate had the main influence on the surface roughness in micro-milling. It was concluded that the optimal feed rates reflects the trade-offs between the kinematic parameters and the minimum chip thickness effect, Fig 2.11. This is the case when machining a single-phase steel, ferrite or pearlite. At the same time, the increase of surface roughness of multi-phase iron slots was attributed to the micro-burr formation at the grain boundaries due to the anisotropic responses of the different phases present within the microstructure.

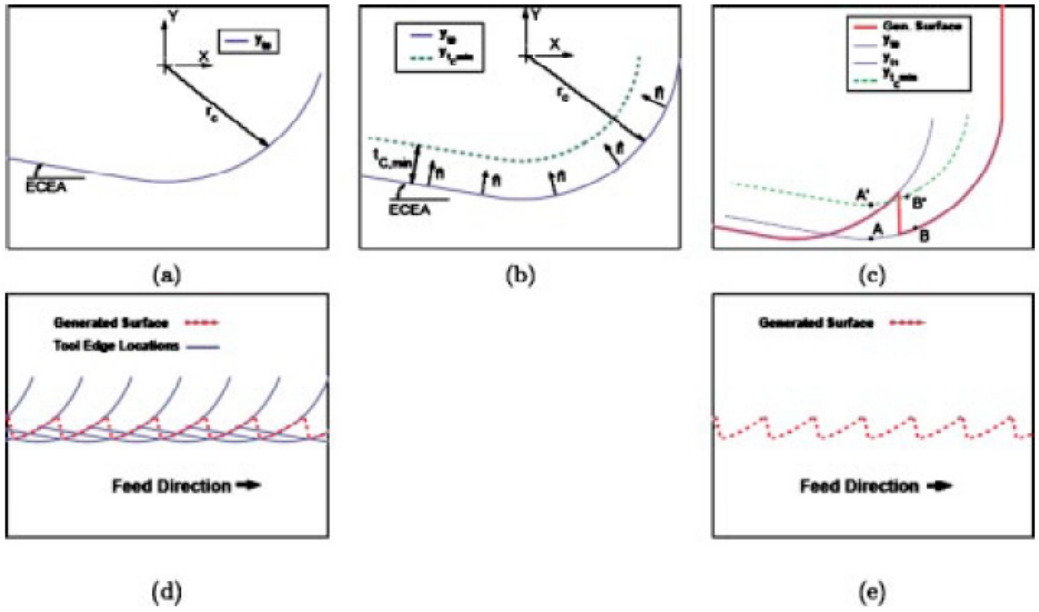

Fig. 2.10: Schematics for surface generation prediction: (a) tool geometry profile, (b) tool geometry and minimum chip thickness offset line, (c) generated surface after second tool pass, (d) final generated surface with tool profiles, and (e) final generated surface (Vogler *et al.* 2004).

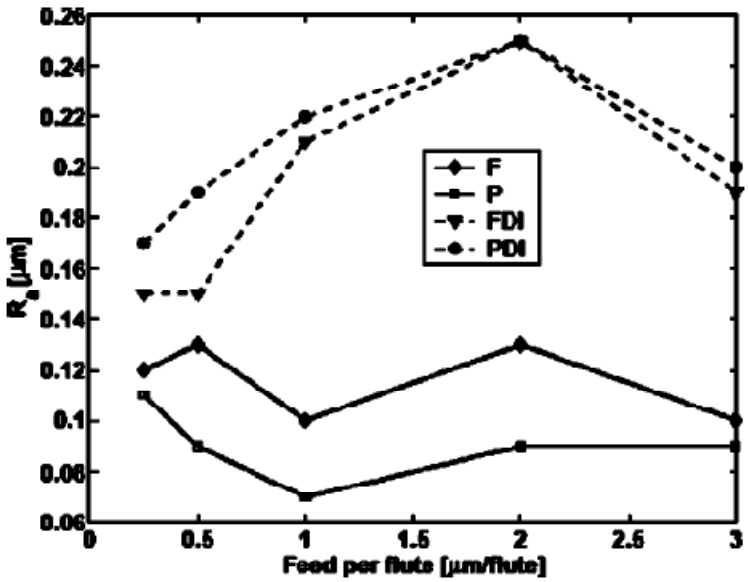

Fig. 2.11: Effect of feedrate on surface roughness (Vogler *et al.* 2004).

Liu and Melkote (2006) concluded that considering only the tool geometry and the process kinematics is no longer adequate to fully explain the surface generation process in micro-machining. This is especially the case at feed rates below the minimum chip thickness. Simultaneously, the side flow in front of the tool due to the strain-gradient is considered the main cause of the higher surface roughness produced at such low feed rates.

Popov *et al*. (2006) studied the machining response of mechanically and metallurgically modified Al 5083 alloy when milling thin features in micro components. They showed that through refinement of the material microstructure it was possible significantly to improve the surface integrity of the machined micro features. For example, by reducing the average grain size from 100–200 μm to 0.6 μm, the surface roughness of thin features in micro components improved three times and the material also became more isotropic. The authors concluded that the roughness of micro features produced by micro-milling was highly dependent on the material grain sizes. Based on this and other results (Presz and Rosochowski 2006; Rosochowski *et al.* 2007a; Rosochowski *et al.* 2007b and Geißdörfer *et al.* 2008), they suggested further research to deal with grain size effects in the manufacturing of micro components for a range of micro engineering applications.

To improve the model proposed by Vogler, Liu *et al.* (2007) developed a more comprehensive surface generation model for predicting roughness of the produced side wall and resulting floor surface in micro-end-milling. The model developed in this research includes two distinctive components: a deterministic/geometric one reflecting the process geometry and a stochastic one to account for the ploughing related phenomena. However, it is important to stress that this model does not consider the effects of the workpiece material

microstructure on the generated surface, especially the increase of the roughness due to the micro-burrs formed at the grain boundaries even at high feed rates.

Li *et al.* (2008) developed a trajectory-based surface roughness model used to predict the surface roughness in micro-milling of OFHC Copper taking into consideration the effects of the minimum chip thickness and tool geometry. To calibrate the model a regression analysis of experimental data was carried out and thus to take into account the effects of the tool wear during the cutting process. The conclusions made in this research were that the minimum chip thickness significantly affects the surface roughness, and its effects become even more severe when the feed per tooth is close to the minimum chip thickness.

Pham *et al*. (2009) investigated the parameters affecting the roughness of surfaces generated after micro-milling of two different materials, Al5083 and Cu99.9E. The materials had a different microstructure, one with coarse grains while the other had an ultra-fine microstructure. The statistical study of the experimental data showed that the material microstructure was the most significant factor affecting the average roughness resulting after micro-milling. Thus, it was concluded that the effects of material microstructure and different machining responses, especially when processing multi-phase materials, should be taken into account in developing new analytical models for simulating the micro-milling process. Such models should account for micro-burr formation at the phase boundaries, and also describe quantitatively their effects on the generated surface.

Mian *et al.* (2009) investigated experimentally the machinability of multi-phase material, ferrite/pearlite AISI 1040 steel, when processing at micro-scale. The authors aimed to

improve the viability of the micro-milling process through identifying cutting conditions and strategies required for machining materials with restricted microstructures. It was found that the edge radius of the tool and sizes of the material grains have a significant influence on the produced surface roughness. Also, the authors concluded that both parameters should be determined prior to the cutting process to optimise the cutting conditions for the best surface quality. Especially, the cutting tool deteriorates rapidly at chip-loads less than the cutting edge radius which in turn leads to higher surface roughness, as shown in Fig. 2.12, and larger burr size. Moreover, to reduce burrs formed during machining such dual-phase materials, it is suggested to use chip-loads larger than the average grain size.

In subsequent research, Mian *et al.* (2010) conducted an experimental comparative investigation of two different steels. One is mostly ferritic steel, AISI 1005, while the other is AISI 1045. The authors examined the effect of the material microstructure on the surface finish, microstructure change, burr formation and tool wear over a range of chip-load. It is found that machining of AISI1005 is more difficult when compared with AISI1045. Particularly, larger burr sizes were observed when machining AISI1005 as shown in Fig 2.13a and 2.13b. Also, more smearing on the machined surface was noticed over the entire range of the feed rates associated with faster tool wear. The investigation proved that both chip-load and workpiece material have noticeable influence on the generated roughness. However, it is found that surface finish was more sensitive to tool edge radius than material grain size. This conclusion was proved based on the improvement of the surface finish that obtained at chip-loads in the vicinity of the tool edge radius for both investigated materials. Also, the authors utilised a nano-indentation test to characterise both material microstructure and suggested that it can be used to relatively assess the machinability of different workpieces.

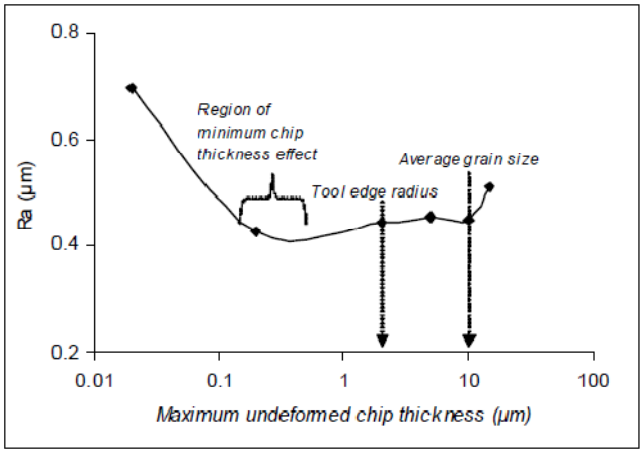

Fig. 2.12: Effect of cutting edge radius on surface roughness (Mian *et al.* 2009).

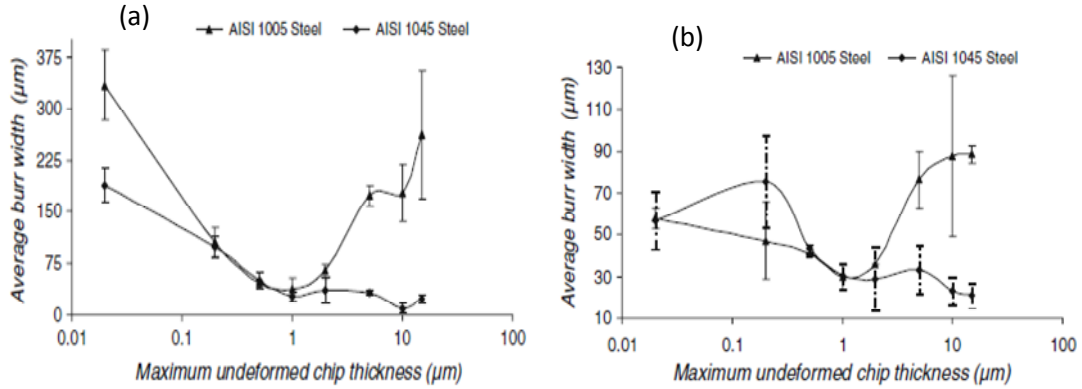

Fig. 2.13: Burr size in (a) down-milling and (b) up-milling (Mian *et al.* 2010).

2.2.3 Surface defects

Surface defects in machined workpieces are real “productivity killers” They make assembly difficult and require additional finishing operations “post-processing” which can damage the part (Dornfeld 2005). Edge burrs appear in both conventional machining and micro-machining. However, since the limitations in part geometry do not allow some of the solutions used in macro-machining, their negative effect is more significant in micro-machining (Dornfeld *et al.* 2006).

Lee and Dornfeld (2002) experimentally investigated micro-burr formation in micro-machining of copper and aluminium under a range of different chip-loads and depths of cut, using 127, 254, and 635 μm cutting tool. It was reported different types of burr. Namely, flag-type, rollover-type, wavy-type, and ragged-type burrs were observed, as shown in Fig. 2.14. The authors observed that, for top burr, up-milling produces a smaller burr than down milling. However, burr size increases with the increase of depth of cut and feed rate. Also, a big wavy-type burr was attributed to the run-out in micro-milling.

Different types of surface defects such as prows, dimples, micro-voids, and floor micro-burrs are always formed in machined multi-phase material (Simoneau *et al.* 2006).

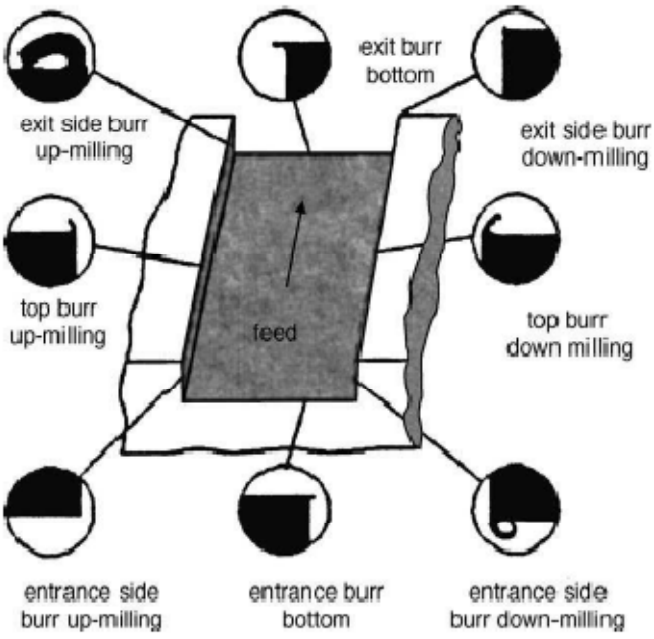

Fig. 2.14: Categorisation of burr types (Robinson and Jackson 2005).

Min *et al.* (2006) investigated experimentally the machinabilty of single-crystal oxygen-free high conductivity (OFHC) copper workpieces. Two-flute uncoated WC endmills of 150 microns in diameter were used in a slot-milling of each workpieces. A noticeable difference in entrance and exit burrs at the top edges of the micro-machined slots was detected. Also, the influence of up and down milling can be clearly seen. Crystallographic orientation was found significantly to affect burr formation, especially, variation of burr height with different orientation in the micromachining of single crystal copper was identified. Also, it is worth stressing that process parameters found have not as significant an effect on burr formation as crystallographic orientation. As a result, paying further attention to the influence of workpiece microstructure on micromachining was suggested. Also, they proposed more refined testing of other crystallographic orientations to see the effect on surface and edge condition. They suggested investigating burr formation in other micro-machining processes, such as micro-drilling, and establishing analytical relationships between crystallographic orientation, cutting direction, and the resulting surface and edge quality.

Wang et al. (2007) found that in multi-phase materials, which comprise different metal grains, the physical characteristics are obviously different. Consequently, the friction coefficient is different and according to the equation developed by the authors which relates the minimum chip thickness to the friction coefficient, the minimum chip thickness is different also. Fig. 2.15 depicts a case where there are four grains dispersed along the cutting edge. Because of their different minimum chip thicknesses, the chip formation statuses are different. For grains with high friction coefficients, chips are formed. However, for grains with lower friction coefficients, only little burrs are created or the material is just compressed.

The effects of the material microstructure on the surface defects resulting after micro cutting were studied by other researchers. It was reported that micro-burrs, one of the common defects in micro cutting of multi-phase materials, account for 20-40% of the total surface roughness (Vogler *et al.* 2004a). In addition, the presence of other defects such as dimples, prows, micro-voids and micro-cracks after machining steel were investigated irrespective of the cutting conditions (Gillibrand 1979; Furukawa and Moronuki 1988; Vogler *et al.* 2004b; Popov *et al.* 2006 and Liu *et al.* 2007). It was reported that these defects should be attributed to the presence of a second phase in the material microstructure.

Simoneau *et al.* (2006a) reported surface defects as dimples, micro-voids, micro-cracks, prows, Fig. 2.15 and Fig. 2.16, on machined surfaces of plain carbon steel. This was attributed to the dual-phase microstructure of the workpiece material, and the effect of the strain mismatch at the grain boundaries due to the absorbed energy by the softer phases before the cutting took place, effectively.

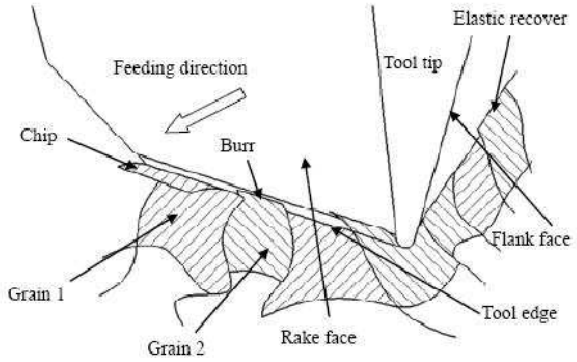

Fig. 2.15: Cutting zone (Wang *et al.* 2007).

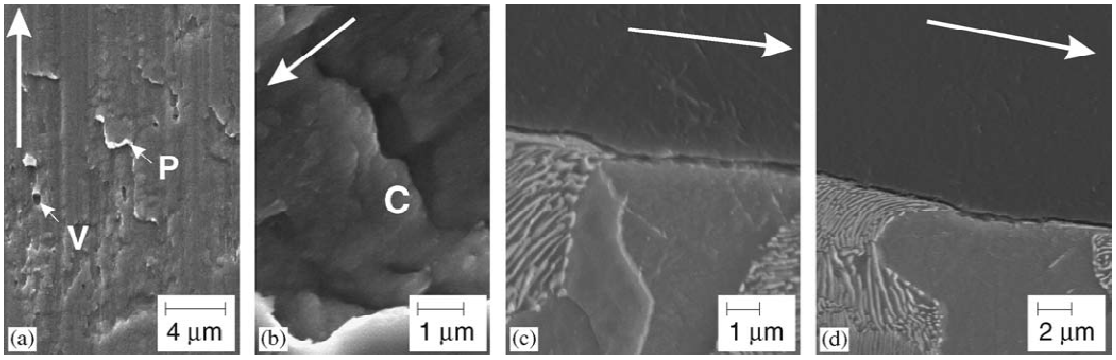

Fig. 2.16: SEM images of the resulting machined surface. The dimpled surface in (a) shows examples of prows (P) and micro-voids (V), while a micro-crack (C) is shown in (b). Cross-sectional SEM images in (c) and (d) of a dimple on the machined surface (Simoneau *et al.* 2006).

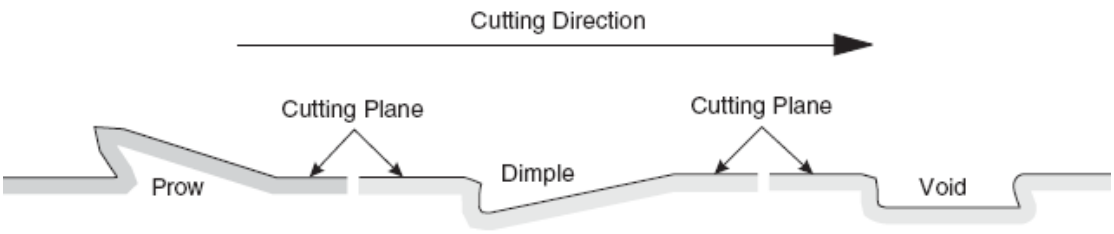

Fig. 2.17: Schematic of different surface defects observed on a machined steel surface (Simoneau *et al.* 2006).

2.3 Tool Wear

Predominantly the tool wear at macro-scale have been investigated, and there are only few studies at micro-scale machining reported due to some limitation of the available inspection technologies and difficulties in conducting empirical research (Jun *et al.* 2008; Li *et al.,* 2008 and Elkaseer *et al.,* 2010b).

Tansel *et al.* (2000) studied experimentally the relationship between the tool wear (usage) and the cutting force in micro-milling during the machining of soft and very hard materials, especially aluminium and steel. Backpropagation-type artificial neural networks (ANN) were used to create models for estimating the tool wear instead of detecting the pre-failure stage investigated by the authors in prior research (Tansel and Rodriguez 1992; Tansel 1994 and Tansel *et al.* 1998). The authors concluded that, in case of aluminium, cutting force variations increased proportionally with the tool usage which was attributed to changes in the shape of the cutting tool while cutting edges gradually losing their sharpness and effectiveness. Also, the created ANN models were able to identify effectively dependence between the tool wear and cutting force during the machining of soft materials. At the same time, the relationship between the tool wear and the cutting force when machining the steel (NAK 55) workpiece was very different from the aluminium response. Therefore, the proposed ANN can only be used to identify the pre-failure stage when machining NAK 55 workpiece.

Rahman *et al.* (2001) experimentally investigated tool wear of 1mm diameter tool when micro-milling of copper. It is concluded that tool helix angle and depth of cut have a noticeable influence on the exhibited wear. However, inverse relationship was detected between the applied depth of cut and resulting tool wear rate. This phenomenon was attributed to the well guiding of the tool by the workpiece at higher depth of cut.

Dow *et al.* (2004) used scanning electron microscopy SEM to monitor the flattening occurred to the cutting edge radius of the tool due to wear. However, the applicability of this method is limited by the long and difficult set-up of the SEM.

Li *et al.* (2008) proposed a regression model of tool wear. The average reduction of the nominal tool radius as a function of the material removal volume and cutting velocity was used to assess the tool conditions. The widths of the machined channels were measured to judge indirectly about the tool wear due to difficulties in measuring small cutters. In this research, the model of the tool wear was employed to calibrate the trajectory-based surface generation model and thus to predict its effects on the surface roughness variation. It was stated that the effect of the tool wear on the resulting surface finish was significant. Especially, for some conditions, the roughness increased several times with the increase of tool wear, and therefore should be considered when modelling the effects of the micro-endmilling process on the machined surface. However, the effects of tool geometry changes due to wear, such as the increase of the cutting edge radius, was not considered in this research.

In spite of the limited publications in this field, it can be concluded that the tool wear in micro-endmilling is an important factor affecting the process performance and at the same time it is a challenging research issue that needs addressing. Especially, the machining performance can be improved by understanding better the effects of cutting conditions (Li *et al.* 2008) and machinability of workpiece materials on tool wear mechanism. In addition, to carry out such an investigation it is necessary to find new ways, e.g. experimental setups, for characterising and monitoring the tool wear.

2.5 Simulation-Based Studies in Micro-Machining Process

Merchant (Merchant 1944) developed the first analytical model of orthogonal machining processes. This model laid the framework for modelling the machining process afterwards (Liu 2005). In particular, later with the high computing power available, there has been notable success in modelling the machining process by investigators. Previous work in modelling-based simulation of machining is reviewed in this section.

2.5.1 Simulation of micro-machining process

During last two decades, simulation of the macro-machining process has lots of interests and ongoing research. In contrast for micro-milling, most of the research reported was experimental in its nature, and only some attempts were made to model the effects of material microstructure in micro milling employing a Finite Element Analysis (FEA) (Vogler *et al.* 2004a; Vogler *et al.* 2004b; Simoneau *et al.* 2006a; Simoneau *et al.* 2006b; Simoneau *et al.*

2006c; Simoneau *et al.* 2007a; and Simoneau *et al.* 2007b). Nevertheless, such simulation models were used mostly to understand better the mechanics of the micro-cutting process, and not as a tool for process optimisation (Simoneau *et al.* 2006b). Also, there are some other drawbacks associated with the use of FEA, in particular the generation of the necessary 3D models for such simulation studies, and their iterative nature and computational complexity. Thus, it is important to describe analytically the influence of material microstructure on the surface generation process and tool wear progression in micro-endmilling.

Liu *et al.* (2006) used a developed model of minimum chip thickness to perform a simulation study for machining three different materials under different cutting conditions. In particular, the simulations were carried out for machining AISI 1040, AISI 1018, Fig 2.18, and Al6082-T6, Fig. 2.19, under cutting velocity ranging between 60-500 m/min and edge radii varying from 0.5 to 5 μm. The authors attributed the proportional relationship between cutting speed and normalised minimum chip thickness of AISI 1040 and AISI 1018 to the predominance of the thermal softening effect over the strain hardening effect. Moreover, it was inferred that increasing cutting edge radius leads to higher normalised minimum chip thickness because ploughing is the dominate cutting regime rather than proper cutting. On the other hand, it is concluded that neither the cutting speed nor the cutting edge radius has significant influence on the normalised minimum chip thickness of Al6082-T6.

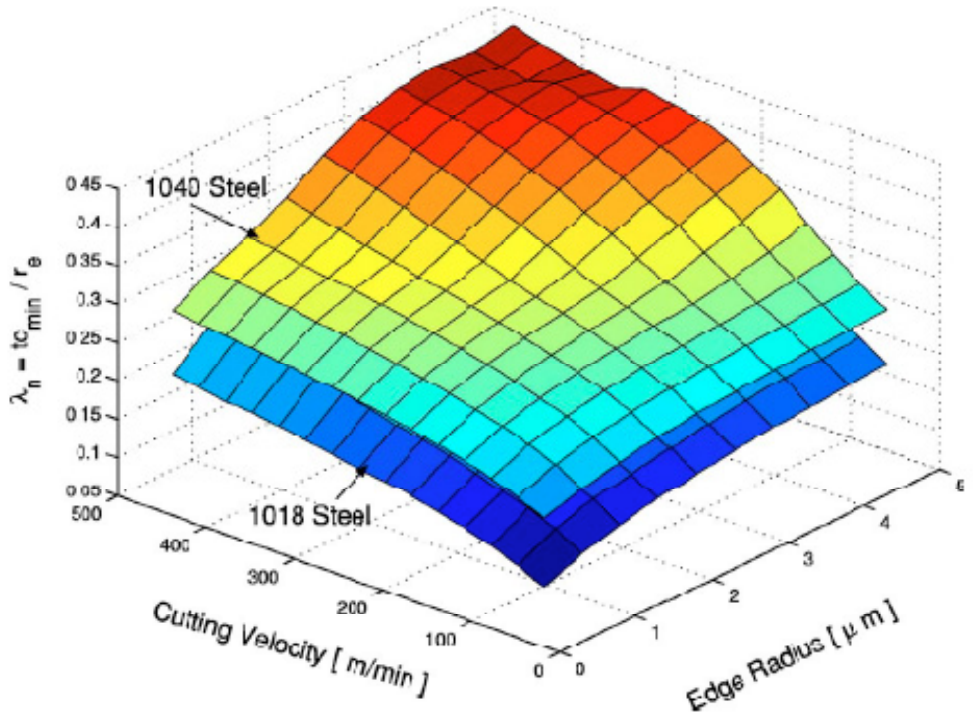

Fig. 2.18: Normalised minimum chip thickness for AISI1018 steel and AISI1040 steel (Liu et al 2006).

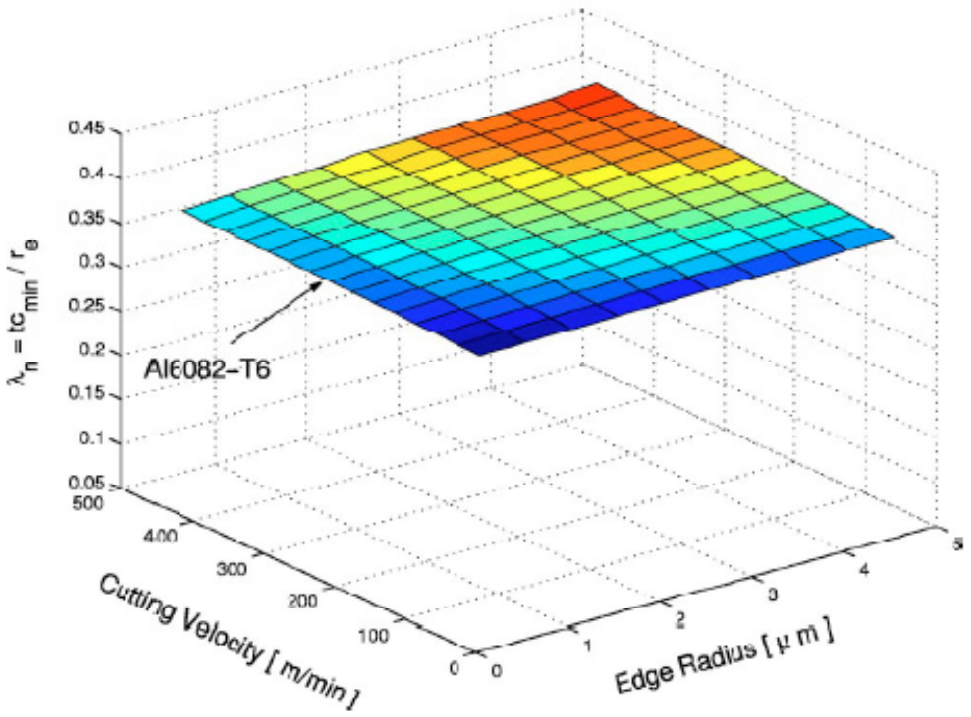

Fig. 2.19: Normalised minimum chip thickness for Al6082-T6 (Liu *et al.* 2006).

In another research, Liu *et al.* (2007b) conducted a simulation trial to study the effects of process conditions, tool geometry and process faults on the generated surface roughness. The authors concluded that feed-rate has a significant contribution to the deterministic floor surface roughness, Fig. 2.20. In addition, large edge radius results in higher surface roughness for both the sidewall and floor surfaces due to the increased influence of the ploughing mechanism. Also, it is found that the stochastic surface roughness component increases while the deterministic surface roughness component of the floor surface decreases when moving from the slot centre to the sidewalls. The author pointed at the positive effect of the vibrations that reduce the total 3D surface roughness of the floor surface at feed rate well below the minimum chip thickness and increases the total 3D surface roughness at high feed rates. Finally, a feed rate of 1–1.5 times of the minimum chip thickness was recommended as a starting point to achieve small surface roughness.

2.3.3 Virtual machining-based modelling

In order to predict precisely the process outcomes such as surface roughness, tool wear and cutting forces, virtual models of different machining operations have been developed by many researchers. However, due to the lack of understanding of the underlying mechanisms of micro-machining process, almost all the reported work is for macro-scale machining processes.

Marinov (2000) proposed a conceptual procedure of how to simulate virtually different machining operations. Subsequently, he applied this approach to develop a virtual turning of

mild steel with a carbide tool. The proposed model simulates the basic process outcomes; tool life, cutting forces, and dimensional accuracy taking into account the stochastic character of the metal cutting process such as elastic deformation, thermal expansion and wear.

Arshad *et al.* (2008) developed a real time virtual simulation for end milling process. The objective of this simulation was to visualise graphs of flank wear against cutting time during the machining process, and hence to enable investigation of the effect of different cutting parameters on the flank wear. 3D objects were modelled using AutoCAD 2002 and then transformed into Virtual Reality Modelling Language (VRML) to simulate the geometrical modelling of end milling process. The analytical modelling of exhibited tool wear was developed based on real data from milling experiments, Fig. 2.21. The authors aimed for simulation software to be used in training purposes, especially for students to increase the understanding of the milling process to avoid purchasing the actual equipment and also accidental damage on the actual machine due to programming errors. However, this simulation examines the effect of cutting conditions on tool wear only and strictly limited with the range of cutting parameters used in the real milling trials.

Additionally, an extensive research was reported in the area of virtual machining at macro-scale (Altintas et al. 2005; Altintas and Merdol 2007; Merdol and Altintas2008a; Merdol abd Altintas 2008b; Merdol and Altintas 2008c; Ferry and Altintas 2008a; Ferry and Altintas 2008b; Zhang 2010), there has been no application for the virtual machining at micro-scale. Therefore, there is a real need to develop a virtual environment which can realistically simulate the machining process. Thus, such model can serve to provide a better physical understanding of cutter/workpiece interactions in micro-milling and aid in optimising the machining conditions.

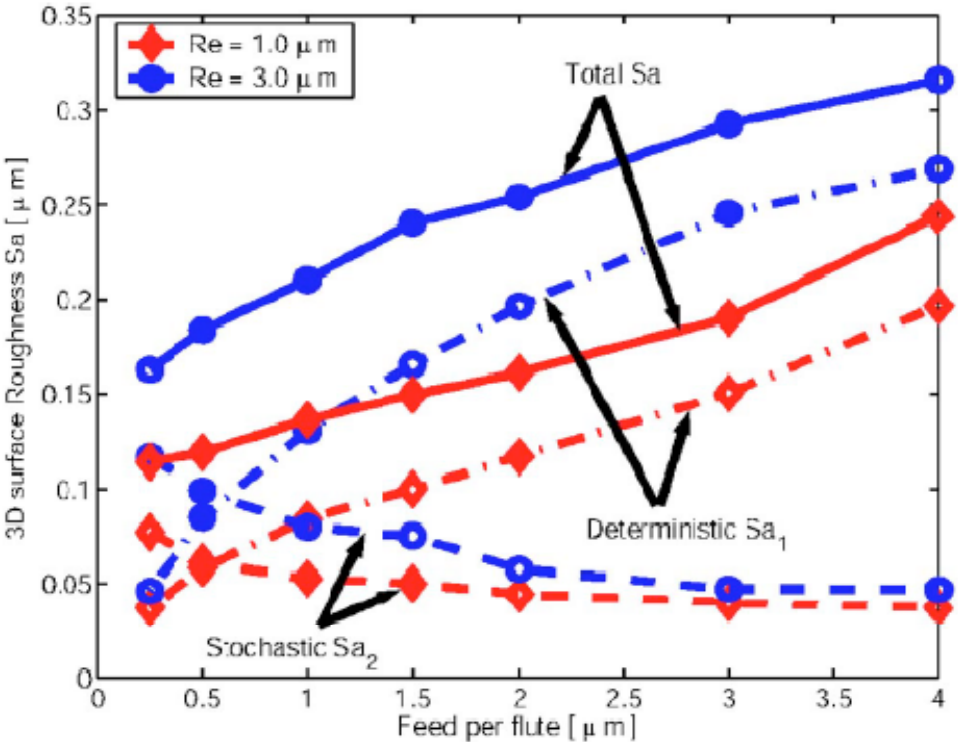

Fig. 2.20: Effect of edge radius on the 3D floor surface Roughness (Liu *et al.* 2007b).

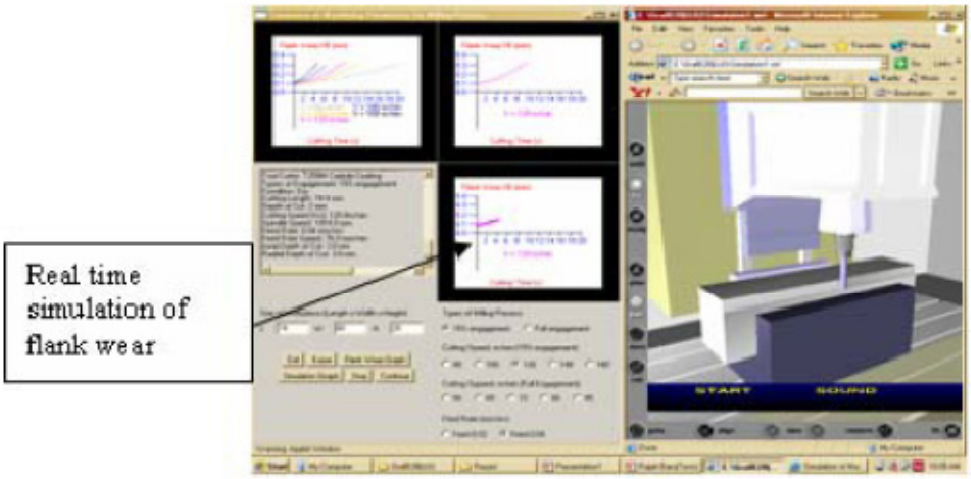

Figure 2.21: Simulation of the virtual end milling process and flank wear (Arshad *et al.* 2008).

2.6 Summary

In summary, there have been several studies in the micro-milling area. However, the main barrier to further development of the micro- milling process is the lack of scientific understanding of the process. Particularly, although, it has been revealed that microstructure has a significant influence on the machining process. So far, there has been no detailed study of the influences of microstructure in the micro-milling of different materials. Such influences are still challenging research issues that need addressing. Therefore, there is a real need to examine some of the process conditions such as scaling issue, material microstructure behaviour and to address their influence on the process, especially, surface quality and tool wear, and thus optimising the process to achieve the best performance. Also, there is a need to develop a reliable virtual machining model which can be utilised to extend the understanding of the process along with saving energy and raw materials for the environmental impact.

CHAPTER 3

INVESTIGATION OF THE EFFECTS OF MATERIAL MICROSTRUCTURE ON THE MICRO-ENDMILLING OF Cu99.9E

3.1 Overview

From the reviewed literature in chapter 2, it is clear that material microstructure, especially grain sizes has a significant effect on machining conditions and surface quality of micro-features produced by micro-milling. So far, there has been no detailed study of the influences of microstructure in the micro-milling of polycrystalline materials. The motivation for this work was to investigate experimentally this effect. In particular, this chapter reports on a series of micro-milling experiments under different conditions to investigate the machining response of metallurgically and mechanically modified Cu99.9E workpieces with coarse and ultrafine grained microstructures. The aim was to determine the effects of material microstructure on machining conditions and surface quality.

Another objective was to demonstrate a new method of assessing material microstructure based on AFM measurement of the coefficient of friction of the individual grains in the material, and to employ that method to evaluate the homogeneity of the modified microstructures. The proposed method enables a

comparative evaluation of the modified microstructures in terms of minimum chip thickness. However, it is necessary to know the minimum chip thickness to have proper cutting and avoid entering the transitional regime associated with intermittent cutting and ploughing.

Following this section, the remainder of the chapter is organised as follows. First, the selected workpiece materials are described. Then, the method to assess microstructures based on AFM measurements is presented. Also, the selected machining conditions, in particular, the cutting tools and cutting parameters used in the trials, are defined and the rationale behind their selection is explained. Next, the results obtained are discussed, focusing on the effects of material microstructure on surface quality and cutting mechanisms. Finally, measurements of the hardness of the machined surface are presented to support the discussion.

3.2 Experimental set-up

This section explains the experimental set-up. First, the microstructures of the workpieces are described. Then, the proposed method of judging the homogeneity of a microstructure is presented. Finally, the selected cutting conditions for the micro-endmilling trials are discussed.

3.2.1 Workpiece material microstructure

The selected workpiece materials had two different microstructures, a coarse-grained (CG) structure with an average grain size of 30 μm (Figure 3.1a) and an ultra-

fine-grained (UFG) structure with an average grain size of 200 nm (Figure 3.1b and 3.1c). The UFG material had been processed by equal channel angular pressing (ECAP) 8 times. The ECAP process is outlined in Appendix A.

3.2 .2 Material characterisation and minimum chip thickness determination

As previously stated, one of the main differences between micro-milling and macro-milling is due to the reduction in chip thickness which becomes dimensionally of the same order as the cutting edge radius of the tools and the material crystalline size. Researchers in micro-milling sometimes refer to the minimum chip thickness effect on the process conditions (Liu *et al.* 2007). The minimum chip thickness can be defined as the minimum undeformed thickness of a chip removed from the workpiece surface with a tool with a given cutting edge radius under ideal conditions as shown in Figure 3.2 (Liu *et al.* 2007). In macro-milling, the chip thickness is sufficiently large and it is not necessary to consider the effects of edge radius and hence the uncut chip thickness. Conversely, as already mentioned, the uncut chip thickness in micro-milling becomes comparable to the tool edge radius. Thus, any small change in the chip-load can have a significant influence on the material removal mechanism by altering machining conditions from proper cutting to ploughing or slipping.

The value of the minimum chip thickness, below which no chip and no material removal will occur, was determined experimentally by other researchers, as mentioned in section 2.2.1. However, this section reports recent work to determine minimum chip thickness employing analytical methods.

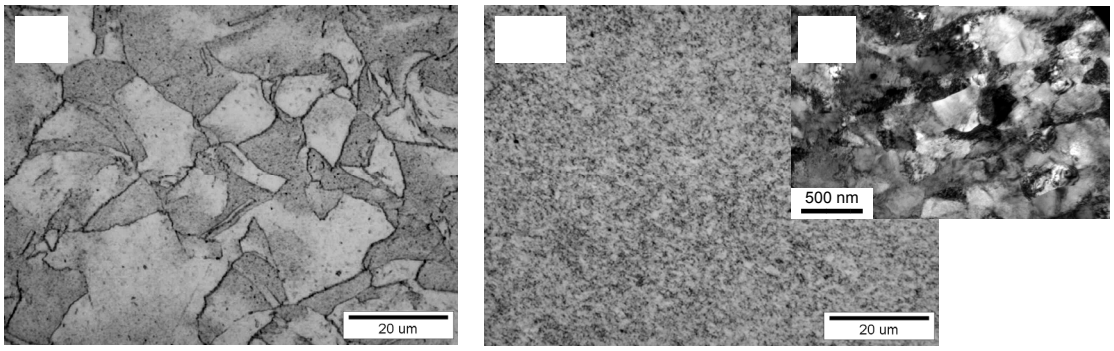

Fig. 3.1: Microstructure of CG (a) and UFG (b, c) Cu99.9E.

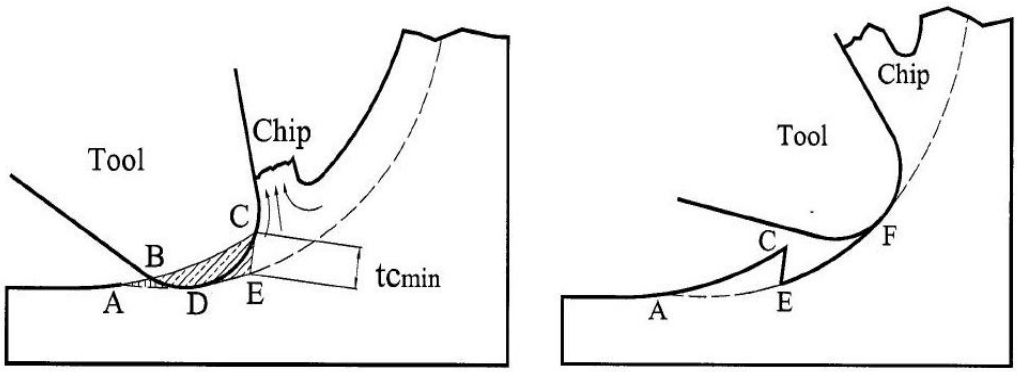

Fig. 3.2: The minimum chip thickness effect (Liu et al. 2007) (t_{cmin} : minimum chip thickness).

Liu *et al*. (2007) developed an analytical model to predict the minimum chip thickness based on the slip-line theory considering the mechanical and thermal properties of the workpiece and cutting tools under different cutting conditions. It should be stressed that the constitutive flow stress model for the processed material is essential to estimating the minimum chip thickness using this approach. However, a number of engineering materials have not yet been tested to identify their constitutive flow stress models. Furthermore, the differences in behaviours of the modified microstructures could be relatively small and they could follow quite similar constitutive flow stress models. As a result this approach can strictly only be applied to standard materials with known characteristics.

Son *et al*. (2005) proposed an analytical model, Equation 3.1, to calculate the minimum chip thickness based on the tool edge radius and the friction coefficient between the workpiece and the tool.

$$t_{c\min} = r * (1 - \cos(\frac{\pi}{4} - \frac{\beta}{2})) \qquad (3.1)$$

where: t_{cmin} is the minimum chip thickness;

r is the cutting tool edge radius;

β is the friction angle between a tool and uncut workpiece.

Generally there are two methods of obtaining the coefficient of friction and thus the friction angle. One is to conduct a friction test to measure the ratio of the tangential force and the normal force between the workpiece and the cutting tool (Son *et al.* 2005). This method requires expensive high-precision equipment (a dynamometer) with a high bandwidth and high sampling frequency capability to provide reliable measurements of the forces generated in micro-milling (Dhanorker

and Özel 2008). As any small amount of noise can give a false cutting force signal, the accurate measurement of very small cutting forces is a challenging issue. The other method of obtaining the coefficient of friction between the workpiece and the cutting tool is to look it up in previous reported work (Wang *et al.* 2007). This method only gives a nominal value of the coefficient of friction which is not useful for the purposes of calculating the minimum chip thickness of heterogeneous materials. There is a real need for an easier and faster method of measuring the coefficient of friction at the grain scale inside the bulk.

In the research reported here, Son *et al.*'s model was used to calculate the minimum chip thickness. The parallel AFM scan method developed by Ruan and Bhushan (2005), as depicted in Figure 3.3, was used to calculate the coefficient of friction according to the following equation (Bhushan 2005):

$$\mu = \left(\frac{(\Delta W_1 + \Delta W_2)}{W_o}\right) * \left(\frac{L}{2 * \ell}\right) \qquad (3.2)$$

where : μ is the coefficient of friction;

$\Delta W_1, \Delta W_2$ are the absolute values of changes in the normal force when the sample is travelling along the direction of the cantilever length forward and backward respectively;

W_o is the applied force between the tip and the sample; W_o ranges from 10 to 200 nN;

L is the length of the cantilever;

ℓ is the vertical distance between the tip of the cantilever and point P (the fixed point of the cantilever).

Force measurements were carried out on a XE-100 AFM from Park Systems. Once the coefficient of friction and the cutting edge radius had been determined, the normalised minimum chip thickness (λ_n) was calculated; λ_n is the minimum chip thickness divided by the tool edge radius and is a material dependent characteristic (Liu *et al.* 2006).

Figure 3.4 shows how the coefficient of friction varied over the AFM measurement range for both UFG and CG Cu; its average value was calculated to be 0.46 and 0.35, respectively. Accordingly, the calculated average minimum chip thickness was 0.397 μm with standard deviation (σ) = 0.039 for UFG Cu99.9E and 0.468 μm with standard deviation (σ) = 0.094 for CG Cu99.9E while the normalised minimum chip thickness was 0.156 for UFG Cu and 0.192 for CG Cu (Figure 3.5). This means that the cutting process started earlier in the case of the UFG Cu sample than for the CG workpiece, and thus a better surface quality would be expected after machining. Also, due to the significant variations in the minimum chip thickness over the scan area for the CG sample, as depicted in Figure 3.6, the cutting process would be unstable and would result in highly fragmented chips and defects in the machined surfaces (Wang *et al.* 2007). Conversely, the high homogeneity of the UFG Cu samples results in much less variation in the coefficient of friction and hence in the minimum chip thickness over the scanned area. Therefore the cutting process would be expected to be more stable and the defects on the machined surfaces to decrease.

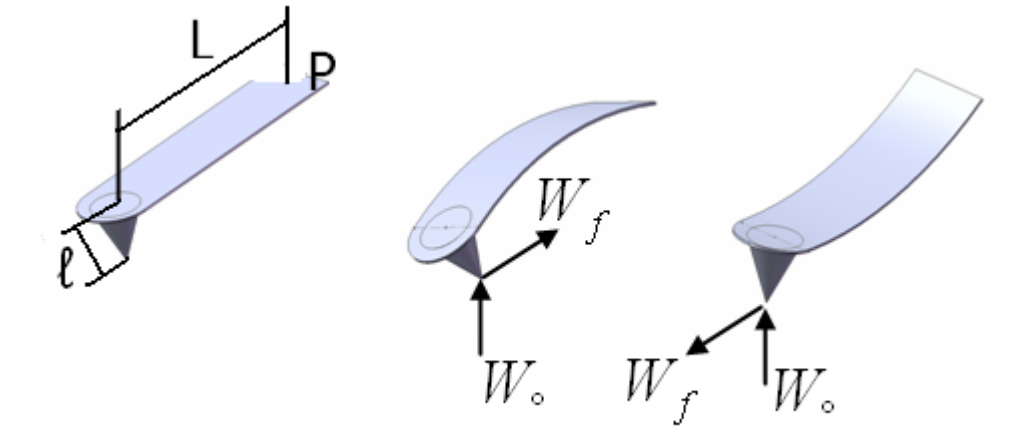

Fig. 3.3: Friction force in AFM parallel scan.

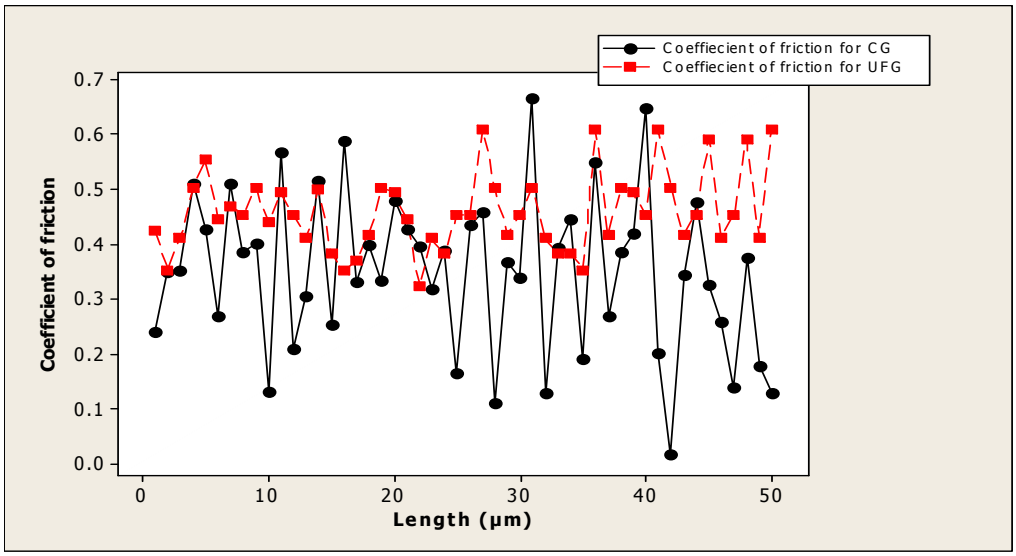

Fig.3.4: Variation of the coefficient of friction over the AFM measurement range.

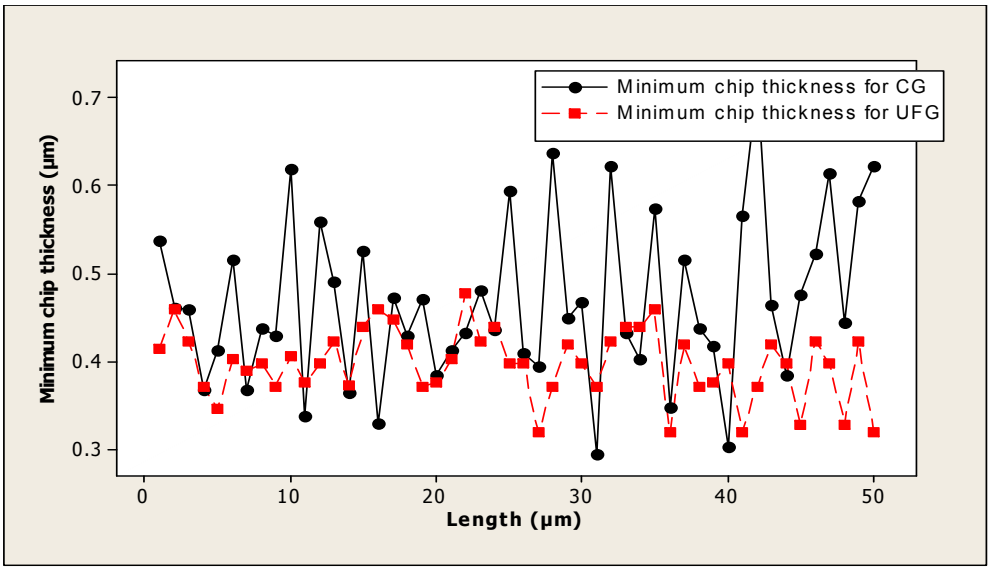

Fig. 3.5: Minimum chip thickness variations over the AFM measuring range.

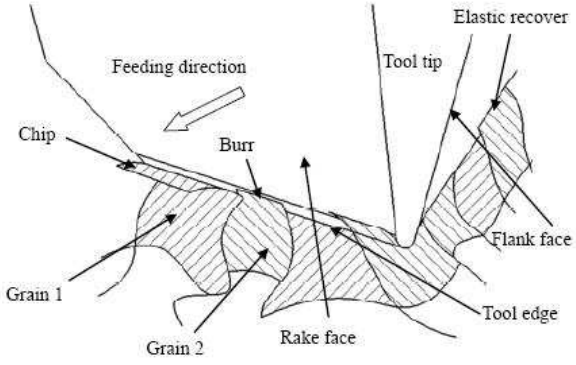

Fig. 3.6: Cutting zones (Wang *et al.* 2007).

3.3 Micro-milling set-up

The machining response of CG and UFG Cu was investigated by carrying out slotting tests on a Kern HSPC 2216 micro-machining centre (Kern Inc. 2011). The polymer concrete mono-block frame of this centre absorbs high frequency vibrations much better than cast iron frames (Popov *et al.* 2006), which is very important in micro-milling. Fine grained tungsten carbide tools coated with TiAlN were used in the machining trials. In particular, 200 μm diameter end-mill cutters with two teeth, and 6° rake and 25° helix angles, were utilised in the experiments. Prior to the cutting tests, each cutter was imaged using a scanning electron microscope (SEM) to measure the approximate radii of the cutting edges as shown in Figure 3.7. It was found that these were in the range 2 to 2.5 μm.

Table 3.1 shows the cutting parameters used in the milling trials. A full factorial experimental design was adopted to study the effects of material microstructure on the resulting surface quality. The undeformed chip thickness was controlled by varying the feed rate per tooth in the slotting operation to achieve values close to the average grain size and in the range of the cutting edge radius.

Cutting speeds were chosen that varied from the maximum available on the machine (40000 rpm) to a low value of 8000 rpm. Only one level of axial depth of cut (7 μm) was applied due to the limited effect of these parameters on the surface roughness in micro-milling (Wang *et al.* 2005).

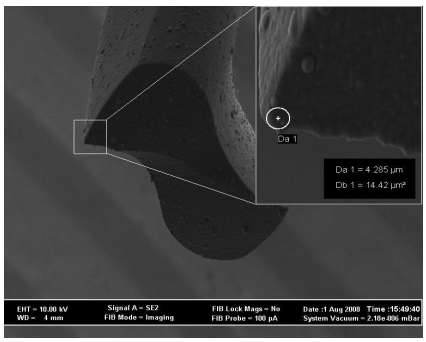

Fig. 3.7: SEM image of the cutting edge radius.

Table 3.1 Cutting conditions

Cutting parameters	Values					
Depth of cut [µm]	7					
Cutting speed [m/min]	25	15	5			
Feed rate [µm/tooth]	8	4	2	1	0.75	0.25

3.4 Results and discussion

The topography of the machined floor surface of the two workpieces was investigated. In particular, roughness and surface defects were examined to elucidate the relationship between the machining response and the material microstructure under different cutting conditions.

3.4.1 Surface roughness

The roughness of the machined surface, at the bottom of the micro-milled slots, was examined using a MicroXAM scanning white light interferometer from Phase Shift Inc (ADE Phase Shift Inc. 2011) with a 40X optical magnification. A 194.15 x 155.65 μm area was sampled with about 1 μm resolution in the X-Y direction (normal to the optical axis) and sub-nanometer resolution in the Z direction (along the optical axis). In particular, the average surface roughness Ra was measured at 5 different places along the centre line of each slot.

For both materials the lowest surface roughness was achieved at the highest speed, 40,000 rpm or 25 m/min, for all different settings as shown in Figure 3.8. The only exception was observed when the highest feed rate, 8 μm/tooth, and the mid-range speed, 24,000 rpm or 15 m/min, were used in the trials. Conversely, the highest roughness was measured at the lowest speed, 8,000 rpm or 5 m/min, for all the settings of the feed rate except for 1 μm/tooth and 2μm/tooth for CG and UFG Cu, respectively, when the surface quality was marginally better at the mid-range setting of the cutting speed.

In the case of CG Cu, reducing the feed rate down to values of 1 μm/tooth led to an improvement in the surface finish. As shown in Figure 3.8, the roughness started to increase when the feed rate was 0.75 μm/tooth, which can be explained by the drastic change in the cutting conditions, in particular, ploughing rather than normal cutting. Further reduction in the feed rate to 0.25 μm/tooth led to an improvement in the surface finish which could be attributed to changes in the cutting conditions to smearing and burnishing.

When the same micro-milling trials were conducted on the UFG Cu sample, a general improvement in the surface finish was observed compared to the CG material. Again, the roughness decreased when the feed rate was reduced. However, this time, the minimum roughness was achieved at a lower feed rate of 0.75 μm/tooth as shown in Figure 3.8. Thus, as far as the resulting surface roughness was concerned, there was a shift in the optimal cutting conditions from 1 μm/tooth for CG to 0.75 μm/tooth for UFG Cu99.9E. This change was associated with a reduction in the minimum chip thickness from 0.48 for CG Cu to 0.39 μm for UFG Cu. It is worth noting that there was a good agreement between the experimental results and the minimum chip thickness calculated based on the AFM measurement of the coefficient of friction. Also, the cutting process became very stable at feed rates 2-3 times the calculated minimum chip thickness in both the CG and UFG workpieces. The increase in roughness at a feed rate of 0.25 μm/tooth suggests that the cutting was already performed below the necessary minimum chip thickness, which led to a change of the cutting conditions from normal cutting to more ploughing.

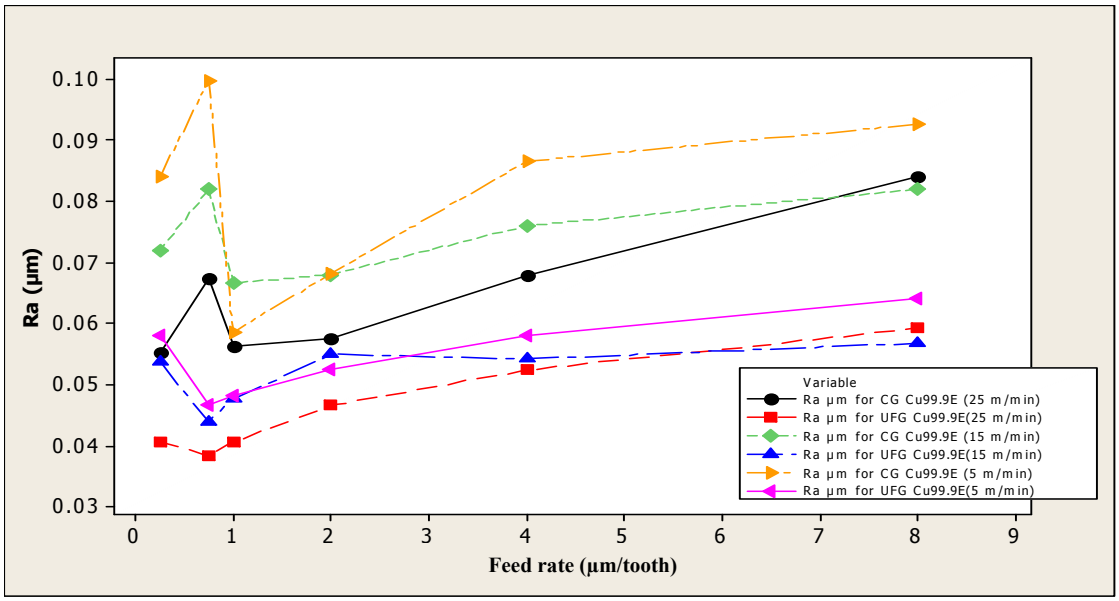

Fig. 3.8: Roughness achieved under different cutting conditions for CG and UFG Cu99.9E.

However, it was reported that an increase in the cutting speed could influence the machining response of a given material in two ways (Liu *et al.* 2006). First, a higher speed will lead to an increase in the cutting temperature, which will have a softening effect on the material. Consequently, the material will tend to be more ductile and hence the minimum chip thickness also increases. Second, at higher speeds, strain hardening effects are also higher, which leads to a reduction in the minimum chip thickness. So, the minimum chip thickness is affected by the changing response of the material to variations of the cutting speed.

In both CG and UFG Cu99.9E, as seen in Fig. 3.8, there is no shift detected in the chip-loads at which the best surfaces were achieved over the cutting speed range. Thus, it can be concluded that the thermal softening and strain hardening effects are equally important and they cancel each other out. One might argue that the range of cutting speeds used in the experiments is not sufficiently large to observe any differences in the minimum chip thickness of Cu99.9E. However, the enhancement in the surface finish at high cutting speeds can be attributed to improvements in the material behaviour with reduced side flows and elastic recovery (Liu and Melkote 2006).

Note that the cutting conditions under which the measurements of the coefficient of friction were conducted are different from the real cutting conditions. However, this method is proposed only to assess the modified microstructures. In particular, this method can be used as a comparative evaluation tool, for example, to assess the improvement in the homogeneity of the modified microstructure which should be associated with a reduced minimum chip thickness. On the other hand, to be generally

applicable to any material, further experimental study is required to calibrate the prediction of the minimum chip thickness. In particular, the difference between scanning and machining conditions has to be examined.

Figure 3.9 shows how the hardness of the machined surface changed with the feed rate for both materials. For CG Cu99.9E, the hardness remained constant at ~105 HV (under a load of 50 g), down to a feed rate of 1 μm/tooth, and then started to increase rapidly to ~230 HV when the feed rate was reduced to 0.25 μm/tooth. This indicates an increase in the work hardening induced at feed rates below 1 μm/tooth and is associated with changes in the cutting conditions from normal cutting to ploughing at very low feed rates. For UFG Cu99.9E, the constant hardness level was ~125 HV. This level was observed at feed rates down to 0.75 μm/tooth. There was only a marginal increase in the hardness to ~130 HV at 0.25 μm/tooth. This again indicates changes in the cutting conditions at feed rates below 0.75 μm/tooth, from normal cutting to ploughing, but the changes were not as severe as in the case of CG Cu99.9E.

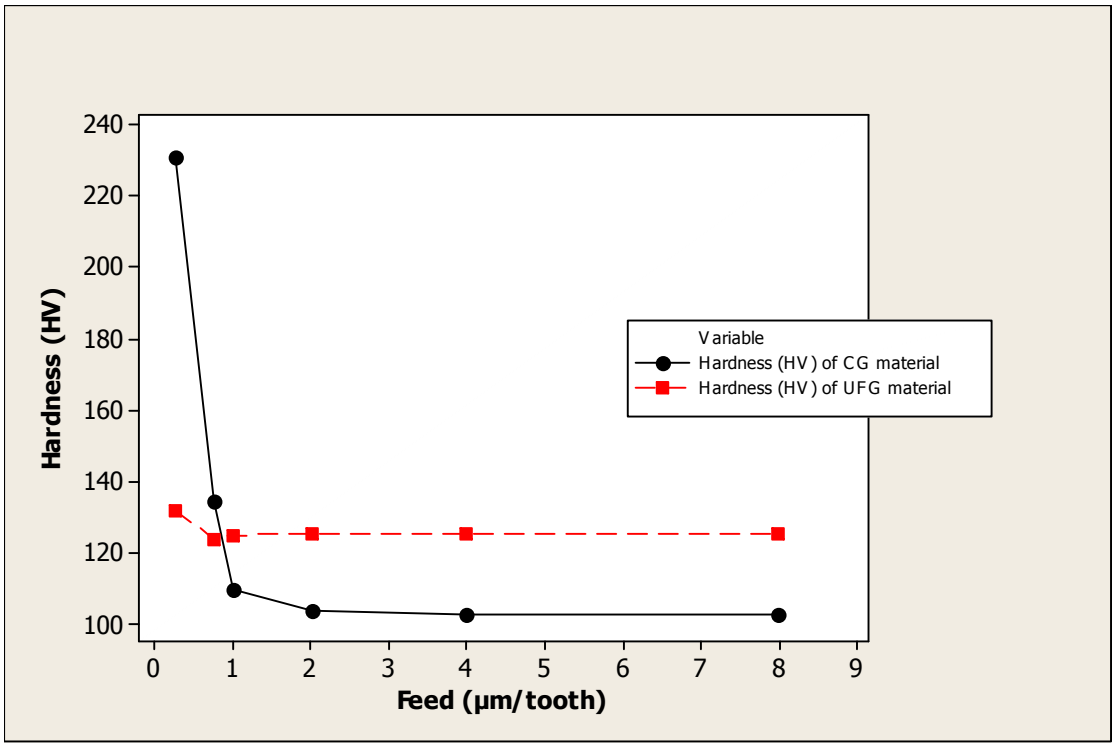

Fig. 3.9: Hardness of the machined surface.

3.4.2 Surface defects

The surfaces of the machined slots were inspected for defects in a scanning electron microscope. For CG Cu99.9E, as shown in Figure 3.10, the surface texturing and features observed at a low feed rate of 0.75 μm/tooth were prows (which are severely strain hardened bits of workpiece material), micro-cracks, voids and floor burrs. As noted by other researchers, prows can be the result of a Built-Up Edge (BUE) that has broken off the tool rake face (Simoneau and Elbestawi 2006a). However, this is not the case in the machining trials conducted by the authors due to the relatively short cutting length. The strain hardening observed on the machined surfaces could be explained by the changes from normal cutting to ploughing at low feed rates due to the cutting edge radius being large compared with the chip-load, and also the relatively high minimum chip thickness required for CG Cu99.9E. In particular, as the chip-load decreased, the cutting tool geometry changed to a negative rake angle and, consequently, cutting was replaced by ploughing. At the same time, the micro-cracks and the floor burrs could be attributed to the heterogeneity of the material microstructure at the grain level (see Figure 3.6) which led to changes in mechanical and metallurgical properties at the boundaries between individual grains. This material anisotropy led to significant variations in the minimum chip thickness and thus to chip fragmentation and formation of micro defects.

Conversely, in the case of UFG Cu99.9E the prows observed on the slot edges were minimal and only small burrs were formed. The reason for this was likely to be the high material homogeneity in comparison to CG Cu99.9E.

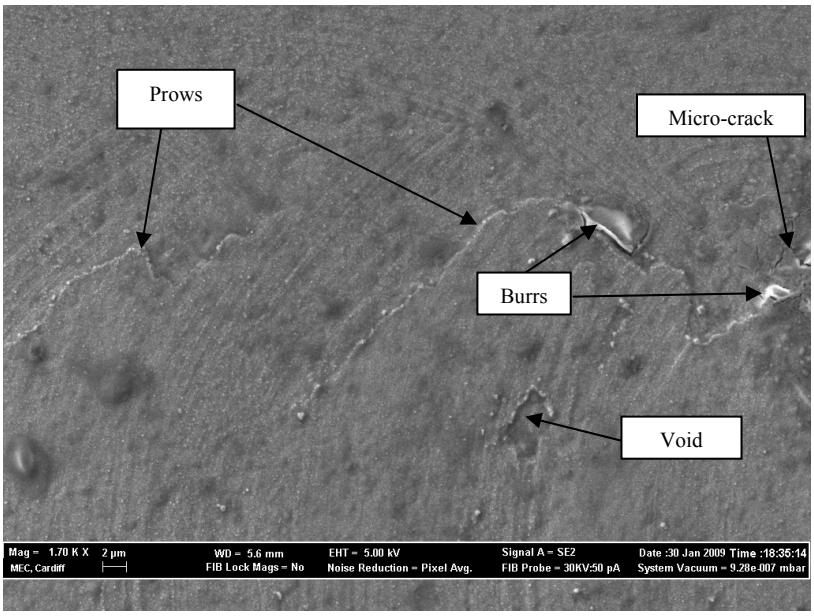

Fig. 3.6: Machined floor surfaces for CG Cu99.9E at a feed rate of 0.75 µm/tooth and cutting speed of 5 m/min.

3.5 Summary

This chapter has reported on the effects of material microstructure on the micro-milling process, especially on cutting conditions and the resulting surface quality. An experimental study was conducted to investigate the machining response of two workpieces with different material microstructures. One workpiece was in "as received" CG Cu99.9E and the other was in UFG Cu99.9E refined by employing the ECAP process. The investigation has shown that through refinement of the microstructure it is possible significantly to improve the specific cutting conditions in micro-milling. This can lead to a reduction in surface roughness and surface defects which are highly dependent on material homogeneity.

An AFM-based method was applied to assess the homogeneity of the material microstructure. The method involved calculating the coefficient of friction of the individual grains inside the workpiece material. This method offers a comparative assessment of the modified microstructures which enables initial prediction of the minimum chip thickness. Estimated values of the minimum chip thickness are necessary to have normal cutting, before entering the transitional regimes associated with intermittent cutting and ploughing. Note that the homogeneity assessment method proposed in the chapter was conducted under cutting conditions different from real conditions. At present, this method can be applied as a comparative evaluation between modified microstructures.

Finally, measurements of the hardness of the machined surface were conducted to investigate the work hardening induced during the cutting process for

the range of applied feed rate. Results pointed out that changes occur in the cutting conditions from normal cutting to ploughing at low feed rate.

CHAPTER 4

MODELLING THE MATERIAL MICROSTRUCTURE EFFECTS IN MICRO-ENDMILLING

4.1 Overview

The underlying material removal mechanisms at micro-scale differ significantly from those at macro-scale. These differences are mainly attributed to the scaling effects in performing milling at micro scale (Liu *et al.* 2004). Particularly, in contrast to those dominating in macro-machining, where the workpiece material can be considered homogeneous and isotropic, and the chip-loads in micro-machining become of the same order of magnitude as the material grain sizes of commonly used engineering materials (Vogler *et al.* 2003). Therefore, when performing machining at micro scale the workpiece material has to be considered heterogeneous and anisotropic (Vogler *et al.* 2003; Mian *et al.* 2009 and Mian *et al.* 2010). Micro-machining of multi-phase materials, such as pearlite/ferrite steel, exemplifies the effects that dominate at micro scale. As the cutter-workpiece engagement may involve only one phase, pearlite or ferrite, and then the other, the machining mechanisms could vary between cutting and ploughing due to the different response of each phase to the selected cutting conditions (Liu *et al.* 2004). Moreover, owing to the variation of the chip-load along the cutter flute due to its geometry, the cutting mechanisms will be altering, too, which could lead to the formation of floor burrs at the grain

boundaries, and as a consequence of this the cutting forces and the resulting surface roughness would be affected, too (Liu *et al.* 2004).

From the carried out literature review in section 2.4, it can be concluded that the resulting roughness after micro-milling is highly dependent on the material microstructure. Most of the research reported was experimental in its nature, and only some attempts were made to model the effects of material microstructure in micro milling employing a Finite Element Analysis (FEA) (Vogler *et al.* 2004a; Vogler *et al.* 2004b; Simoneau *et al.* 2006a; Simoneau *et al.* 2006b; Simoneau *et al.* 2006c; Simoneau *et al.* 2007a; Simoneau *et al.* 2007b and Özel *et al.,* 2011). However, such simulation models were used mostly to understand better the mechanics of the micro-cutting process, and not as a tool for process optimisation (Simoneau *et al.* 2006b). Also, there are some other drawbacks associated with the use of FEA, in particular the generation of the necessary 3D models for such simulation studies, and their iterative nature and computational complexity. Thus, it is important to describe analytically the influence of material microstructure on the surface generation process in micro-endmilling. In this context, the motivation of the research presented in this chapter is to develop and validate a model that can be used to predict the resulting surface topography in micro-endmilling of multi-phase materials. Also, the aim is to use such a model for optimising the machining conditions, and thus to improve the surface roughness when machining materials with different microstructures.

This chapter is organised as follows. First, the chapter presents a multi-phase microstructure mapping procedure developed to incorporate the effect of the machined microstructure into the surface generation model. Then, modelling the

cutting tool trajectory and the minimum chip thickness effect on the surface generation process are discussed. Next, an experimental study conducted on two different dual-phase steel samples to validate the proposed model is described. Finally, the comparison between simulation and experimental results is discussed.

4.2 Surface generation model

In this section, the surface generation mechanism of multi-phase materials is discussed taking into consideration the trajectory of the cutting tool, the tool geometry associated with the varying chip-load and the effect of the minimum chip thickness for each phase within the microstructure.

4.2.1 Multi-phase microstructure mapping

To model the micro-milling process when machining multi-phase materials, a map of the metallurgical microstructure is created to capture the effects of the materials morphology on the cutting conditions.

Vogler *et al.* (2003) made an attempt to use a map of the material microstructure to study its effects on the cutting forces in micro-milling. However, in their model, the microstructure was mapped applying a statistical approach, in particular measurements of the size, shape and distribution of the different grains, as shown in Fig. 4.1.

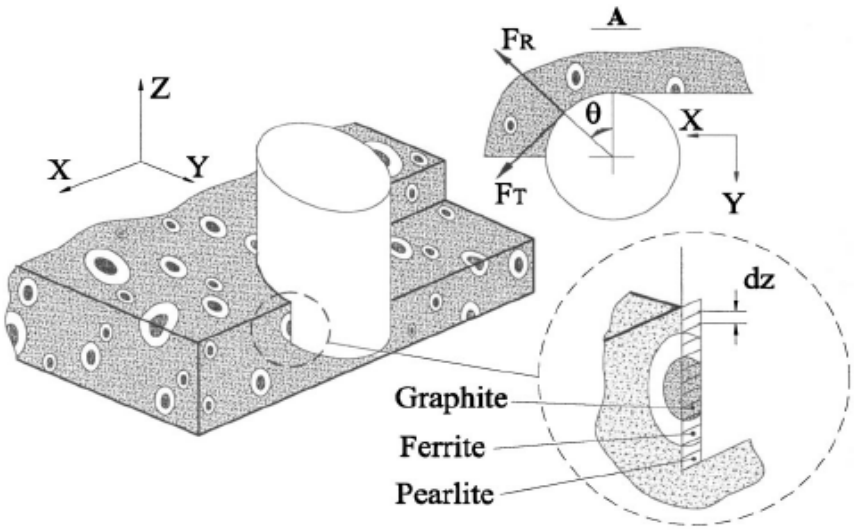

Fig. 4.1: Tool workpiece engagement (Vogler *et al.* 2003).

The simple procedure proposed in this research to represent realistically the material's microstructure differs from that suggested by Vogler *et al.* (2003) and relies on image processing techniques. Fig. 4.2 depicts the sequence of steps applied to model the microstructure of the AISI 1040 steel, a dual-phase material used to validate the proposed model. This material was selected due to the two distinctive and well balanced phases in its microstructure, ferrite and pearlite.

First, an AISI 1040 sample was polished and etched with a standard 'nital' reagent. Then, its surface was imaged employing an optical microscope in polarisation mode, Fig. 4.2a, and thus to obtain as clear as possible definition of the edges representing the boundaries between any two phases. Second, the Matlab image processing software was employed to process the captured micrographs and convert them into a gray-scale images as depicted in Fig. 4.2b. Subsequently, a simple image processing technique, thresholding, was applied to segment the phases within the material microstructure into white and black 2D fields, for the ferrite and pearlite phases, respectively, as shown in Fig. 4.2c. By conducting this segmentation, a planer map of points (X_i, Y_i, 0 or 255) is generated, where X_i and Y_i are the coordinates of each pixel and the third binary number gives information about the phase, white or black, at each point on the map. Fig. 4.2d shows a contour image of the phase boundaries where the occurrence of micro-burrs can be expected.

Fig. 4.3 depicts the pseudo code of the proposed image processing algorithm that was applied to map the material microstructure of a dual-phase steel and thus to account for the effects of its variation on the cutting process.

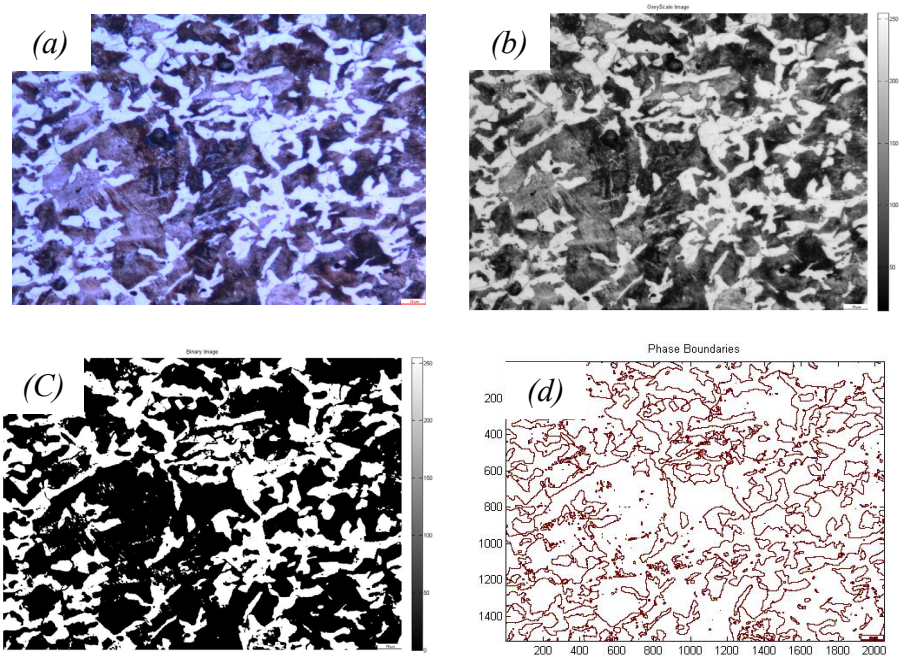

Fig. 4.2: Material microstructure mapping procedure, (a) Captured picture of the AISI 1040 sample, (b) Gray-scale picture, (c) Binary picture, and (d) Phase boundaries' picture.

```
LOAD captured picture of the material microstructure

CONVERT the picture into a grayscale image with values from
0 to 255 for each pixel

//Thresholding of all the pixels and separating them into
two groups

FOR All the pixels in the picture:
  IF the grayscale value < 140 THEN
    The pixel grayscale value = 0

  ELSE
    The pixel grayscale value = 255

  ENDIF
ENDFOR

GENERATE matrixes of the material microstructure and contour
maps
```

Fig. 4.3: Pseudo code of proposed image processing technique.

4.2.2 Cutting tool trajectory and the minimum chip thickness effect

The following sequence of steps is applied to generate the surface topography considering the cutting tool trajectory and the cutting flute geometry. Accordingly, any variation of the chip-load along the contact profile of the cutting edge with the workpiece material is considered by adapting the model developed by Liu *et al.* (2007a). In particular, with this model it is possible to account for the effects of moving from one phase to another in the material microstructure throughout the cutting process.

First, the trajectory of the tool centre in XY plane, C (X_c, Y_c), is determined by adapting the dynamic model developed by Liu *et al.* (2007a). Especially, the coordinates of the centre point C (X_c, Y_c), as shown in Fig. 4.4, can be determined as the intersection point between the tool axis and the horizontal plane defined by the centre points of the cutting edges as follows (adopted: Liu *et al.* 2007a):

$$X_c = N_p * f_t + \frac{f_t * P_i}{n * 180} \tag{4.1}$$

$$Y_c = 0 \tag{4.2}$$

where: $\boldsymbol{N_p}$ is the number of revolutions already completed before counting the current cut, $\boldsymbol{f_t}$ is the feed per tooth, $\boldsymbol{P_i}$ represents a point corresponding to the rotational angle of the cutter, and $\boldsymbol{n}$ is the model sensitivity factor and represents the number of points that should be calculated at each degree of the cutter rotation. To simplify the calculations, the process conditions were "idealised". In particular, zero run outs of the tool and zero vibrations were assumed and also, no tool manufacturing errors was considered, as shown in Fig. 4.4a. By taking these assumptions, the trajectory of the centre point of the cutter edge corner **f** ($\boldsymbol{X_f}$, $\boldsymbol{Y_f}$), as shown in Fig. 4.4b, can be determined employing the following equations:

$$X_f = X_c + (R - r_c) * \sin(\theta) \quad (4.3)$$

$$Y_f = Y_c + (R - r_c) * \cos(\theta) \quad (4.4)$$

where: X_c and Y_c are the coordinates of the cutter centre point in X and Y direction respectively, $\boldsymbol{R}$ is the nominal cutting tool radius, $\boldsymbol{r_c}$ is the cutting edge corner radius and θ is the rotational angle of the cutter.

Then, the distance between each two corresponding cutter flute centre points at different rotational angles across every two subsequent revolutions of the cutter are determined, as shown in Fig. 4.5. This distance represents the local chip thickness, $\boldsymbol{t_c}$, at a given position (Liu *et al.* 2007a). The intersection points $\boldsymbol{p}^{\boldsymbol{i}}_{\theta}$ and $\boldsymbol{p}^{\boldsymbol{i\text{-}1}}_{\theta}$ of each profile, ***i***, with the two profiles generated in the follow up, ***i+1***, and preceding, ***i-1***, revolutions, respectively, can be determined based on the local chip thickness and the flutes' geometries as presented in Fig. 4.5a. The subscript in the figure denotes the rotational angle, $\boldsymbol{\theta}$. Next, as can be seen in Fig. 4.5b, $\boldsymbol{p}^{\boldsymbol{i}}_{\theta,j}$ and $\boldsymbol{p}^{\boldsymbol{i\text{-}1}}_{\theta,j}$ are the two corresponding points along the current, ***i***, and the previous, ***i-1***, flute profiles, respectively and the second subscript, ***j***, denotes the position of a given point along the profile. Then, the part of cutter profile between these two intersection points, $\boldsymbol{p}^{\boldsymbol{i}}_{\theta}$ and $\boldsymbol{p}^{\boldsymbol{i\text{-}1}}_{\theta}$, is sliced into a number of point representing this profile. The coordinates of the current point, $\boldsymbol{p}^{\boldsymbol{i}}_{\theta,j}$ **(**$\boldsymbol{l}^{\boldsymbol{i}}_{\theta,j}$, $\boldsymbol{z}^{\boldsymbol{i}}_{\theta,j}$**),** are calculated taking into account the cutting tool geometry, especially the tool corner radius and the end cutting edge face. In particular, $\boldsymbol{l}^{\boldsymbol{i}}_{\theta,j}$ is the horizontal coordinate of $\boldsymbol{p}^{\boldsymbol{i}}_{\theta,j}$ in relation to the centre point of the tool corner radius while $\boldsymbol{z}^{\boldsymbol{i}}_{\theta,j}$ is the vertical coordinate of $\boldsymbol{p}^{\boldsymbol{i}}_{\theta,j}$ relative to the same centre point. So, $\boldsymbol{z}^{\boldsymbol{i}}_{\theta,j}$ can be calculated employing the following equations (Vogler *et al.* 2004a):

$$z^{i}_{\theta,j}\left(l^{i}_{\theta,j}\right) = \begin{cases} -\sqrt{r_c^2 - l_{\theta,j}^{i^2}} & \text{when } \boldsymbol{l}^{\boldsymbol{i}}_{\theta,j} > -\, r_c * sin(ECEA) \\ -r_c * \cos(ECEA) - \left[l^{i}_{\theta,j} + r_c * \sin(ECEA)\right] * \tan(ECEA) & \text{when } \boldsymbol{l}^{\boldsymbol{i}}_{\theta,j} < -\, r_c * sin(ECEA) \end{cases} \quad (4.2)$$

and ECEA is the end cutting edge angle.

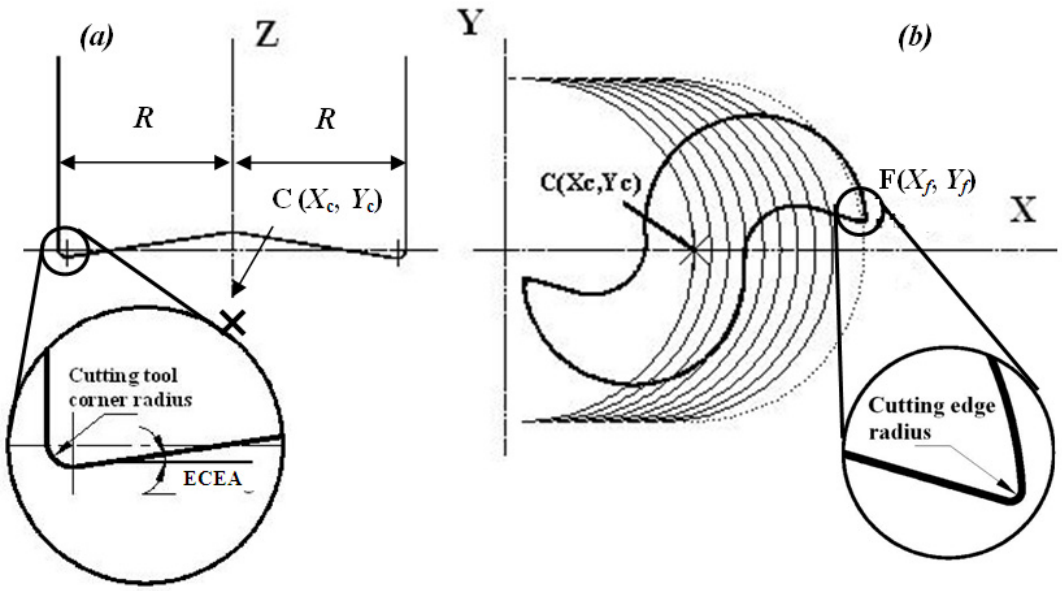

Fig. 4.4: Tool geometries and flute trajectories under perfect process conditions (a) Side view and (b) plan view.

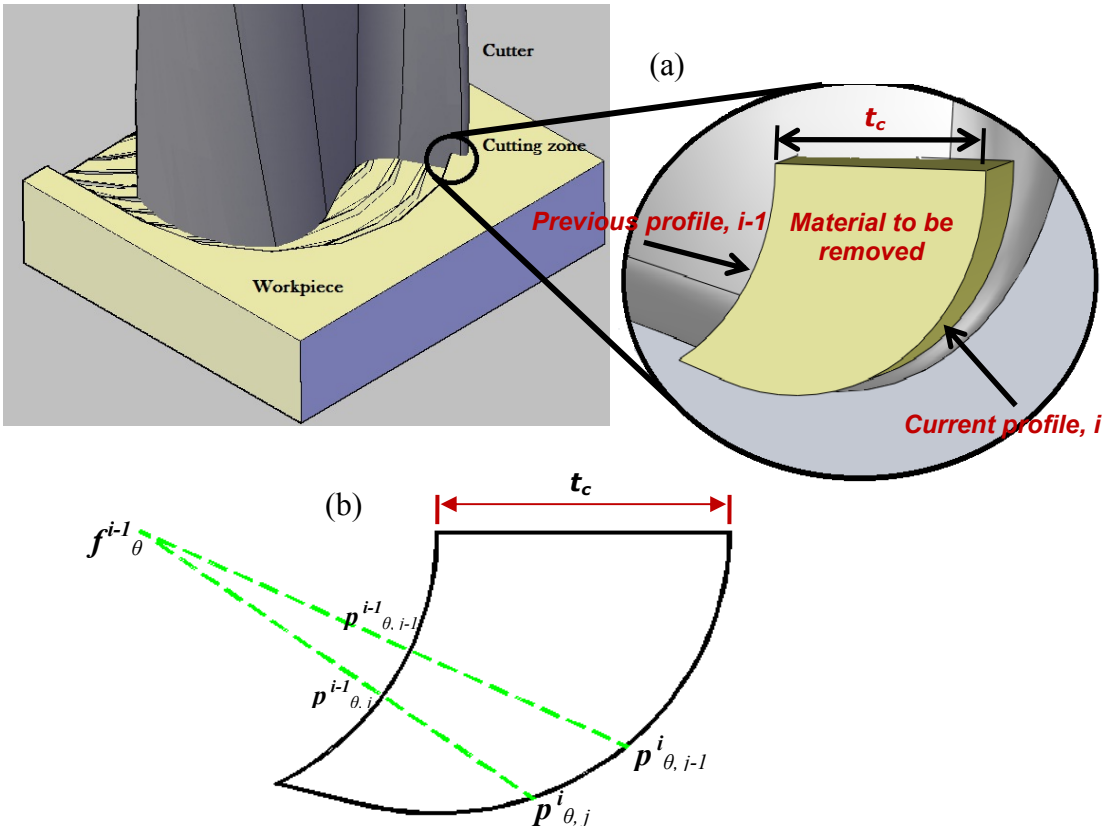

Fig. 4.5: Tool geometry effects on surface roughness.

The next step is to determine the coordinate of the corresponding point $\boldsymbol{p}^{i-1}_{\theta,j}$ which represents the intersection between the previous profile, ***i-1***, with the line through $\boldsymbol{p}^{i}_{\theta,j}$ and $\boldsymbol{f}^{i-1}_{\theta}$, the centre point of the ***i-1*** profile as shown in Fig. 4.5b. Then, the distance between $\boldsymbol{p}^{i}_{\theta,j}$ and $\boldsymbol{p}^{i-1}_{\theta,j}$ can be calculated, and by comparing the results with the minimum chip thickness values for the ferrite and pearlite phases, t_{cmin}^{f} and t_{cmin}^{p}, three different cases can be identified. The normalized minimum chip thickness values for the ferrite and pearlite phases, λ_{nf} and λ_{np}, were chosen to be 0.35 μm and 0.2 μm, respectively, based on the results reported by Vogler *et al.* (2004a) at the applied cutting speed (Vogler et al. 2004a). Thus, the three possible cases are as follows.

Case 1

$\boldsymbol{p}^{i}_{\theta,j}\boldsymbol{p}^{i-1}_{\theta,j} > t_{cmin}^{f}$ - cutting is the dominant condition and point $\boldsymbol{p}^{i}_{\theta,j}$ defines the end of a segment belonging to the surface at this position. So, the resulting topography is represented by a family of $\boldsymbol{p}^{i}_{\theta,j}$ as shown in Fig. 4.6a.

Case 2

$\boldsymbol{p}^{i}_{\theta,j}\boldsymbol{p}^{i-1}_{\theta,j} < t_{cmin}^{p}$ - ploughing is the prevailing machining mechanism and the segment that defines the resulting surface is $\boldsymbol{p}^{i-1}_{\theta,j}$ as a complete elastic recovery of the material was assumed in the model and the generated surface is represented by a family of $\boldsymbol{p}^{i-1}_{\theta,j}$ as shown in Fig. 4.6b.

.

Case 3

$t_{cmin}^{f} > \boldsymbol{p}^{i}_{\theta,j}\boldsymbol{p}^{i-1}_{\theta,j} > t_{cmin}^{p}$ – the dominant machining mechanism is then determined depending on the phase type in a in-progress position, in particular, its

coordinates on the microstructure map. Again, if it is a pearlite phase then cutting takes place similarly to **Case 1**, while if the phase is ferrite then ploughing is the dominant mechanism, and once more the family of $\boldsymbol{p}^{i-1}_{\theta,j}$ defines the resulting surface topography.

It can be concluded that the alterations of the machining mechanisms due to varying conditions in any given position of the cutting flute on the material microstructure map are the main cause of the micro-burr formation. In particular, this is due to the transition from ploughing to cutting and back to ploughing when the cutting flute moves from one phase to another with a small chip-load as depicted in Fig. 4.6c and 4.6d. In this way the mechanism of micro-burr formation at the phase boundaries can be defined clearly, and thus can be taken into account in assessing its effects on the surface roughness.

The total surface roughness, S_a, can be calculated based on the Z position of all generated points, $\boldsymbol{p}^{i}_{\theta,j}$, when the cutting flute moves from one phase to another. Finally, this sequence of steps is applied on five different microstructure maps each time, and then the average value is taken in order to obtain more precise predictions.

The sequence of the steps applied to simulate the surface generation process in micro-endmilling of multi-phase materials are summarised in Fig. 4.7 that represents the pseudo code used in the implemented algorithm.

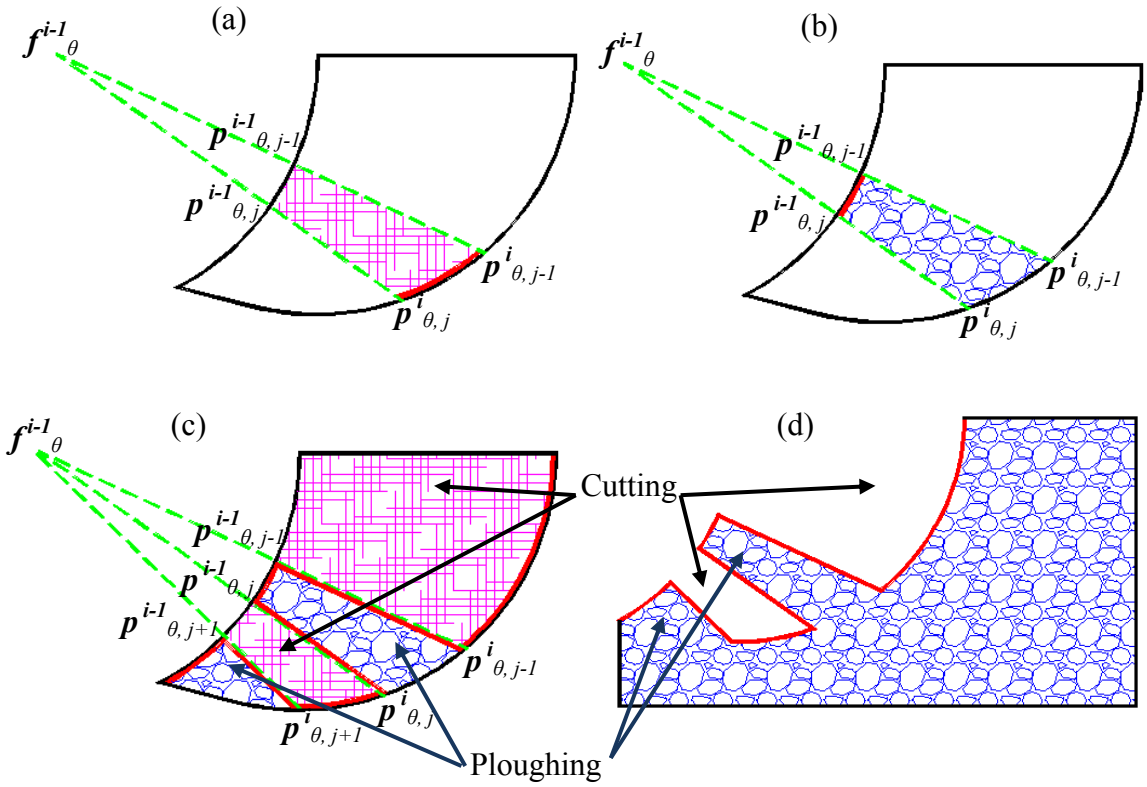

Fig. 4.6: Surface generation cases: (a) Cutting, (b) Ploughing and (c) Mixing between cutting and ploughing (d) Generated surface with defects due to altering machining conditions, cutting and ploughing.

```
INITIALISE Cutting tool geometry, workpeice microstructure and
           cutting parameters

//Determine trajectory of the tool centre C(Xc,Yc)
FOREACH Cutting revolution:
FOR All cutting edge centres
 CALCULATE Xc and Yc

 //Determine the trajectory of the centre of the cutter edge
corner f(Xf,Yf)
  CALCULATE Xf and Yf
ENDFOR

CALCULATE local chip thickness by determining the distance
between each two corresponding cutter flute centres at different
rotational angles across every two subsequent revolutions of the
cutter

DEFINE the two intersection points of each profile with the
preceding and follow up profiles based on the local chip
thickness & cutting flute geometry

FOR ALL points along the profile between the defined two
intersection points

DETERMINE the coordinates of the corresponding point on the
previous profile

CALCULATE the distance between THIS point and the determined
corresponding point

//Compare the results with the minimum chip thickness for
ferrite and pearlite
IF distance > minimum chip thickness of ferrite THEN
  //Cutting is the dominant mechanism
  KEEP this point to represent the resulting topography
ENDIF

IF distance < minimum chip thickness of pearlite THEN
  //Ploughing is the prevailing mechanism and complete
    elastic recovery takes place
  REPLACE this point with the correspondent point to represent
  the resulting topography
ENDIF
```

```
 IF distance < minimim chip thickness of ferriete AND distance >
 minimum chip thickness pearlite THEN
 //The dominant mechanism is dependent on the phase type
 RETRIEVE the multiphase microstructure map to determine the
phase type at the in-progress position
IF phase = pearlite THEN
    //Cutting is the dominant mechanism
    KEEP this point to represent the resulting topography
ENDIF

IF phase = ferrite THEN
    //Ploughing is the prevailing mechanism and complete
    elastic recovery takes place
    REPLACE this point with its correspondent point to represent
    the resulting topography

ENDIF

ENDFOR
ENDFOR

CONSTRACT the predicted surface Topography based on the
calculations

CALCULATE surface roughness based on Z position of all generated
points on the map

REPEAT the algorithm on five different microstructure maps each
time
CALCULATE the average value to obtain more precise predictions.
```

Fig. 4.7: The pseudo code of proposed image processing technique.

Note that the applied depth of cut could be in the range of tens of micrometers which could be larger than the grain sizes of the phases present within the microstructure. Therefore, the axial engagement of cutter-workpiece may involve more than one phase at once. However, it is worth stressing that the heterogeneous material being machined with the axial flute could affect the surface generation process of the side wall and not the floor surface. This is because the floor surface generation process only related to the floor cutter-workpiece engagement. In particular, the part of the cutter profile between the two intersection points, $\boldsymbol{p}^{i}_{\theta}$ and $\boldsymbol{p}^{i-1}_{\theta}$, as shown in Fig. 4.8, is the part concerning the floor surface generation. This part of cutter-workpiece engagement depends on the geometry of the tool and the applied feed rate. As an example, in case of extreme large geometry, 5 μm corner radius and 10 ***ECEA,*** and 7 μm feed per tooth, the engagement height related to the floor surface generation is less than 0.7 μm which is much less than the grain size of any phase. As a result, the planar map of the microstructure is valid to model the effect of a multi-phase microstructure in the generation of the floor surface and not sufficient for the side wall surface.

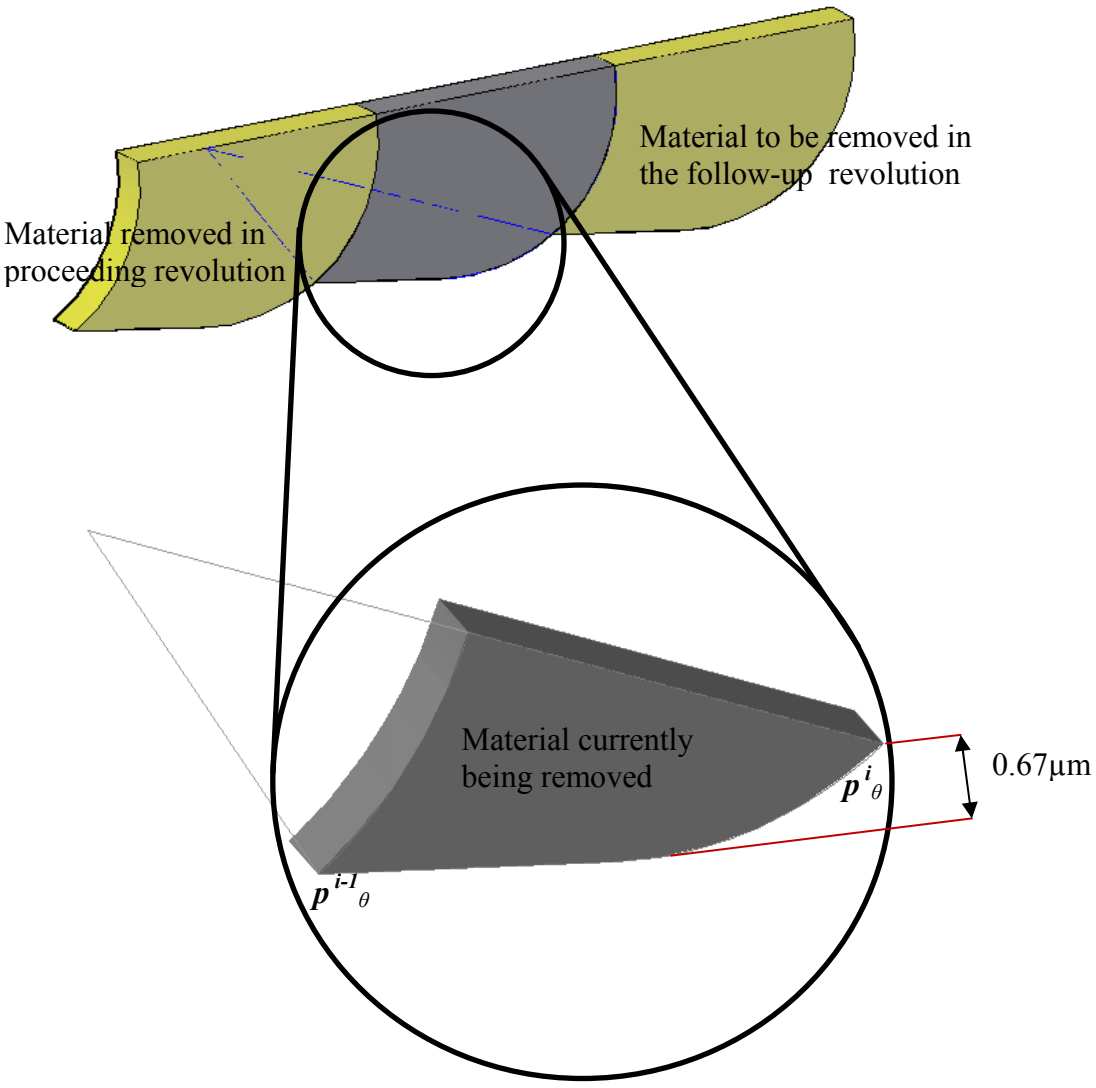

Fig. 4.8: Floor surface generation process.

4.3. Experimental validation

To validate the proposed model, an experimental study was conducted on two different dual-phase steel samples and thus to compare the simulation with the machining results. In particular, AISI 1040 and AISI 8620 steels were selected to conduct the slotting tests due to different ratios of ferrite and pearlite in their microstructure. Fig. 4.9a and 4.9b show the microstructure of AISI 1040 and AISI 8620 steel samples, respectively. The two phases can be seen clearly; especially the dark one is pearlite while the bright is ferrite. The micrographs of both samples were taken to create the maps of their metallurgical microstructure and then to calculate the percentage of pearlite and ferrite in them, respectively. For the AISI 1040 steel the ratio between pearlite and ferrite is well balanced, 48% and 52%, respectively, while for the AISI 8620 sample the ferrite phase was dominant, 68%. This higher content of ferrite, with its higher minimum chip thickness value than that for pearlite, is expected to lead to a different machining response. In particular, when compared with the AISI 1040 sample more ploughing rather than cutting is expected under the same cutting condition.

A micro-machining centre, Kern HSPC 2216, was used to cut the slots by using 400 μm diameter tungsten carbide tools. A set of cutters was imaged using a scanning electron microscope (SEM) to assess their geometry before starting the tests. The cutters selected for this experimental study had the following geometric parameters, cutting edge radiuses $\boldsymbol{r}$ in the range of 1.5 to 3.5 μm, and end cutting edge angles **ECEA** between 7° and 11°. Also, the cutting tool corner radiuses $\boldsymbol{r_c}$ were in the range of 2 to 5 μm.

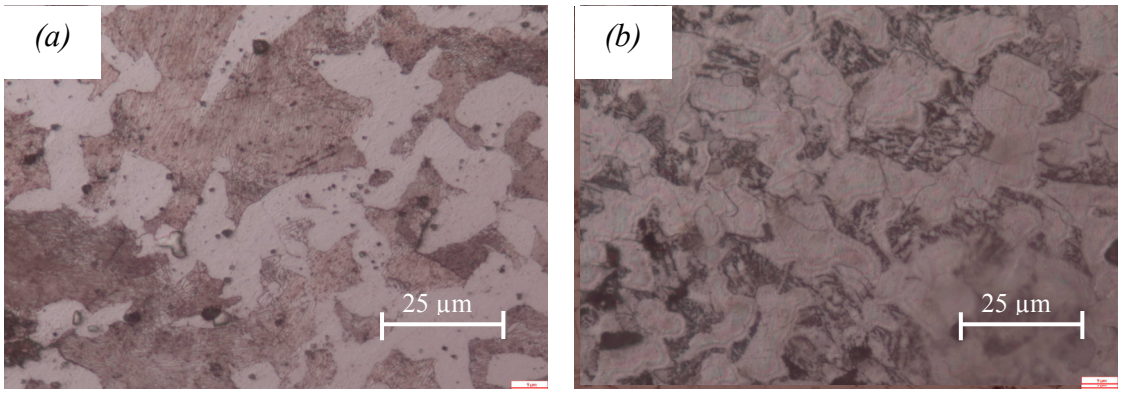

Fig. 4.9: Micrographs of the two samples, (a) AISI 1040 and (b) AISI 8620.

The cutting parameters used during the experiments are presented in Table 4.1. Particularly, in order to reveal the effects of the minimum chip thickness on the cutting mechanism, its alterations between cutting and ploughing, the experiments covered a wide range of feed rates from 5 to 0.6 μm/tooth while the other two machining parameters, were kept constant. The maximum available spindle speed of 40,000 rpm was selected which was equivalent to 50 m/min and also, one level of axial depth of cut, 10 μm, was applied.

Table 4.1: Cutting conditions

Cutting parameters	Values								
Depth of cut [μm]	10								
Cutting speed [m/min]	50								
Feed rate [μm/tooth]	5	4	3	2	1.6	1.2	1	0.8	0.6

4.4 Results and discussion

4.4.1 Surface roughness

The roughness of the machined surface, at the bottom of the micro-milled slots, was examined using a scanning white light interferometer, Micro-XAM from Phase Shift Inc, with a 12.5X optical magnification. A 656.48 x 427.19 μm area was scanned with about 1 μm resolution in the X-Y plane, normal to the optical axis, and sub-nanometre resolution in the Z direction, along the optical axis. In particular, the average surface roughness, $\mathbf{S_a}$, was measured for each slot.

Fig. 4.10 shows the surface roughness results obtained on the AISI 1040 sample over the considered feed rate range and the cutting tool geometry used in the tests. The material machining response in regards to the resulting surface roughness is presented in Fig. 4.10. The results reflect the trade-offs between the kinematic parameters and the minimum chip thickness effects, and also they are in agreement with those reported by Vogler *et al.* (2004a). In particular, the improvement of the resulting surface roughness with the decrease of the feed rate from 5 μm to 2 μm/tooth is due to the effects of the kinematic factors such as the cutting parameters and the tool trajectories. Conversely, the roughness increase at feed rates below 1.2 μm/tooth can be explained with the effects of the minimum chip thickness, especially in case of multi-phase materials where burrs and surface defects are formed repeatedly. However, further reduction in the feed rate to 0.6 μm/tooth led to improvements in the surface finish which could be attributed to changes in the cutting mechanisms to predominantly burnishing rather than ploughing or cutting.

Also, one can argue that the critical range of the feed rates is between 2 and 1 μm/tooth where the value of the feed is in the vicinity of the cutting edge radius. The best roughness values were achieved in this range, and also noticeable variations of the roughness can be easily seen, which indicates the importance of optimising machining parameters. Thus, the proposed model has the potential to address this need in micro-milling by providing a means to optimise the cutting parameters before starting any machining, and thus to be able to achieve the required surface quality.

In Fig. 4.10, the simulation results obtained by applying the proposed model are also provided. The model was implemented employing the Matlab software. The same cutting parameters and tool geometries as those applied in the experimental study were fed into the model together with the material microstructure maps of the multi-phase AISI 1040 steel sample, generated as it was described in Section 4.2.1. Comparing the simulation and experimental results in Fig 4.10, it is not difficult to conclude that in general they are in a good agreement with an average error of 14.5%. The only exception is the results obtained at the very low feed rate of 0.6 μm/tooth where the error is higher, up to 40%. This can be explained with the changes in the cutting mechanisms to predominantly burnishing rather than ploughing or cutting. This cutting conditions was not considered in the proposed model. However, it should be stressed that such low feed rates are not applied in practice.

In the case of AISI 8620, the trend observed during model validation is relatively similar to the AISI 1040 steel as shown in Fig. 4.11. Again, the improvements in surface quality achieved with the reduction of the feed rate from 5 μm to 1.6 μm/tooth are attributed to the effects of the kinematic factors, such as the

cutting parameters and the tool trajectories. Also, the rougher surfaces generated at law feed rates of 1.2 and 1 μm/tooth can be explained with the effects of the minimum chip thickness, resembling again the results obtained on the AISI 1040 sample. Conversely, the alteration in the cutting mechanisms to predominantly burnishing at the very law feed rate of 0.6 μm/tooth can be considered the main reason for the surface roughness improvements at these regimes.

The simulation results obtained by applying the proposed model are also plotted in Fig. 4.11. The simulation runs were conducted under the same machining conditions, cutting parameters and tool geometries, as those applied in the experimental study, while the material microstructure maps of the dual-phase AISI 8620 steel sample were fed into the model. It is not difficult to see that the model predictions are very close to the experimental results. Thus, again there is a good agreement between the simulation and experimental results at the feed rates of 5 to 0.8 μm/tooth, an average error of 17.6%. However, the error increases at low feed rates of 0.6 μm/tooth, and becomes very high, up to 80%. This can be attributed again to the burnishing mechanism that dominates, as it was the case with the AISI 1040 sample at these machining regimes. In addition, the differences between the optimum cutting conditions in regards to resulting roughness are relatively small; in particular 1.6 and 2 μm/tooth for the simulation and experiment results, respectively, and can be explained with the assumption taken to simplify the model by idealising the machining conditions.

Comparing the results obtained for both materials, AISI 1040 and AISI 8620, there are clear evidences of significant influence of the material microstructure on the

achieved surface quality. This conclusion can be easily drawn based on the differences between the roughness measured on the AISI 8620 and AISI 1040samples that was achieved under the same cutting conditions and relatively similar cutter geometries. However, micro-burrs and surface defects are formed repeatedly for both materials, as shown in Fig. 4.12a and 4.12b, the increase of roughness in the case of the AISI 8620 sample can be attributed to the higher percentage of ferrite phase present in the microstructure with its higher minimum chip thickness than the pearlite one. Hence, the differences in their machining responses are associated with the differences in their mechanical properties. The ferrite phase is characterised by a higher toughness and therefore ploughing can be the predominant machining mechanism rather than cutting when compared with the cutting behaviour of pearlite under the same conditions. In addition, the higher ductility of the ferrite contributes to the material 'build-up' on the tool leading to more intensive tool wear and a higher surface roughness associated with it. At the same time, pearlite is more 'brittle' which lead to a smaller minimum chip thickness required to initiate the cutting process. Also, pearlite is susceptible to the formation of smaller chips and favourable cooling conditions of the tool edge which again have a positive effect on the resulting surface.

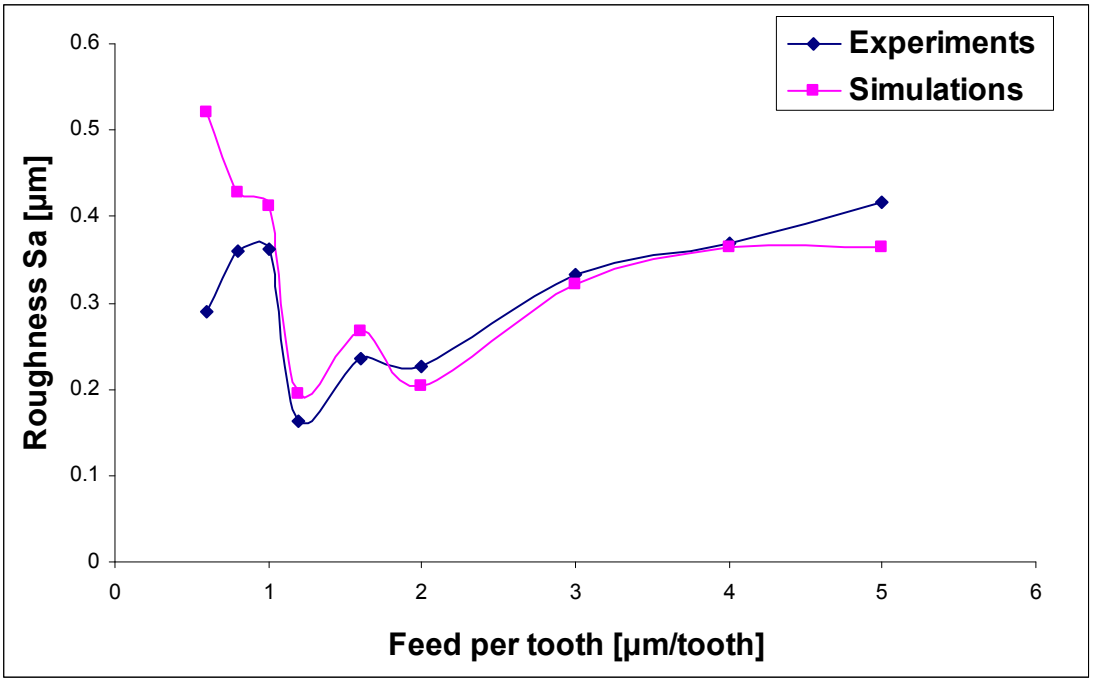

Fig. 4.10: Comparison of experimental and simulation results in micro milling a dual-phase AISI 1040 steel.

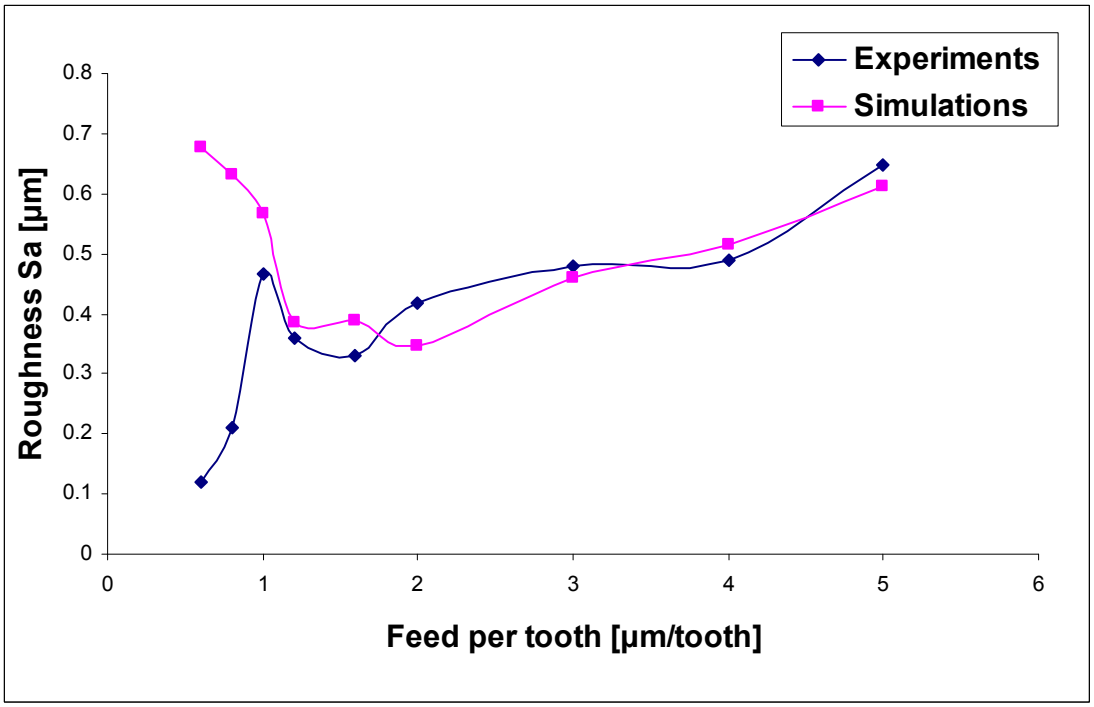

Fig. 4.11: Comparison of experimental and simulation results in micro milling a dual-phase AISI 8620 steel.

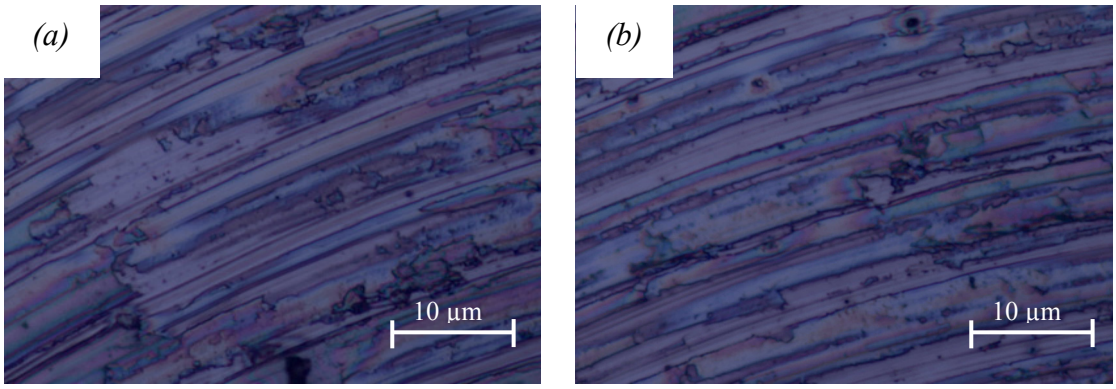

Fig. 4.12: Optical images of the machined surfaces (a) AISI 1040 and (b) AISI 8620.

4.4.2 Comparison of simulation and experimental results

The differences between the simulation and experimental results can be explained with the idealised cutting conditions used in the simplified model, especially at low feed rates. Their cumulative effect at the very low feed rates can be considered as the main reason for these discrepancies. In particular, at such machining regimes when the maximum feed rate at the centre of the slot is less than the minimum chip thickness, the cutting does not take place at every pass, but only after a certain number of unsuccessful passes. In this way the thickness of the material that has to be removed increases incrementally from pass to pass until it exceeds the minimum chip thickness and only then the cutting occurs (Liu et al. 2007a). To simplify the model this phenomenon is not considered, and therefore the error is so high at very low feed rates. Another reason for the difference between the simulation and experimental results at very low feed rates can be the very small chip-load that alters the cutting mechanism from cutting and ploughing to rubbing and burnishing. Such machining conditions can produce less roughness but with a high tool wear due to the high forces exerted to the end cutting edge face. In addition, to the aforementioned reasons, there are two more factors contributing to the occurrence of this error. First, it is the effect of the end cutting edge when moving over prominent burrs left after the previous cutting passes. Secondly, this can be due to the measurement uncertainty associated with the use of the scanning white light interferometer to inspect the machined surface, especially prominent burrs in the form of undercuts as shown in Fig. 4.13, which are more likely to occur at low feed rates.

Thus, based on the obtained results one can argue about the validity and applicability of the proposed model to predict the surface roughness after micro-milling multi-phase materials under various machining conditions, while excluding only those at very low feed rates. However, as it was already stated such cutting regimes are not suitable for most practical applications taking into account the available cutters' geometries, specially the manufacturing constraints in producing tools with very small cutting edge radiuses.

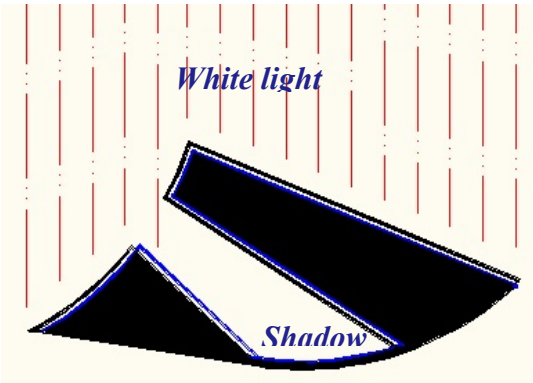

Fig. 4.13: White light microscope limitation.

4.5 Summary

This chapter has presented a model to simulate the surface generation process during micro-milling of multi-phase materials together with an experimental study to validate it. The proposed model of the micro-endmilling process has been developed especially to simulate the surface generation process associated with the machining of multi-phase materials. It takes into account the effects of the feed rate as the most important cutting parameters affecting the material machining response but also the cutting tool geometry, in particular the cutting edge radius, the cutter corner radius and the end cutting edge angle. In addition, as the workpiece cannot be considered anymore homogeneous at this scale of material removal, a special attention is paid to its microstructure. The model takes into account any variations of the minimum chip thickness when moving from one phase to another by feeding maps of the material metallurgical microstructure into the model. Such maps are created by employing image processing techniques to process micrographs of the material microstructure and thus to convert them into planer maps of points that represent the coordinates of each pixel with the third binary number giving information about the phase at each point on the map.

An experimental study was conducted on two different dual-phase steel samples to validate the proposed model. In particular, slotting tests were performed on AISI 1040 and AISI 8620 samples under a range of chip-loads, especially feed rates ranging from 5 down to 0.6 μm per flute, and thus to assess the effect of their microstructure on the generated surface. Subsequently, the roughness of the generated

surfaces were measured and compared with the predictions of the proposed model under the same cutting conditions.

The study showed a good agreement between the experimental and simulation results, with an average error of 14.5% and 17.4% for the AISI 1040 and AISI 8620 samples, respectively. Based on these results, a conclusion can be made that the model can be used both to predict the surface quality after micro-milling multi-phase materials under various machining conditions, and also as a tool to optimise the micro-milling process. Only at very low feed rates, below 1 μm per flute, the error is much higher, and thus the model cannot be applied at such cutting regimes. However, it is worth stressing that they are not suitable anyway for most practical applications taking into account the available cutters' geometries, especially the manufacturing constraints in producing tools with very small cutting edge radiuses. Another important feature of the model is that it allows the micro-burr formation at the phase boundaries to be taken into account in assessing the resulting surface roughness. Finally, the results of this research show clearly that a special attention should be paid to the selection of the workpiece material, especially multi-phase ones, and then the cutting conditions for their processing at micro-scale.

CHAPTER 5

TOOL WEAR IN μ-ENDMILLING: MATERIAL MICROSTREUCTURE EFFECTS, MODELLING AND EXPERIMENTAL VALIDATION

5.1 Overview

This chapter reports an investigation of material microstructure effects on tool wear in micro-scale machining of multi-phase materials. Conversely to macro-scale machining, as has been mentioned earlier, the cutting edge radius of micro cutters is at the same order of magnitude to the chip-loads and both are comparable with the grain sizes of the machined materials (Liu *et al.* 2004; Vogler *et al.* 2004a; 2004b and Pham *et al.* 2008). Hence, the effects of the material microstructure on tool wear have to be considered in micro-endmilling operations. These scale effects become even more pronounced in the case of multi-phase materials because they are a "blend" of a finite number of phases with distinct properties and therefore can have a different machining response under the same cutting conditions. So, these effects have to be investigated in order to optimise the process and identify processing windows, cutting conditions, which can reduce the resulting surface roughness while extending the tool life.

However, tool wear is associated with changes in the tool geometry, especially, cutting edge radius and cutting tool corner radius. This is mainly attributed to the significant increase of the friction between the tool and the workpiece associated with a thermal growth and wear (Chae *et al.* 2006), and also the small chip-load usually applied in micro-milling. Consequently, surface roughness is directly affected by such changes in the tool geometry. And, ultimately the tool wear affects the quality and dimensional accuracy of the machined parts. Moreover, an increase in the cutting edge radius can alter the machining condition from cutting to ploughing and hence also leads to changes in cutting forces. Therefore, one can advocate that getting a better understanding of the mechanism and progression of tool wear in micro-endmilling is very important for advancing further this technology.

The structure of this chapter is as follows. First, the most relevant research to the work presented here is reviewed. After that, the proposed experimental setup is described. Then, the selected machining conditions, especially, workpiece materials, cutting tools and cutting parameters used in the trials are defined and the rationale behind their selections is explained. Next, the results are presented and discussed, especially; focusing on the material effects on tool wear. This is followed by the creation of two regression models based on these trials and their experimental validation to demonstrate their applicability to predict tool wear when machining a wide range of multi-phase steels and iron. Finally, a summary is made about the effectiveness of the proposed approach for modelling the tool wear behaviour.

5.1.1 Related work

Due to some limitation of the available inspection technologies and difficulties in conducting empirical research, there are only few studies of tool wear at micro-scale machining have been reported (Jun *et al.* 2008 and Li *et al.* 2008). However, in addition to the work reviewed in section 2.3, this section reports on two of the most relevant research investigation to the work presented in this thesis.

Jun *et al.* (2008) studied experimentally the effects of the cutting and ploughing machining conditions on the tool wear by applying different feed rates. Also, the authors introduced a new parameter to quantify tool wear during micro-endmilling. In particular, the increase of the edge radius, denoted as ***Δr,*** was defined as a new wear parameter, which was calculated employing the following equation:

$$\Delta r_e = \frac{1}{3}\left[\left(r_{1,w} - r_{1,n}\right) + \left(r_{2,w} - r_{2,n}\right) + \left(r_{3,w} - r_{3,n}\right)\right] \quad (5.1)$$

where r_1, r_2 and r_3 are the cutting edge radii for the first, second and third flutes, respectively, while the subscript, w or n, denotes worn and new tools, Fig. 5.1. In addition, dependence between the applied feed rates and the wear mechanisms was identified and thus it was possible by varying the feed rates to avoid an increase of the "round" wear and consecutively the minimum chip thickness effect. The authors stressed that by selecting an appropriate processing window favourable machining conditions could be maintained, especially normal cutting above the minimum chip thickness and predominantly flat flank tool wear without increase in the cutting edge radius. However, it is worth noting that the tool wear parameters were assessed only

before and after the machining trials.

Malekian *et al.* (2009) examined experimentally the effect of cutting conditions on tool wear in micro-endmilling, and proposed a monitoring method that replied on sensory data obtained employing accelerometers, and force and acoustic emission sensors, Fig. 5.2. Subsequently, a neuro-fuzzy method was used to combine such data and thus to study the condition of the cutting tool, especially whether it was sufficiently sharp for normal machining to continue. To verify the proposed monitoring method cutting trials were performed using 500 μm diameter flat micro-end mills, while an optical microscope was utilised to investigate the actual tool conditions by examining the status of the cutting tool corner radius, Fig. 5.3. According to the authors, the proposed method can be used to monitor the conditions of the micro-end mills during the cutting process and thus to provide warnings when the tool reaches the pre-failure stage. However, it is important to stress that in this research only the conditions of the cutting tool corner radius were monitored to estimate the tool wear, and not the cutting edge radius, which has a higher influence on the resulting surface finish and cutting forces.

In spite of the limited publications in this field, it can be concluded that the tool wear in micro-endmilling is an important factor affecting the process performance and at the same time it is a challenging research issue that needs addressing. Especially, the machining performance can be improved by understanding better the effects of cutting conditions (Lia *et al.* 2008) and machinability of workpiece materials on tool wear mechanism. In addition, to carry out such an investigation it is necessary to find new ways, e.g. experimental setups, for characterising and monitoring the tool wear.

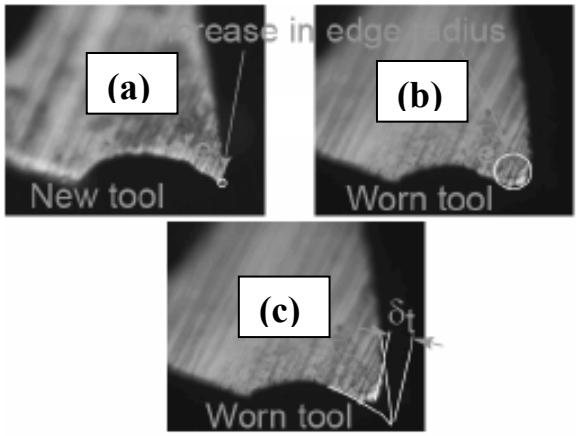

Fig. 5.1: Tool wear (a) before cutting and (b) and (c) after cutting at feed rate of 1.0 µm/flute (Jun *et al.* 2008).

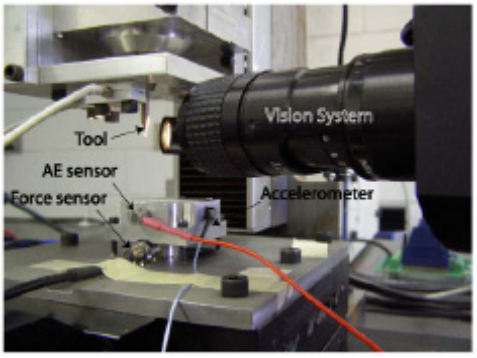

Fig. 5.2: Experimental setup (Malekian *et al.* 2009).

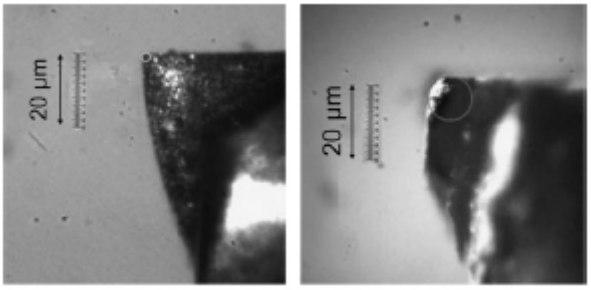

Fig. 5.3: Edge radii of good andworn tools: (a) good tool (r=1_m) and (b)worn tool (r=6_m) (Malekian *et al.* 2009).

5.2. Experimental set-up and experiment design

This section describes the experimental setup used to investigate the tool wear during micro-endmilling. In particular, it outlines the basic procedure that was applied to perform the experimental trials, and also explains the rationale behind the selected materials, cutting tools and cutting parameters for the trials.

Changes in the cutting edge radius and the cutter flute profile were chosen to quantify the tool wear. These process characteristics were identified by the author as very important factors for modelling the processes and also for predicting the resulting surface roughness after micro-endmilling. To investigate the effects of these two parameters after machining a workpiece without taking off the cutters, a new experimental setup was designed and implemented as depicted in Fig.5.4. By employing this set-up it was considered more likely the cutter conditions to be maintained unchanged during the trials which in turn could minimise uncertainties associated with the replacement of the cutting tools.

The adopted procedure to investigate experimentally the tool wear in micro-endmilling includes the following steps. After removing a certain volume of material, the cutter was cleaned employing Delta GT-7810A ultrasonic cleaner for 30 sec. Then, a Blum NANO laser system, P87.0634, was used to measure nominal diameters of the cutters at different heights and thus to characterise the cutter flute profile after each trial. Next, Dino-lite digital microscope with 500X optical magnification was employed to image the bottom of the cutter as shown in Fig 5.4. To measure the cutting edge radius of the three cutter flutes, the software supplied with the microscope, DinoCapture 2.0, was used. Fig. 5.5 depicts some of the software capabilities employed to assess the tool wear.

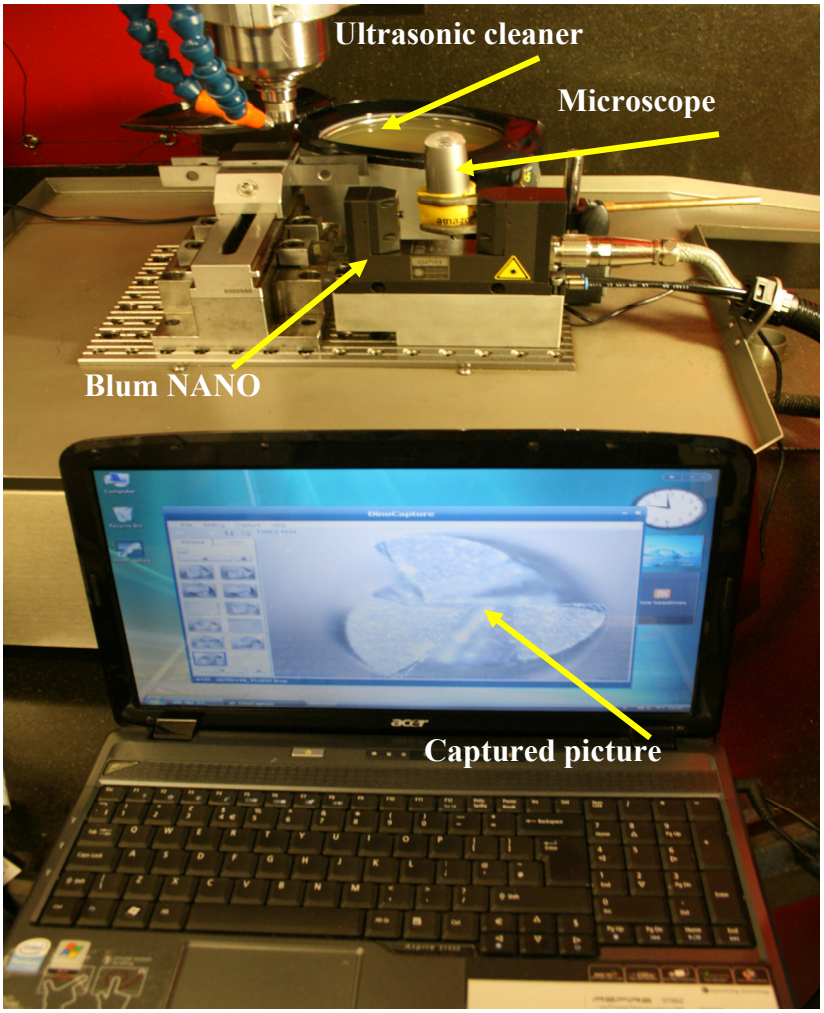

Fig. 5.4: Experimental setup.

To examine the effect of the material microstructure on the tool wear progress, two different materials were selected for the first part of this research. In particular, SAE01 high carbon steel (0.85-1.05%C) and SAE101 low carbon steel (0.08-0.13%C) were used because of their pure pearlite and pure ferrite microstructures, respectively. The effects of each phase on the tool wear behaviour were studied individually under different cutting conditions. The objective was to create two regression models for predicting tool wear (Δr) based on the results obtained from these experimental trials. The models should be able to predict tool wear as a function of cutting speed, feed rate per tooth and material removal volumes for each phase separately. Then, it was aimed to apply them to estimate the tool wear for a wide range of multi-phase steels and irons, composed predominantly of these two phases but with different ratios between them, when performing machining at micro-scale.

The machinability in terms of tool wear of pearlite and ferrite phase independently was investigated by carrying out slotting tests on a micro-machining centre, Kern HSPC 2216. Fine grained tungsten carbide tools coated with TiAlN were utilised in these machining trials. In particular, 800 μm end-mill cutters with three teeths were utilised in the experiments. Prior to the cutting tests, each cutter was imaged using an optical microscope to measure approximately the radii of the cutting edges as shown in Figure 5.6a. It was found that for the cutters used in the trials they were in the range from 2 to 5 μm. The undeformed chip thickness was controlled by varying the feed rate per tooth, and thus to achieve values in the vicinity of the average cutting edge radius, in particular 4 and 8 μm/tooth, for which the best surface roughness was achieved. The other cutting parameters used in the trials were two levels of cutting speeds, 20,000 and 5,000 rpm equivalent to 50 and 12.5 m/min respectively, and only one level of axial depth of cut, 30 μm.

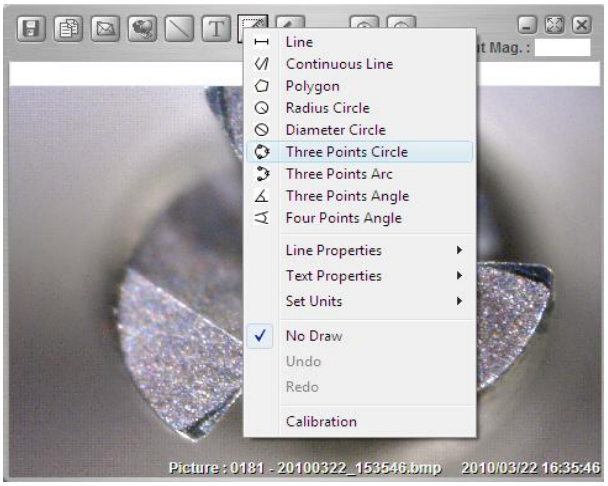

Fig. 5.5: Measurement functions of the Dino-Capture 2.0 software.

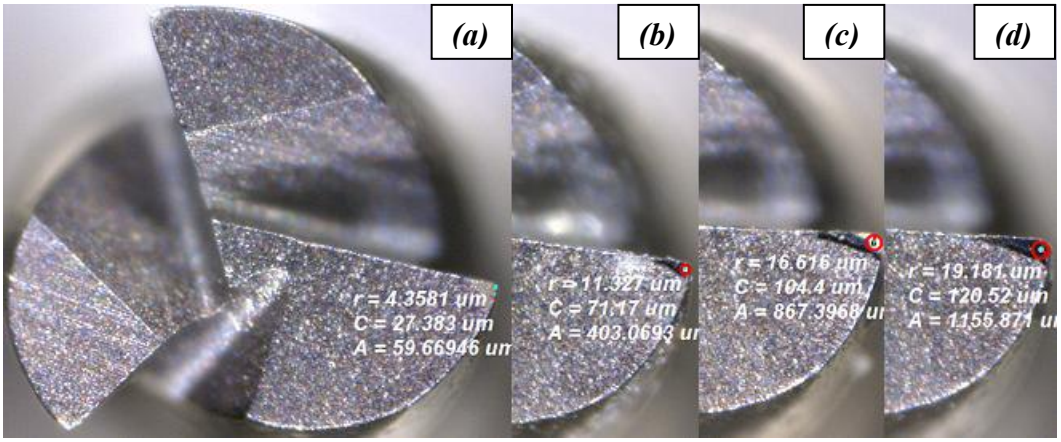

Fig. 5.6: The tool wear evolution in micro-endmilling (a) a new tool, (b) a worn tool and (c) and (d) severely worn tool.

5.3 Results and Discussions

5.3.1 Measurement uncertainty

As the measurements of cutting edge radius were conducted manually, there was uncertainty in performing this inspection procedure. To minimise measurement errors, the maximum magnification allowed by the software was used to inspect the selected features. In addition, measurements were taken after relatively large increments in machining time, and hence removed volumes, in order to judge clearly about any increases of tool wear. However, to validate the measured value of cutting edge radius obtained for a given cutting condition, measurement uncertainty has to be studied.

An existing methodology for calculating uncertainty in measurement was utilised to determine the uncertainty associated with the cutting edge radius, ***r,*** (Kirkup and Frenkel 2006). Also, as all ***r*** measurements are taken at the same digital magnification it can be assumed that the sources of uncertainty in radius measurements are the same for the all measurements. Hence, the formula for calculating the standard uncertainty, ***u***, is:

$$u = \frac{s}{\sqrt{no}} \qquad (5.2)$$

where ***s*** is the estimated standard deviation for all measurements and ***no*** is the number of measurements in the set.

To apply this procedure, five measurements were conducted for three different cutting edge radii. In particular, the smallest and largest cutting edge radii in addition to a mid-range radius were measured five times each in order to judge the uncertainty of the measurement. Fig.5.7 illustrates the measurements of the different cutting radii. The standard deviation, ***s***, was calculated to be 0.265 µm, 0.158 µm and 0.112 µm and the standard uncertainty of measurements was calculated to be 0.12 µm, 0.07 µm and 0.05 µm for radii with mean values of 2 µm, 10.65 µm and 20.4 µm, respectively. Based on the results, it can be concluded that there is an inverse relationship between the measurement uncertainty and the size scale of the measured radii. However, the maximum measurement uncertainty was determined to be 0.12 µm for a 2 µm cutting edge radius which is considered acceptable. Therefore, all measurements were repeated five times and the average was selected to represent the real value of the measurement.

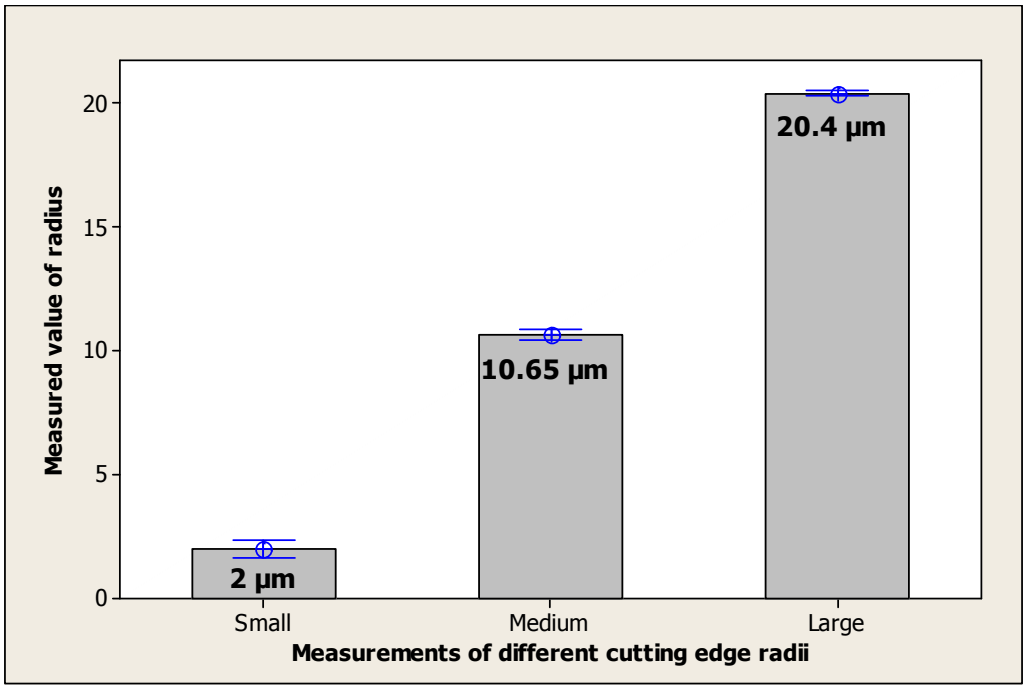

Fig. 5.7: Five measurements for different cutting edge radii.

5.3.2 Tool wear

The images captured with the microscope were used to assess the wear of the cutting edge radius after removing certain volumes of material. Fig. 5.6 illustrates the evolution of the wear with the increase of the removed volume of material and also how this was assessed using the proposed experimental set-up.

The increase of the edge radius, Δr, was calculated using Eq. 5.1 and thus to judge about the average wear increase of the three flutes of the cutters. The results obtained for pearlite and ferrite are presented in Fig. 5.8 and Fig. 5.9, respectively.

For pearlite, the tools exhibited the highest wear when the lowest settings for the cutting speed and the feed rate were applied, whereas the lowest wear was experienced at their highest settings as shown in Fig. 5.8. Hence, it is worth stressing that such inverse relationships between the exhibited wear and the applied feed rates and speeds are contrary to those at macro-scale machining but are in agreement with those reported by Filiz *et al.* (2007). This increasing trend for the tool wear at low feed rates can be attributed to the effect of the minimum chip thickness when the ploughing regime dominates the cutting mechanism. Especially, a higher force was exerted on the cutter due to a higher friction between the cutting tool and the workpiece which in turn leads to a higher wear. Besides the minimum chip thickness becomes significant at low cutting speeds because the engagement time of the tool/workpiece is longer. Moreover, it is not difficult to see that the tool wear, in particular, Δr is highly dependent on the selected cutting speed.

In contrast for ferrite, there is a small variation of Δr when the results for the two different settings of the cutting speed and the feed rate are compared. In addition, the linear increase of the tool wear is much more pronounced as can be seen in Fig. 5.9. Moreover, as could be expected, a higher tool wear was observed when machining ferrite than pearlite under the same cutting conditions. This phenomenon is explained with differences in mechanical properties of these two phases. The ferrite phase is characterised by a higher toughness, especially when alloyed even with small quantity of Mn, which contributes to the material 'build-up' on the tool. Therefore, ploughing can be the prevailing machining mechanism rather than cutting when compared with the response of pearlite under the same conditions. This regime dominates due to the effect of the minimum chip thickness associated with higher forces exerted on the tool edge and more intensive wear of the cutting tool. At the same time, pearlite is more 'brittle' and susceptible to a lower minimum chip thickness, shorter chip formation and favourable cooling conditions of the tool edge.

The cutting tool radii at different heights were measured, and an example printout of these results is provided in Fig. 5.10 and Fig. 5.11 for pearlite and ferrite, respectively. The black arrow indicates the reduction of the nominal cutter radius due to the tool wear. These measurements are affected by such factors as tool run out and vibrations, its thermal elongation during machining and also the presence of some chips due to insufficient cleaning time. These factors can explain the measured bigger radius of the cutter than its nominal value of 400 μm for a new tool. Also, it should be noted that the repetition accuracy of the Blum NANO laser system, which allows cutting tools with diameters down to 30 μm to be measured with a repetition accuracy of ±1 μm (Popov *et al.* 2010).

When comparing the results for both cases, pearlite and ferrite materials, at the same cutting conditions, less tool wear in terms of nominal cutter radius exhibited in case of pearlite, as shown in Fig. 5.10. However, higher wear occurred when ferrite was machined under the same cutting conditions, Fig. 5.11. In particular, the reductions of the nominal cutter diameter were 12 μm and 28 μm for pearlite and ferrite phases, respectively. These results are in agreement with the other wear parameter, cutting edge radius, where machining of pearlite exhibited less wear than those experienced when machining ferrite. Again, this phenomenon can be attributed to the mechanical properties of these two phases, as mentioned earlier.

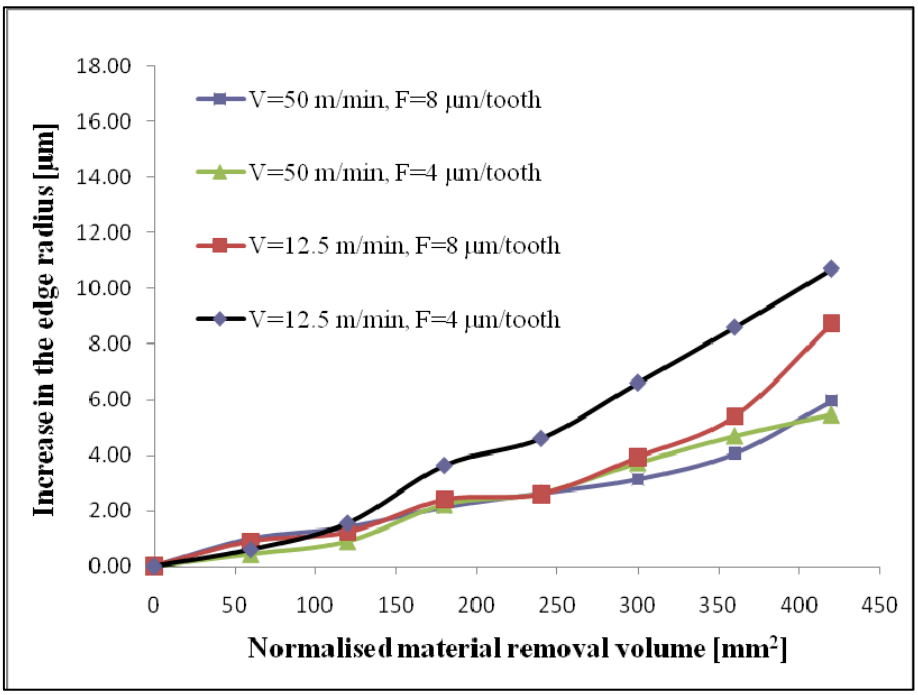

Fig. 5.8: The average increase of the cutting edge radius for pearlite.

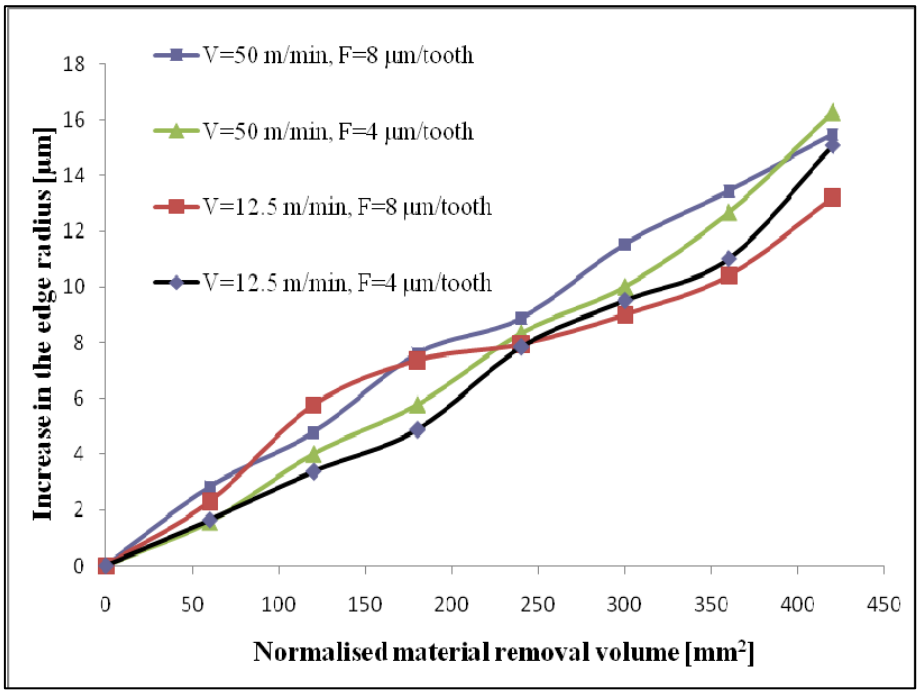

Fig. 5.9: The average increase of the cutting edge radius for ferrite.

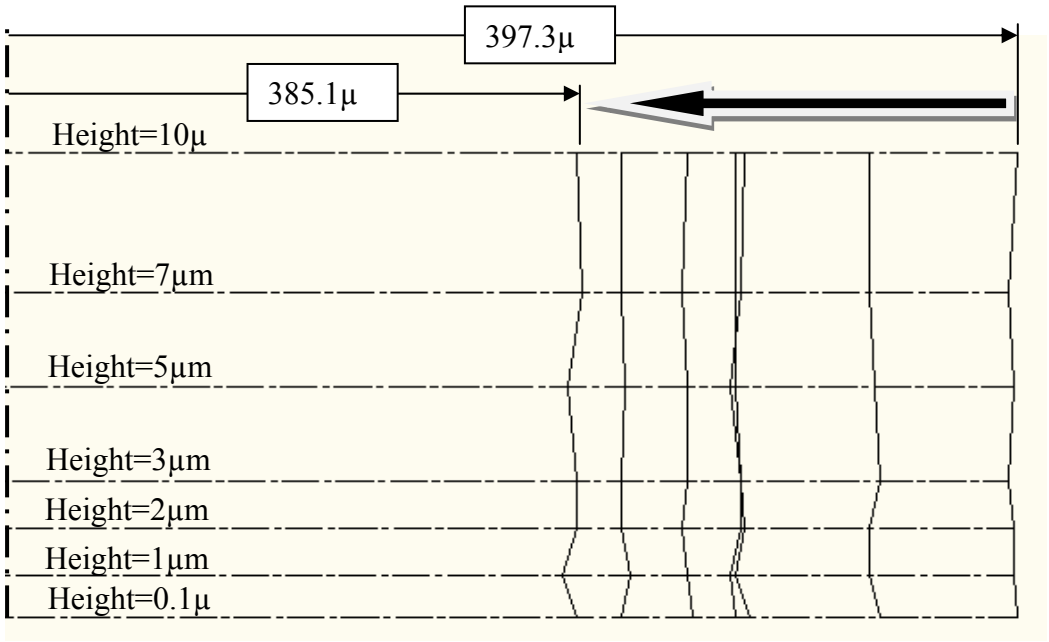

Fig. 5.10: Cutter radius measurements at different heights for pearlite.

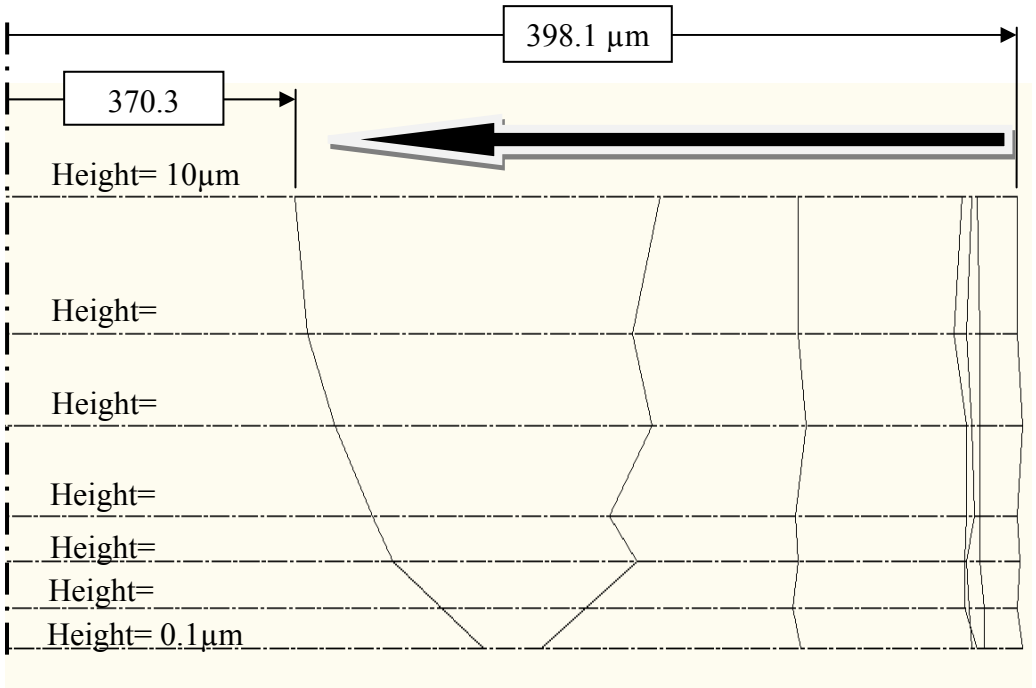

Fig. 5.11: Cutter radius measurements at different heights for ferrite.

5.4 Regression-based modelling

It is considered that ANNs can model the tool wear better than regression based models (Özel and Karpat 2005 and Palanisamy and Shanmugasundaram 2008). However, to create such ANNs large data sets are required in order to train and then test such models. This is a major constraint because of the high cost of running such experimental studies due to relatively large numbers of expensive cutting tools necessary, usually one for each of the investigated cutting conditions' settings. Therefore, the experiments were conducted at only two levels of cutting speeds and feed rates and seven levels of removal rates for each material. Preliminary trials were carried out to train an ANN using 70% to 100% of the available input data. However, the model performed poorly during both the training and testing stages due to the occurred under-fitting. Therefore, for this experimental study regression modelling was selected to estimate the increase of the cutting edge radius when machining multi-phase materials.

In this research, two regression models were created to estimate the tool wear, Δr_p and Δr_f for pearlite and ferrite, respectively, as a function of cutting speed, $\boldsymbol{V}$, feed rate per tooth, $\boldsymbol{f_t}$, and normalised material removal volume, $\boldsymbol{MR_n}$, the removed volume divided by the depth of cut. Minitab 15 software was used to generate the models based on the experimental data obtained by machining the SAE 01 and SAE 1010 samples.

For pearlite, taking into account the observed trend of the tool wear in Fig. 5.8, an

exponential model, Eq. 5.3, was adopted as it was considered to have the best fit.

$$\Delta r_p = \alpha_o * MR_n^{\alpha_1} * V^{\alpha_2} * f_t^{\alpha_3} \quad (5.3)$$

Then, a logarithmic transformation was applied to convert Eq 2 into the following linear analytical form as shown in Eq.5.4:

$$\ln(\Delta r_p) = \ln(\alpha_o) + \alpha_1 * \ln(MR_n) + \alpha_2 * \ln(V) + \alpha_3 * \ln(f_t) \quad (5.4)$$

The least squares estimation technique was applied to compute the coefficients, and thus to create this regression model for estimating the tool wear when machining pearlite steel at micro-scale.

In case of ferrite, as the tool wear trend was very close to linear, as shown in Fig. 5.9, a linear regression model was adopted. Once again, the least squares estimation technique was applied. In this way, the coefficients were determined and the proposed regression model was created.

The models that were created for pearlite and ferrite phases are given in Eq. 5.5 and Eq. 5.6, respectively.

$$\Delta r_p = 0.01133 * MR_n^{1.21} * V^{-0.233} * f_t^{-0.103} \quad (5.5)$$

$$\Delta r_f = -1.45 + 0.0342 MR_n + 0.0231 V + 0.134 f_t \quad (5.6)$$

Based on the obtained coefficient of determination for both models, R-Sq, the prediction accuracy for the average wear, Δr_p and Δr_f, were within 91.2% and 97.3% for pearlite and ferrite, respectively. Also, the normal probability plots, shown in Fig. 5.12 and Fig. 5.13 for pearlite and ferrite models, respectively, indicate that most factors considered in the analysis affect the tool wear.

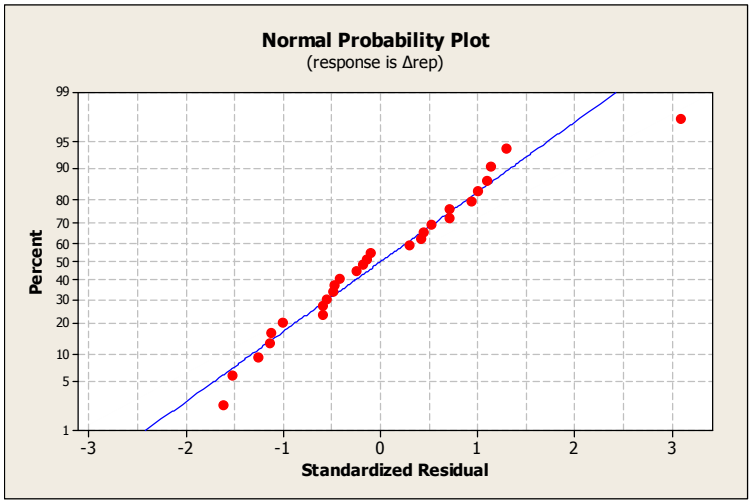

Fig. 5.12: Normal probability plot of the wear model for pearlite.

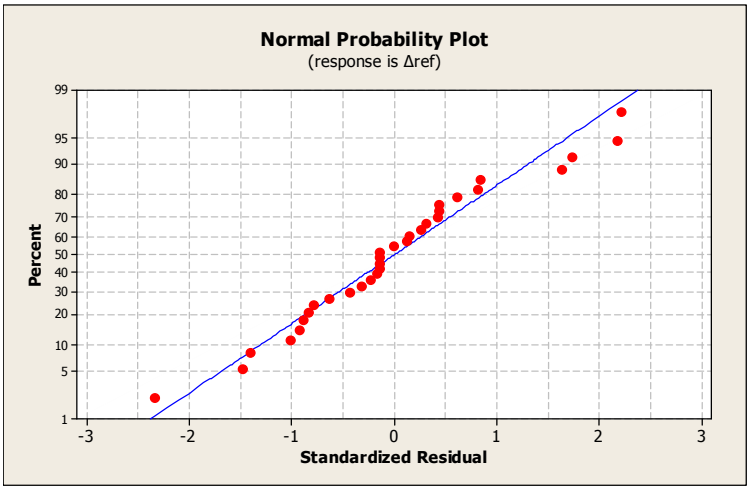

Fig. 5.13: Normal probability plot of the wear model for ferrite.

5.5 Experimental Validation

The objective of the second series of experiments was to demonstrate the validity of the proposed method and also to validate developed regression models. So, the proposed approach was evaluated at two different levels and under different conditions in order to compare the predicted values of the tool wear with the machining results. Firstly, the proposed models were used to estimate the tool wear when machining two different dual-phase (pearlite and ferrite) steel samples, particularly AISI 1040 (0.37-0.44%C) and AISI 8620 (0.18-0.23%C) carbon steels. The machining trials were conducted with 800 μm cutting tools similar to those used in the initial experimental trials. Then, to demonstrate the soundness of the proposed method, another experimental study was performed by using the models to estimate the tool wear of cutting tools smaller in size than those used in the first trials. In particular, 600 μm and 400 μm two-fluted tools were utilised to analyse the wear when an AISI 1040 workpiece was machined at micro-scale. All these validation trials were conducted under cutting conditions similar to those used in the initial experimental trials, in particular, feed rate of 6 μm/tooth and cutting speed of 25 m/min were applied. However, the depth of cut was 30 μm in the first validation trials when a 800 μm cutter was used, while in the second trials, when smaller tools were investigated, a smaller depth of cut, 20 μm, was applied to reduce the load and thus to avoid tool breakages.

As it was already mentioned the normalised, as received, AISI 1040 and AISI 8620 steels were selected to conduct the slotting tests due to different ratios of ferrite and pearlite in their microstructure. Fig. 5.14a and 14b show the microstructure of

AISI 1040 and AISI 8620 steel samples, respectively. The two phases can be seen clearly; especially the dark one is pearlite while the bright is ferrite. The micrographs of both samples were taken to create the maps of their metallurgical microstructure and then to calculate the percentage of pearlite and ferrite in them, respectively. For the AISI 1040 steel there is a good balance between pearlite and ferrite, 48% and 52%, respectively, in the microstructure while for the AISI 8620 sample the ferrite phase was dominant, 68%. This higher content of ferrite, with its higher minimum chip thickness than that for pearlite, was expected to lead to more ploughing rather than cutting, when compared with the AISI 1040 sample, under the same cutting condition. Again, as mentioned before, this ploughing mechanism increases the force exerted on the cutting edge due to the significant increase of the friction between the tool and the workpiece which in turn leads to a thermal growth and a higher wear.

Based on this data, it is possible to account for the effects of these two different phases on the tool wear, and thus to estimate it using Eq. 5.5 and Eq. 5.6. The same approach can be applied to other multi-phase materials.

As an example, the tool wear model for the dual-phase materials can be defined as follows:

$$\Delta r = \Delta r_p * R_p + \Delta r_f * R_f \qquad (5.7)$$

where: Δr is the tool wear for the dual-phase material; Δr_p and Δr_f is the tool wear for pearlite and ferrite, respectively; and R_p and R_f are the percentages of these two phases in the dual-phase material.

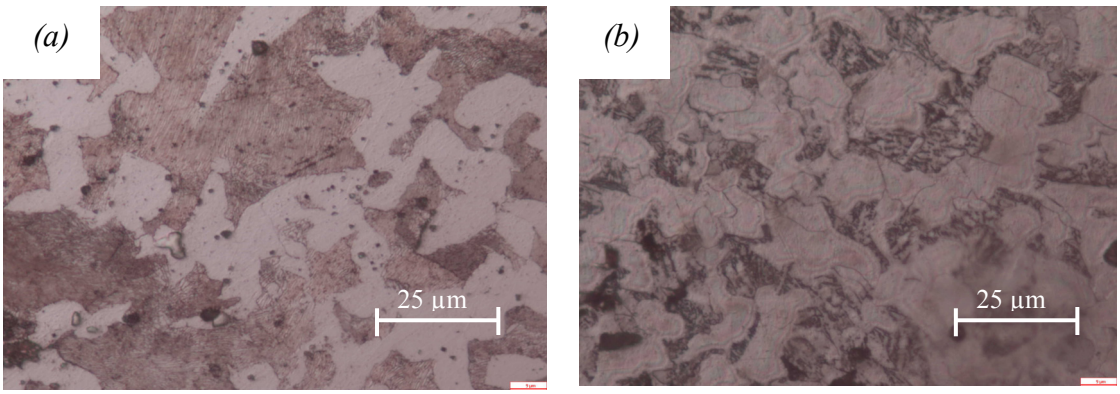

Fig. 5.14: Optical microstructure micrograph of (a) AISI 1040 and (b) AISI 8620 steels.

Fig. 5.15 shows a comparison of the predicted and experimental results of the tool wear exhibited when machining the AISI1040 workpiece with 800 μm tool by applying 25 m/min cutting speed, 6 μm feed rate per tooth and 30 μm depth of cut. The experimental results have a non linear trendline in contrast to linear one for the prediction; however, the discrepancy between the estimated tool wear and the experimental results is in average 14.7%.

Fig. 5.16 shows a comparison between the prediction and experimental results when machining the AISI 8620 sample under the same cutting conditions as those used for the AISI 1040 one. As it can be seen from the figure, the trend is quite similar to that observed during the machining of the AISI 1040 steel (Fig. 5.15). Again, there are differences between the prediction and experimental results but again they are relatively low, within 17.5%. Thus, it can be judged that these results support the use of the proposed approach and the models created by applying it can be applied to predict tool wear when machining dual-phase steels.

Studying the experimental results obtained for both materials (Fig. 5.15 and Fig. 5.16), it is not difficult to notice the higher tool wear resulting from the machining of the AISI 8620 workpiece in comparison with the AISI1040 one under the same cutting conditions. This was expected and was attributed mostly to the higher percentage of ferrite in the AISI 8620 microstructure. Also, the models predicted accurately the wear in both case as depicted in these two figures. Hence, it can be concluded that the influence of the material microstructure on the tools' wear is significant and by accounting for this models can be created to predict the tool wear when machining dual-phase materials.

Fig. 5.17 and Fig. 5.18 represent the results from the second validation trial that was conducted to demonstrate the applicability of the proposed generic approach for predicting the wear of smaller tools as discussed previously. In particular, in Fig. 5.17 the predictions are compared with the experimental results when machining the AISI 1040 workpiece with 600 μm cutter. Similarly, Fig. 5.18 depicts the predictions vs. the actual tool wear when machining the same workpiece with a 400 μm tool under the same cutting conditions. Again, there is a good agreement between the predictions and the experimental results in both cases. Especially, the average error was 20% and 19% for the 600 μm and 400 μm cutters, respectively, under the same cutting conditions.

Taking into account the results from all trials it is evident that the proposed approach can be used to model the tool wear behaviour when machining dual-phase materials. It can be argued that the differences between the predictions and experimental results can be reduced by increasing number of experiments conducted on the pearlite and ferrite steels' samples independently. Additionally, the engagement of a tool with more than one phase at once could be another reason for the observed discrepancies. However, it can be judged that the obtained results demonstrated the applicability of the proposed approach for estimating tool wear when machining dual-phase materials. Besides, the same approach can be adopted for predicting the tool wear when machining multi-phase materials, especially by conducting similar experimental trials for all phases present within their microstructure and thus to model their effects on the tool wear. Also, it should be noted that the regression models created in this way can be easily refined to account for any new experimental data and thus to improve their prediction capabilities.

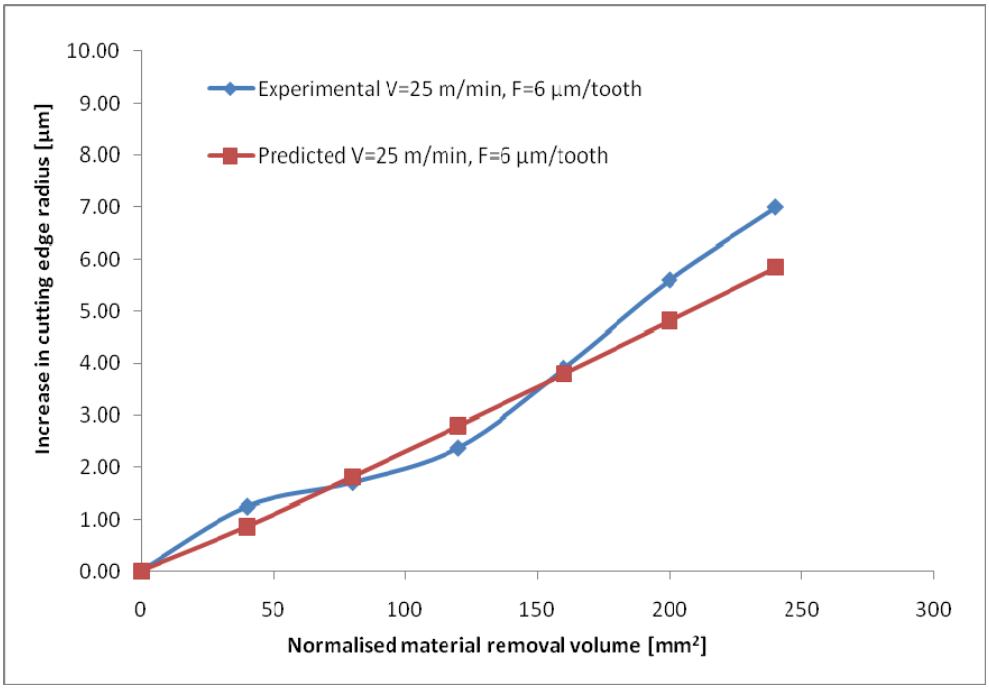

Fig. 5.15: Comparison between experimental and estimated tool wear when machining the AISI 1040 workpiece with 800 µm tool.

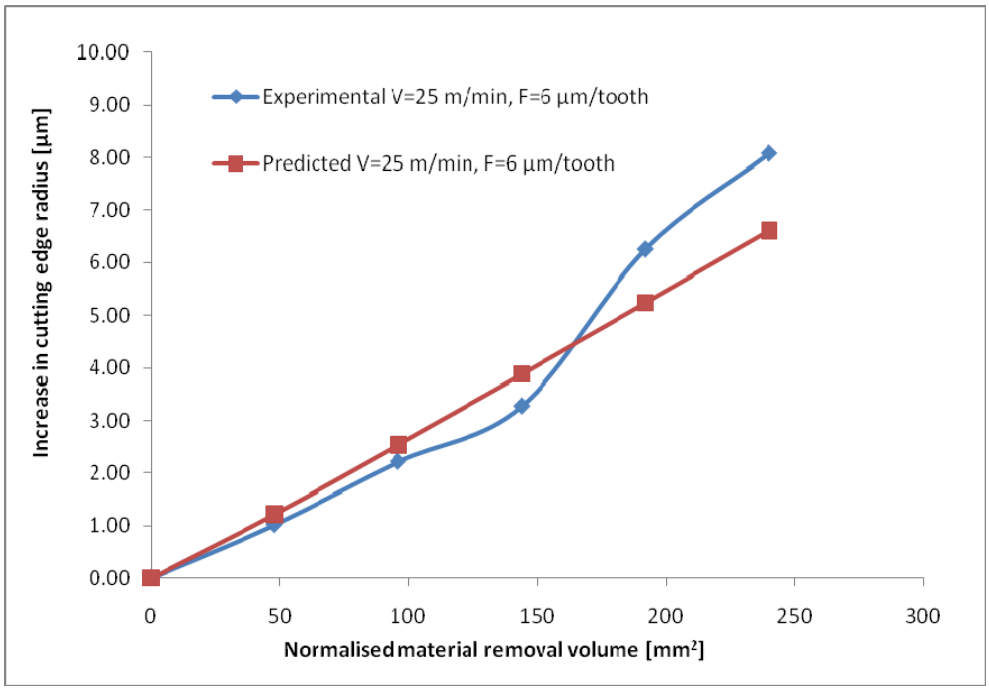

Fig. 5.16: Comparison between experimental and estimated tool wear when machining the AISI 8620 workpiece with the 800 µm tool.

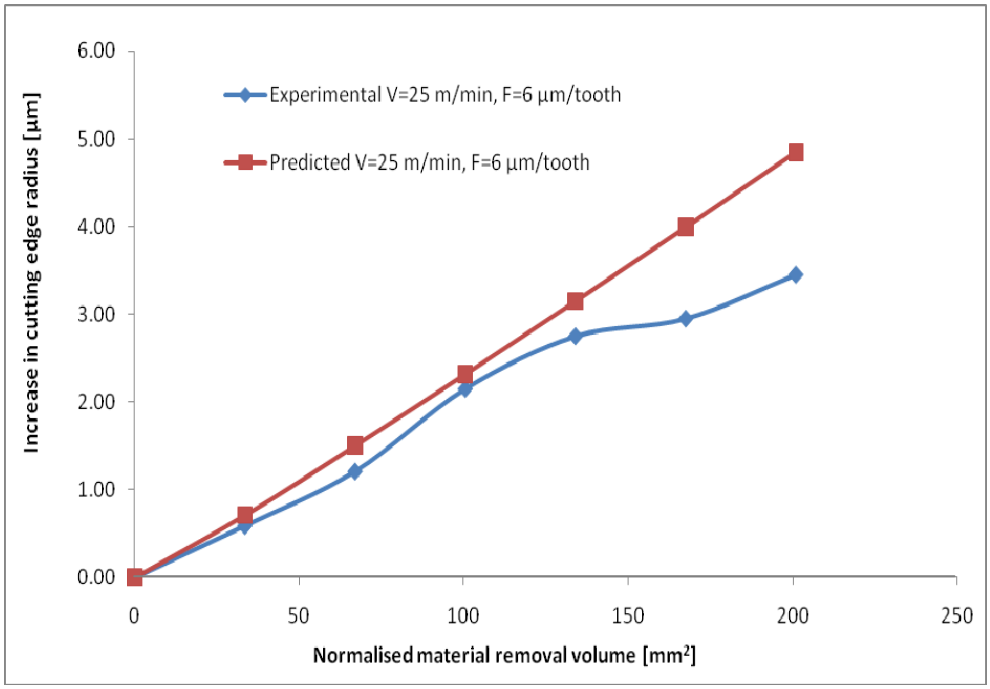

Fig. 5.17: Comparison between experimental and estimated tool wear for 600 µm tool and AISI 1040 workpiece.

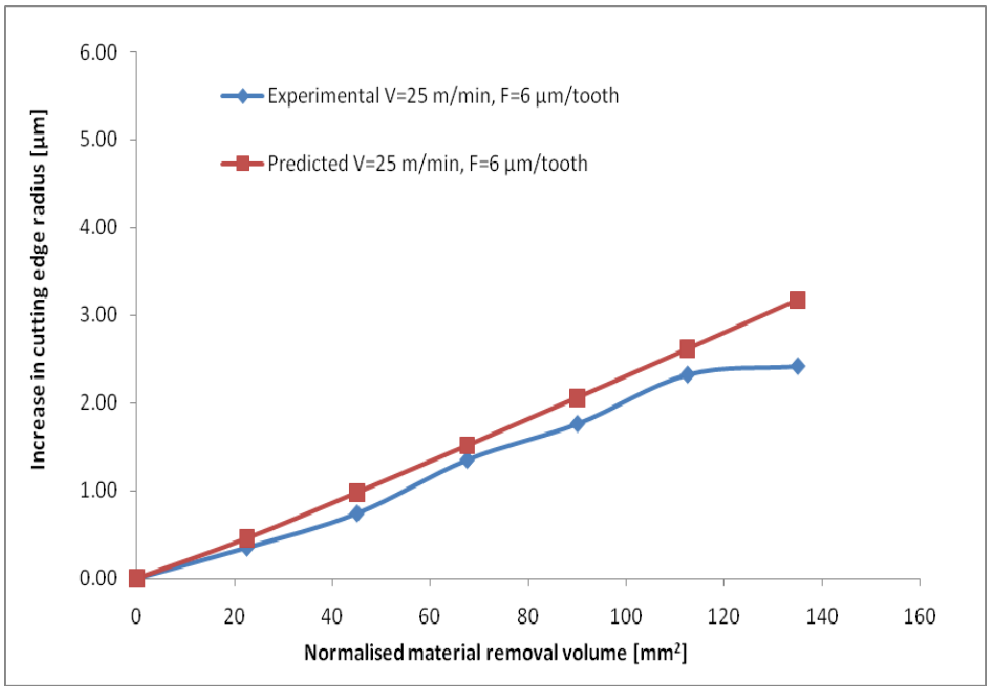

Fig. 5.18: Comparison between experimental and estimated tool wear for 400 µm tool and AISI 1040 workpiece.

5.6 Summary

In this chapter, various factors affecting the tool wear in micro-endmilling were examined and discussed. Special attention was given to the effects of the material microstructure on tool wear. The average values of cutting edge radius and tool flute profile were used to assess the tool wear. A new experimental setup was proposed to determine these two tool parameters, and then a series of experiments on pearlite and ferrite steel were conducted to investigate the effects of their distinctive properties on the tool wear. The factors that affect the accuracy of the flute profile measurements were also discussed. Then, two regression models were created based on the experimental data in order to estimate the increase of the cutting edge radius of pearlite and ferrite steels independently. The aim was by combining them to be able to predict the tool wear when machining dual-phase steel workpieces predominantly composed from these two phases with different ratios.

To demonstrate the applicability of this generic method and at the same time to validate the models, the proposed approach was evaluated in two different experimental studies under different conditions, especially by machining two different dual-phase steel samples, AISI 1040 and AISI 8620, with different cutting tools. The results showed a good agreement between the estimated and the actual tool wear, especially the average error was in the range from 14.7% to 20% in all experimental trials.

This empirical research demonstrated the validity of the proposed generic method for modelling the tool wear behaviour when machining dual-phase and potentially

multi-phase materials. The differences between the predictions and experimental results were attributed to the limited number of experiments conducted on single-phase steels' samples independently. In addition, there were two other factors contributing to the observed discrepancies. In particular, the resulting tool wear was measured manually, and hence there was some uncertainty in performing this operation, and also it was not taken into account the engagement of the tools with more than one phase at the time. Finally, it should be noted that the tool wear models created by applying this approach could be easily refined to account for any new experimental data and thus to improve their prediction capabilities.

CHAPTER 6

SIMULATION-BASED STUDY OF THE μ-ENDMILLING PROCESS

6.1 Overview

As previously mentioned, to achieve optimum machined surfaces at the micro-scale, the selection of workpiece microstructures and the cutting conditions for their processing is one of the challenging issues that need addressing (Vogler *et al.,* 2004a). The motivation for this work was to investigate the effects of cutting conditions, tool wear and workpiece microstructure on floor surface roughness generation with the goal of using the results of this study to optimise the machining process. Using the models discussed in chapters 4 and 5, simulations have been performed over a wide range of cutting conditions and modified workpiece microstructures. The study will enable appropriate selection of workpiece material (especially multi-phase) and cutting conditions for their micro-scale processing. In addition, a virtual micro-milling environment has been created that implements the developed surface generation and tool wear models. Thus, the generated VR model would provide a better physical understanding of cutter/workpiece interactions in micro-milling and aid in optimising the machining conditions (Elkaseer *et al.,* 2009b).

The chapter begins by presenting a simulation of the roughness generated for AISI 1040 and AISI 8620 under a wide range of cutting conditions. Next, the likely improvement of the surface generation model obtained by incorporating a tool wear model is discussed. After that, the modification of the microstructure of the materials to be investigated is presented. Next, a discussion is presented of the optimisation of the cutting conditions for the microstructures to be studied. The final section presents the virtual simulation of the micro-endmilling process.

6.2 Simulation of Surface Roughness

This section outlines the simulation study of the surface roughness model experimentally validated as previously discussed in Chapter 4. First, the model was used to simulate the effect of a wide range of cutting conditions on the surface generation of two different materials, AISI1040 and AISI8620, under a wide range of cutting conditions. Fig. 6.1a and 6.1b illustrate the microstructures of AISI1040 and AISI8620, respectively. Simulation trials were performed with cutting speeds ranging from 5-100 m/min and with a feed rate varying between 0.5 and 20μm/tooth. Next, the surface generation model was extended to include the tool wear model (see Chapter 5) so that it considers the effects of tool wear on the resultant roughness.

6.2.1 Cutting conditions based-simulation of surface roughness

This section presents a simulation of surface roughness obtained in micro-endmilling of the two dual-phase materials being used. The simulation was conducted using the model described in Chapter 4 with the aim of investigating the effects of cutting conditions on the surface roughness obtained using AISI 1040 and AISI 8620. All these simulation trials were carried out using a 400μm diameter tool assumed to have a cutting edge radius of 2.5μm, 3μm cutter corner radius and end cutting edge angle of 7º.

Figure 6.2a shows the results for the simulated microstructure obtained when the proposed model was applied to AISI 1040 over the given ranges of feed rate and cutting speed. It can be seen clearly that the relationship between the feed rate and the resulting surface roughness is a non-linear. With the decrease of feed rate from 20 to 4.5 μm/tooth, there was a reduction in surface roughness which can be attributed mainly to tool geometry and process kinematics. However, at very low applied feed rates, particularly at less than 1μm/tooth, an opposite relationship was observed and a rapid increase in surface roughness is clearly seen. This can be ascribed to the effect of the minimum chip thickness which dominates the machining regime at such low feed rates. In particular, the maximum chip-loads are much smaller than the cutting edge radius of the tool, and hence the material flows beneath the rounded tool edge. As a result, ploughing is the only machining mechanism that occurs and no chips are formed. Note that because the model being used assumes full elastic recovery of the material, very high surface roughness is generated. However, in the real cutting

process at very low feed rates less rough surfaces are achieved than those predicted by the model. This is because the machining mechanism is more likely to be shining and burnishing rather than ploughing. Thus, the model is not valid at very low feed rates, see Section 4.4.2.

However, when the feed rate is between 1 and 4.5 μm/tooth, the generated roughness is influenced by the interaction between the minimum chip thickness effect and the effect of the process kinematics. Especially, this interaction could lead to formation of the micro-burr repeatedly at the phase boundaries due to the different response of each phase to the cutting process. As clearly seen in Figure 6.2a, the best resultant surface is a result of trade-offs between the effect of the process kinematics and the minimum chip thickness effect, as also reported by Vogler *et al.* (2004a). Also, a noticeable variation in the resultant surface roughness is seen when the feed rates are near the cutting edge radius. Thus, the feed rates should be the result of careful consideration based on the geometry of the cutting tool used and the processed microstructure.

In case of AISI 8620, the trend obtained from the model simulation is very similar to that with AISI 1040 steel, see Figure 6.2b; with improvement in surface quality as the feed rate is reduced from 20 to 4.5μm/tooth. This is attributed to the kinematic factors. However, the rougher surfaces obtained at low feed rates (1 and 0.5μm/tooth) are explained by the effects that occur due to the minimum chip thickness. Again, as with AISI 1014, variation of the resultant roughness is seen when the values of the feed rates are in the vicinity of the cutting edge radius.

The differences between the simulated surface roughness achieved with AISI 1040 and AISI 8620 using the same cutting conditions and cutter geometries is taken as clear evidences of the importance of material microstructure on surface quality, especially at low feed rates. The relative surfaces roughness of the two materials can be described as: Very small differences at higher feed rates (20 to 4.5μm/tooth) where the process is more similar to macro-scale machining rather than micro-machining. At these relatively high feed rates the effects of the material microstructure and minimum chip thickness are negligible, and process kinematics and tool geometries dominate the machining mechanism. However, at lower feed rates where edge radius of the tool and chip-loads are comparable in scale (4.5 to 1μm/tooth) the ploughing regime becomes increasingly dominant due to the minimum chip thickness effect. Now the surface roughness obtained from the machining process reflects the different properties of the material microstructure. The surface roughness for the AISI 8620 sample is 7% greater on average than for AISI 1040, and this is can be attributed to the higher percent of the ferrite phase present in the microstructure with its consequent higher minimum chip thickness.

Note that the red lines in Fig 6.2a and Fig 6.2b refer to the minimum roughness's achieved for the studied range of cutting parameters.

Because the surface roughness model does not consider cutting speed as having an effect on surface roughness there was no difference in the roughness over the studied range of cutting speeds. However, in the next section, a tool wear model which considers the effect of cutting speed is incorporated into the surface generation model.

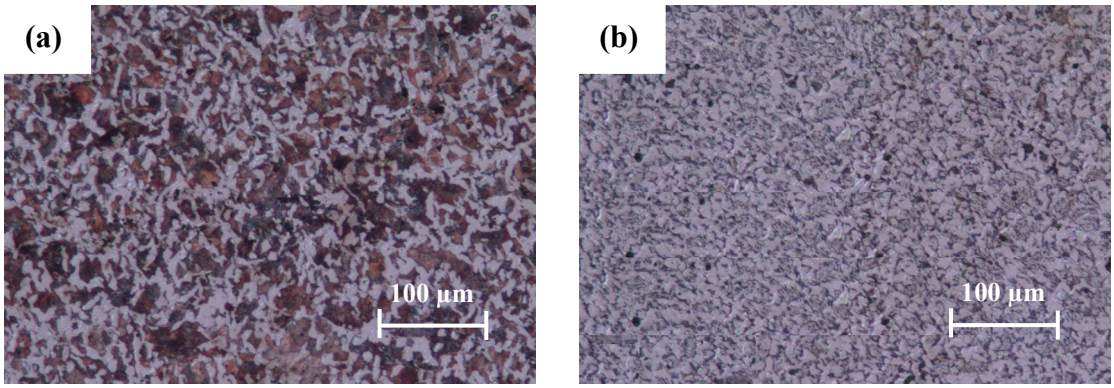

Fig. 6.1: Material microstructure of (a) AISI 1040 and (b) AISI 8620.

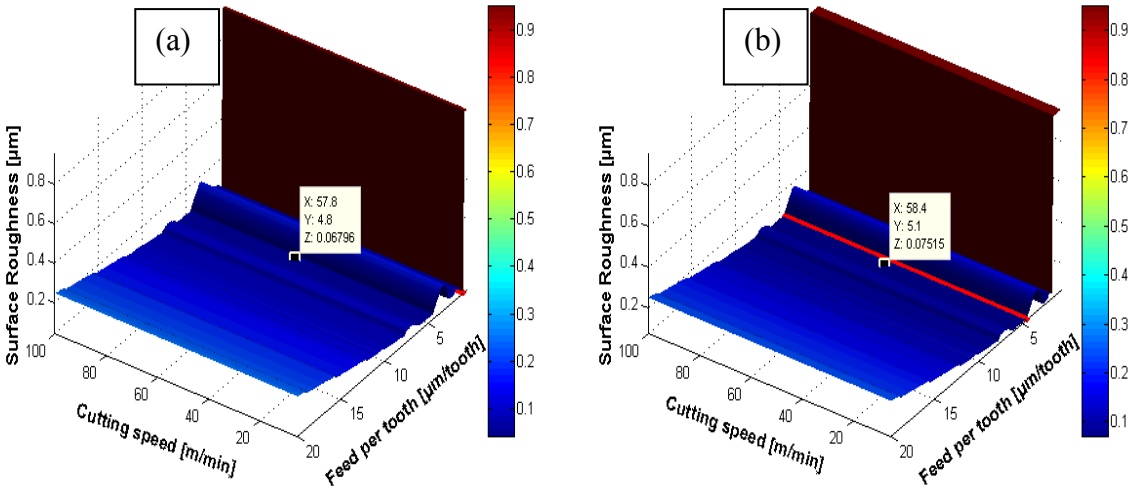

Fig. 6.2: Simulation of cutting conditions effect on surface roughness for (a) AISI 1040 and (b) AISI 8620.

6.2.2 Surface roughness model considering tool wear

In the second part of this simulation, the tool wear model described in chapter 5 is incorporated into the surface generation model to increase its capability. So, the increase of the surface roughness due to tool wear progression is presented.

Surface roughness was investigated for the same range of cutting speeds and feed rates as discussed in Section 6.2.1. However, to include the effect of tool wear on the roughness generated, the simulations were performed for five cutting lengths of 0, 150, 300, 450 and 600 mm. A 400μm cutting tool was used for the simulation trials.

Figure 6.3a shows the roughness obtained for AISI 1040 with the given cutting conditions. The increase in surface roughness with amount of material removed can be seen clearly. In the simulation this is because tool wear increases the cutter edge radius after a certain amount of material has been removed and as a consequence ploughing rather than cutting occurs with consequent higher surface roughness. With the increase in cutting edge radius, minimum chip thickness effect dominates a greater range of feed rates while the range over which process kinematics dominates decreases. For zero cutting length, the minimum chip thickness effect dominates the cutting process for feed rates between 1 and 4.5μm/tooth. However, when cutting length was extended to 600μm/tooth upper limit of the minimum chip thickness range shifted to 12.5μm/tooth. This meant that the feed rate for least surface roughness increased with increase in material removed. Thus, the strategy of micro-milling should, in part, include consideration of the total material to be removed and

the required surface roughness to be achieved. In particular, feed rate has to be increased after the removal of a certain volume of material to maintain surface roughness within the required limit.

However, the surface roughness model does not include consideration of cutting speed but tool wear depends on cutting speed. Thus, as can be seen in Figure 6.3, there is a relatively obvious change in surface roughness over the considered range of cutting speed. Based on these simulation trials for AISI 1040, cutting speed should vary with the increase in the amount of machined material to maintain surface roughness within the required limit.

In case of AISI 8620, tool wear gave the same general results on surface roughness, with the simulated roughness increasing with increase in material removed but the surface roughness was greater than that found with AISI 1040. This difference in surface roughness increased with increase in the volume of material removed due to the greater influence of the microstructure with increase of minimum chip thickness effect. Comparing the microstructure of the two sample materials, the higher percentage of the ferrite phase in AISI 8620 increases the effect of the minimum chip thickness which increases the generated surface roughness.

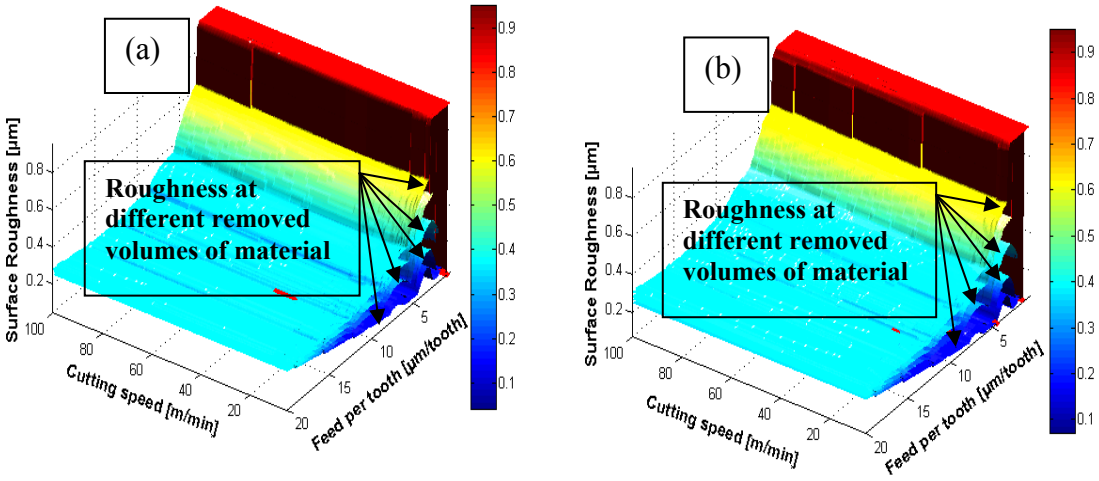

Fig. 6.3: Simulation of tool wear effect on surface roughness under considered cutting condition range for (a) AISI 1040 and (b) AISI 8620.

6.3 Optimisation of the Micro-Endmilling Process

This section discusses optimisation of the micro-endmilling process. The AISI 1040 was heat-treated to modify the size of the grains of the phases in its microstructure. Then, simulation experiments similar to those presented in Section 6.2.2 were carried out to compare their machinability. Finally, the simulation trials which were performed on AISI 1040, AISI 8620 and the modified AISI 1040, are used to optimise the cutting parameters, e.g. feed rate and cutting speed, for the best possible surface.

6.3.1 Optimisation of the material microstructure

AISI 1040 was chosen for these experiments because its structure and properties are well known. Its composition (0.37-0.44%C; 0.60-0.90%Mn, <0.04%P, <0.05%S) make its machinability good. That is because the ferrite and pearlite phases in the microstructure of the steel gives reliable chip control (George, 2002).

Different morphologies of the pearlitic grains in the AISI 1040 samples were obtained by using two types of heat-treatment (Buchkov and Kanev, 1998 and Smith, 2006). The steel was heated above its critical austenitising temperature (AC3, 900^{o}C) for 1 hour to assure that all the ferrite transformed into austenite. After this the AISI 1040 samples were cooled following ‘full annealing’ and ‘normalisation’ conditions:

Full annealing: To produce a coarse pearlitic structure with thick "bands" of pearlite, see Figure 6.4a, the cooling is slow, 50°C/hr. After this treatment the AISI 1040 is

soft and ductile, with no internal stresses and lowered toughness and impact strength, see Table 6.1. These factors mean the properties of the material are such that there is increased build-up on the tool and reduced machinability (eFunda, 2011).

Normalising: To produce a fine pearlitic structure and a more-uniform morphology air-cooling is used to give a cooling rate of about 50°C/min. Normalised AISI 1040 has a higher hardness and strength than its annealed counterpart but with increased brittleness, see Table 6.1. These factors mean the properties of the material are such that there is reduced build-up on the tool, lower cutting force and better machinability (eFunda, 2011).

The simulation trials were repeated for both fully annealed and normalised AISI 1040 and the results are presented in Figure 6.5 (a and b). Based on the results shown it can be concluded the surface roughness achieved was very similar for both fully annealed and normalised AISI 1040 and for the as-received AISI 1040 for the condition where only small volumes of the material were removed, see Figures 6.3a and 6.5a. However, with the increase in volume removed, differences between the obtained surface roughnesses appeared. A higher roughness was found for the normalised microstructure than for the fully annealed. This observation appears to contradict what was stated earlier about the relationship between grain sizes and achievable surface roughness. However, that relationship is valid only for the cases of single-phase microstructures or multi-phase materials when the grain size is small enough for the microstructure to be considered homogeneous, particularly when compared with the applied chip-loads. The increase of surface roughness with relatively small grain sizes, similar to normalised AISI 1040, can be attributed to an increased number of phase boundaries and associated micro-burr formation.

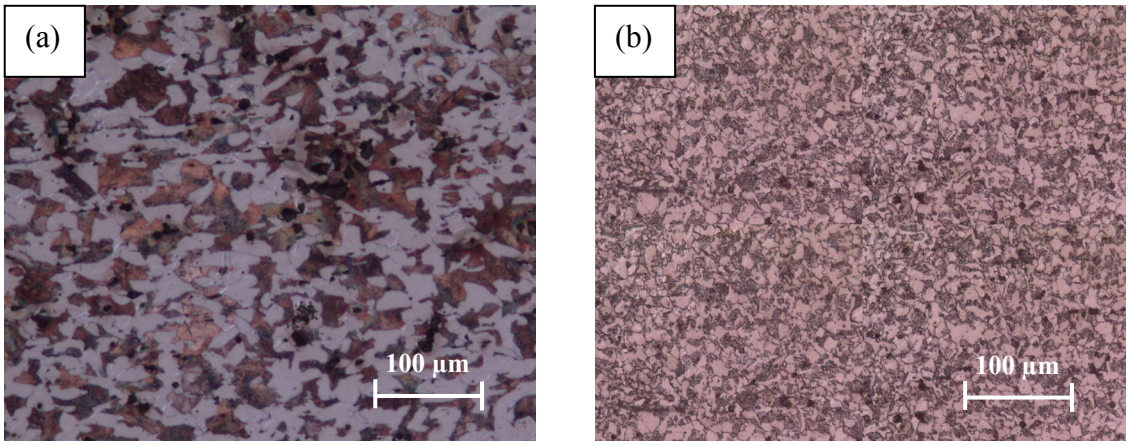

Fig. 6.4: AISI 1040 steel after heat treatment (a) full annealing and (b) normalising.

Table 6.1. Properties of AISI 1040 steel after annealing and normalisation.

Heat treatment	Hardness (Brinell)	Izod Impact Strength, J
Annealed	149	44
Normalised	170	65

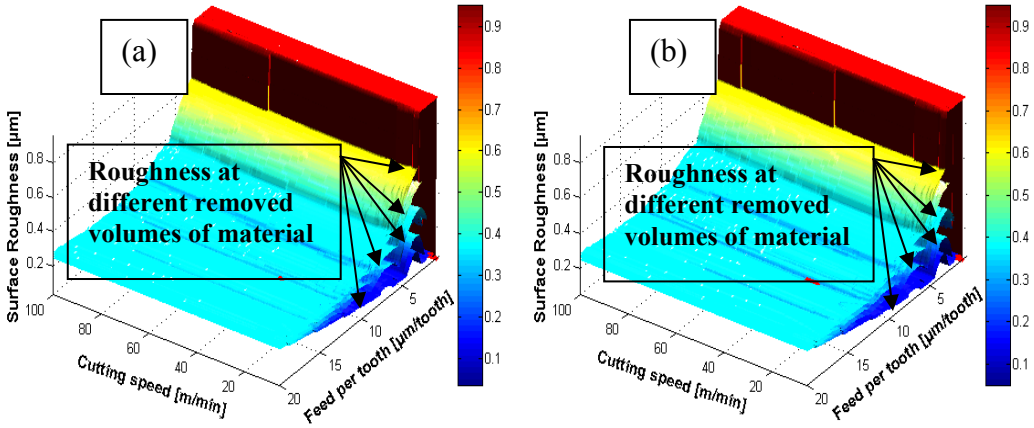

Fig. 6.5: Simulation trials for AISI 1040 steel after heat treatment (a) full annealing and (b) normalising.

6.3.2 **Optimisation of the cutting condition**

The algorithm for modelling the surface roughness (S_a) can be presented as a function:

$$Sa = f_t(Constants,\ f_t \text{ and } V)$$

where f_t represents the feed rate in μm/tooth and V is the cutting speed in m/sec. The boundary conditions chosen for feed rate and cutting speed are:

$$0.5 \leq f_t\ (\mu m/tooth) \leq 20\ \mu m$$

$$5 \leq V\ (m/sec) \leq 100$$

Material microstructure, cutter geometries and other parameters are considered to be constant.

A number of Matlab optimisation algorithms have been applied to find the optimum for S_a:

- Interior-point algorithm,
- SQL algorithm,
- Active-set algorithm, and
- Trust-region-reflective algorithm.

These algorithms are available as part of Matlab Optimisation toolbox (Mathworks, 2011) but it was found that none of them performed well in finding the minimum of S_a. This is because the output of the S_a algorithm will be a constant for certain ranges of values of f_t and V. In particular, for a certain range of values of V it was found that the rate of change of S_a with V is zero. Such behaviour means the optimisation algorithms cannot find a minimum for the S_a fitness function. Thus, a

different strategy was necessary to find the optimum value of S_a. A two-dimensional grid for the given range of inputs for the parameters f_t and V was created and value of S_a found for every given pair of f_t and V. Then, the minimum of S_a and the related range of input parameters were determined. The step sizes for the grid were:

- f_t **= 0.5:0.1:20 [µm/tooth]**
- V**=5:0.2:100 [m/min]**

Figure 6.6 shows the simulated surface roughness for the input variables, f and V**.** Also, the minimal S_a and the corresponding inputs $f_{t\ op}$ and V_{op} was determined. Figure 6.7 shows the results of the optimisation for a combination of different materials and cutting lengths. In Fig. 6.6, AR_AISI1040 denotes the as-received AISI 1040, LG_AISI1040 refers to the large-grained (fully annealed) AISI 1040 and SG_AISI1040 denotes the small-grained (normalised) AISI 1040.

Note that, due to the noticeable variation in the resultant surface roughness when the feed rates are near the cutting edge radius, very low and higher levels of surface roughness could be obtained over a small range of feed rates. On the other hand, the grid assumes zero machine/tool vibration and manufacturing error which would adversely affect the roughness values. Therefore, the grid of results can help in the selection of more conservative inputs parameters, rather than those recommended by the algorithm and are associated with less uncertainty risk. So, the results of this research show that the cutting process has been optimised by the identification of processing windows, cutting conditions and material microstructure, which will reduce resulting surface roughness.

Cutting length	AISI 8620	AR_AISI 1040	LG_AISI 1040	SG_AISI 1040
L=0 mm	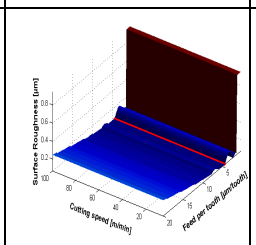	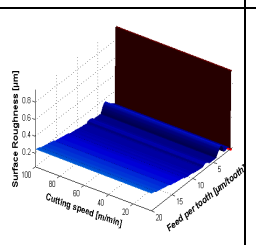	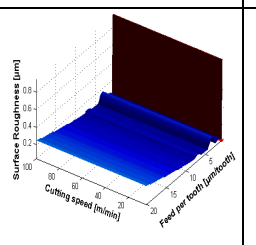	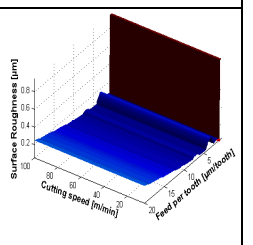
L=150 mm	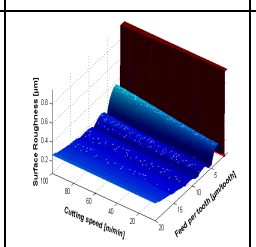	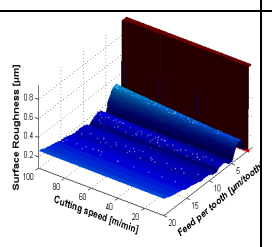	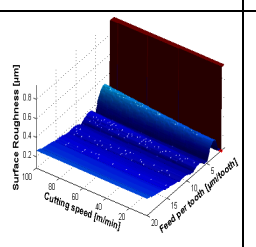	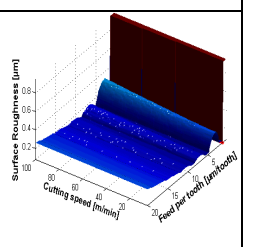
L=300 mm	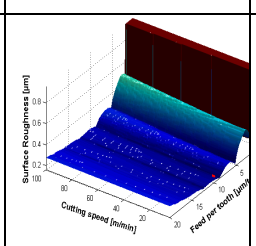	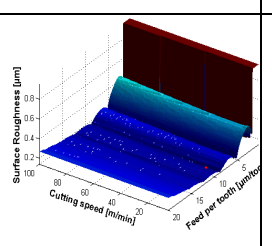	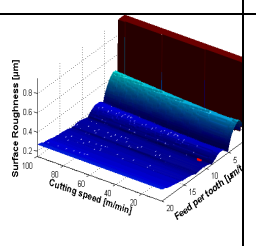	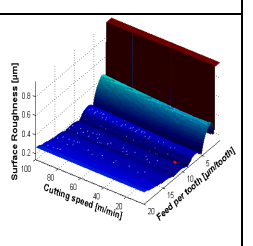
L=450 mm	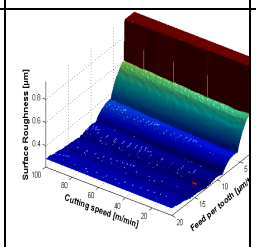	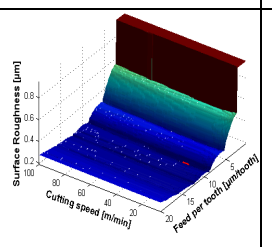	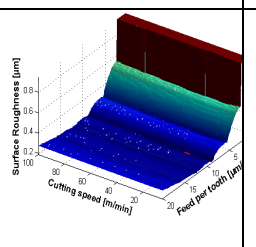	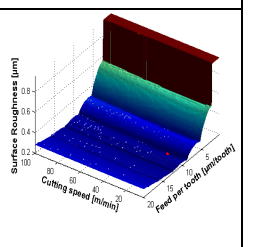
L=600 mm	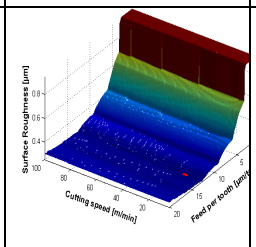	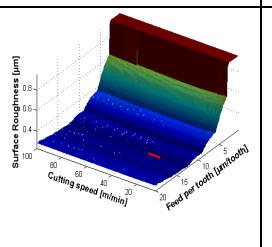	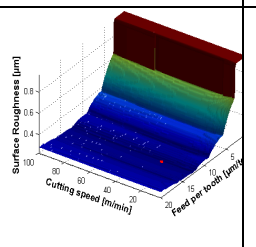	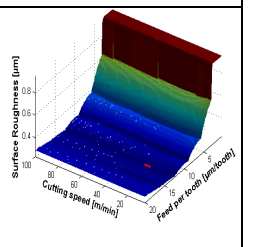

Fig. 6.6: Simulated surfaces for five cutting lengths (f_t = 0.5:0.1:20 [µm] and V=5:0.2:100 [m/min]).

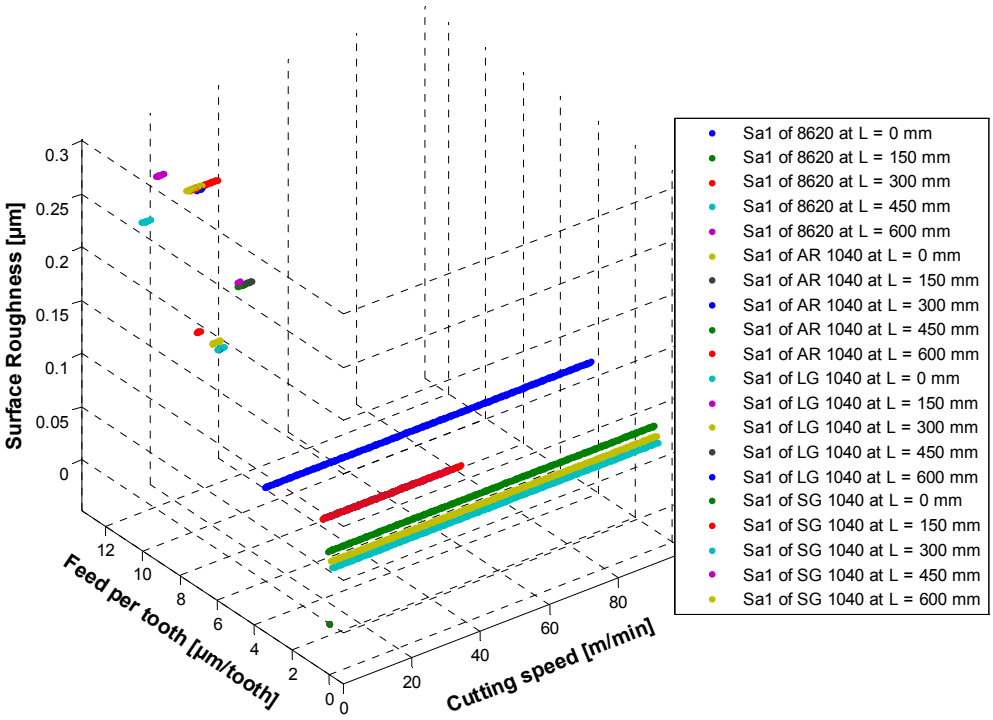

Fig. 6.7: Optimum surface achievable for different material microstructures and under different levels of removed materials.

6.4 Virtual Reality-Based Simulation

Virtual Reality (VR) is an interactive simulation technology which can be used to visualised the micro-milling processes in order to evaluate the feasibility of the process (Arshad *et al.* 2008). Also, it allows a user to study factors affecting the quality of the machined part prior to the real machining process takes place. However, it is worth stressing that both real and abstract systems can be represented using VR technology (Arshad *et al.* 2008). In this section, a VR-based model is proposed based on the aforementioned detailed surface roughness model. The VR model is utilised to visualise the micro-endmilling process of multi-phase materials. In particular, the model considers the effect of the processed material microstructure along with the applied cutting condition on the resultant surface. A real-time graph of the generated surface against local chip-loads applied simultaneously with the microstructure being in contact with the cutting tool is displayed.

a. Material microstructure-based modelling

This section presents the generation of a 3D geometrical model of the microstructure to be processed, and its import into the VR-model.

The first step was to adapt the procedure developed for mapping the multi-phase microstructure (see Section 4.2) and use it to capture the microstructure of fully-annealed AISI 1040 with large grain sizes, see Figure 6.8a. By processing of this microstructure picture, the grain boundaries between the different phases are

delineated. Hence, the contour of the ferrite phase can be separated from the rest of the microstructure. The coordinates of this contour are converted to a "*.dxf" file and imported to CAD software (Solidworks). Then, the software is used to extrude the imported contour to generate a 3D geometrical model of the ferrite phase, as seen in Fig. 6.8b. The second phase, pearlite, is treated as the base of the microstructure and is represented as a blind cube. The two geometries were then merged to provide a virtual representation of the processed microstructure of fully-annealed AISI 1040, see Figure 6.8c. Finally this 3D model was exported into a Virtual Reality Modelling Language format (VRML.*wrl).

b. 3D modelling of cutting tool

A 3D VR geometrical model was created to represent a micro-endmill tool. Figure 6.9 (a and b) shows the real micro-endmilling tool and the VR-model of the tool respectively. The geometry of the cutter was based on the description given in Section 6.2.1: a cutting edge radius of 2.5 μm, cutter corner radius of 3 μm, and 7º end cutting edge angle, see Figure 6.9c. Again, the 3D model was exported to VRML format (.*wrl).

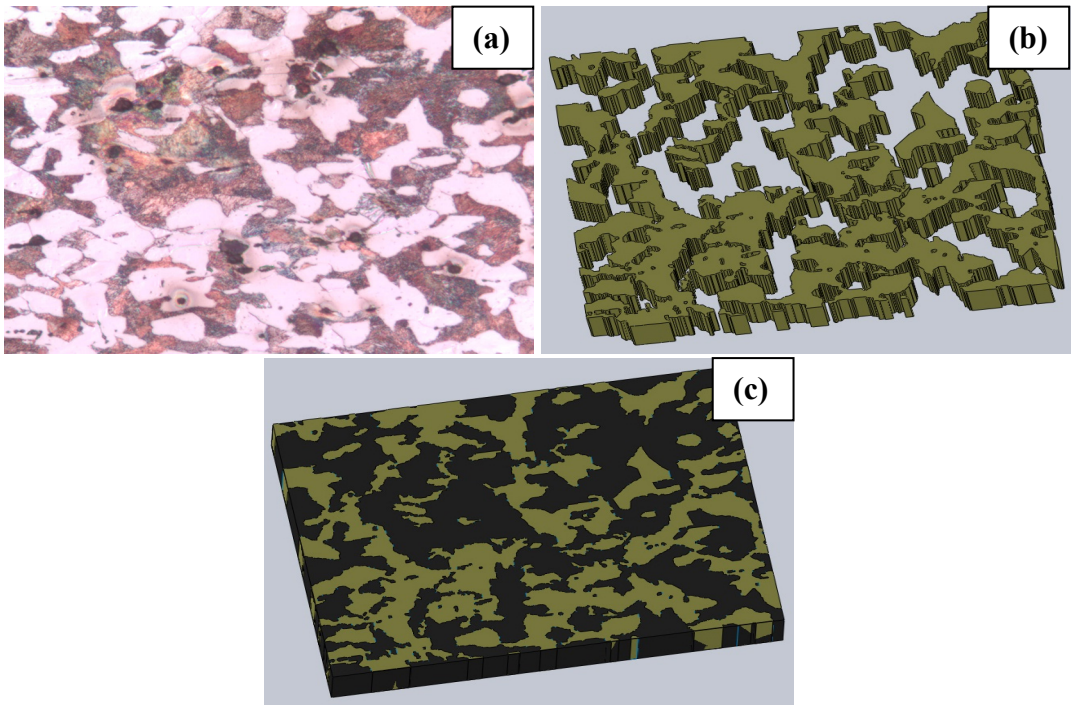

Fig. 6.8: Material microstructure modelling steps (a) Captured picture of the fully annealed AISI 1040 sample, (b) Geometrical model of ferritic phase and (c) 3D model of fully-annealed AISI 1040 microstructure.

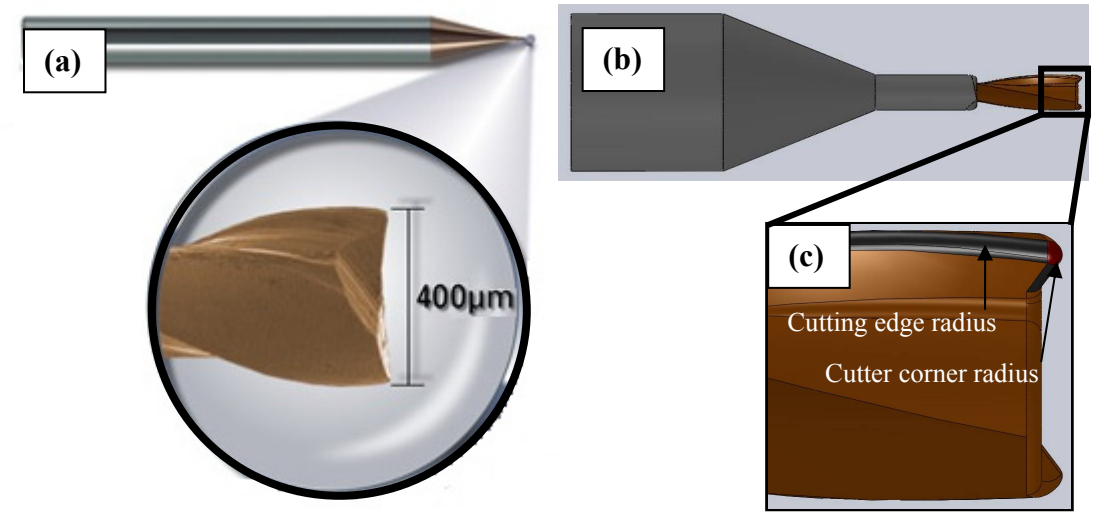

Fig. 6.9: Micro-end mill tool (a) real tool, (b) and (c) 3D model of the cutting tool.

c. Virtual micro-endmilling simulation

Once the 3D models of the processed material microstructure and the cutting tool have been exported to the VRML format (*.wrl), they are gathered to complete a VRML model as seen in the Fig. 6.10. Hence, the virtual micro-endmilling process world is completed and ready to be explored through any VRML browser, Matlab virtual reality browser was used in this case.

In this application, the proposed detailed surface roughness model presented in section 6.2.2 was used to manipulate the virtual model. The virtual environment has been utilised to perform simulation trials. In particular, the movement of the cutting tool through the processed microstructure with the applied cutting parameters and the resultant surface at each position can be simulated. Fig. 6.10 represents the achievable surface at a very small feed rate, 1.55 μm, relative to the cutting edge radius, 5.6 μm. No cutting takes place at such a small feed rate and the ploughing regime dominates the cutting mechanism. Therefore, as can be seen in Fig. 6.10, the generated surface is represented by a straight line and has the original height of the material. However, with the increase of feed rate to 2.49 μm, the cutting mechanism becomes a mixture between cutting and ploughing as shown in Fig. 6.11. When the feed rate increases to 4.3 μm, close to the cutting edge radius, the cutting mechanisms becomes the dominant regime and a good surface is produced as seen in Fig. 6.12. Also, Fig. 6.13 illustrates the micro-burr formation due to the engagement of more than one phase with the cutting edge at once. Different regimes and generated surface owing to the process parameters and the nature of the workpiece microstructure are exercised. Thus, it can be concluded that the proposed virtual model provides a tractable means

to extend understanding and improve knowledge of the micro-endmilling process. In particular, the model simulates the influence of different microstructures on the alteration of the cutting regime, and thus elucidates the underlying mechanism of micro-burr formation at the phase boundaries.

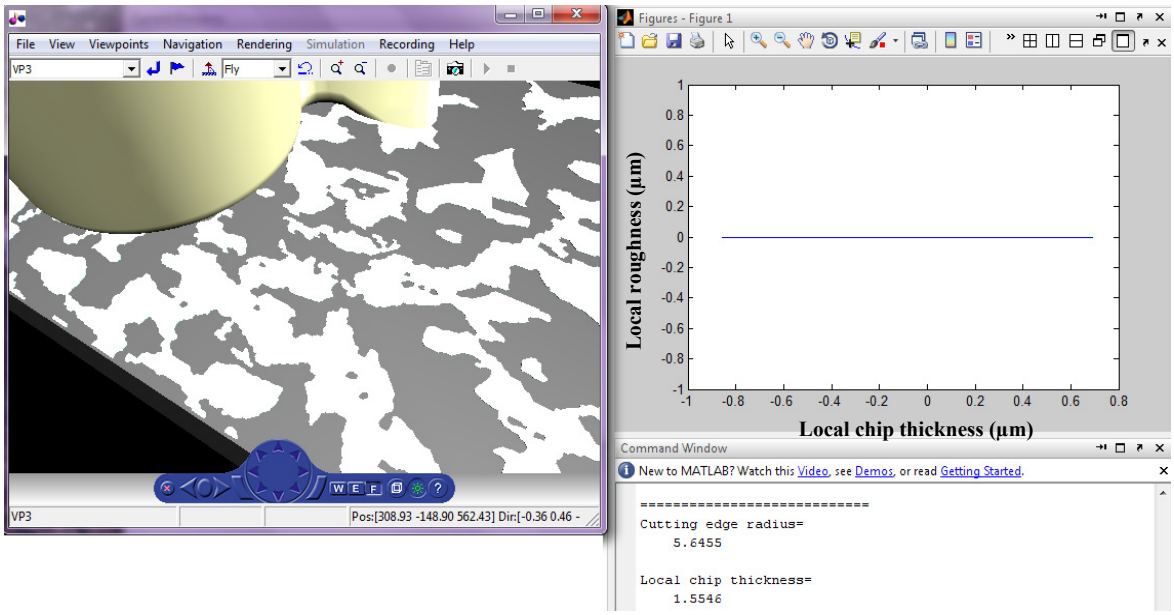

Fig. 6.10: Virtual micro-endmilling simulation: Ploughing and complete elastic recovery of the machined surface.

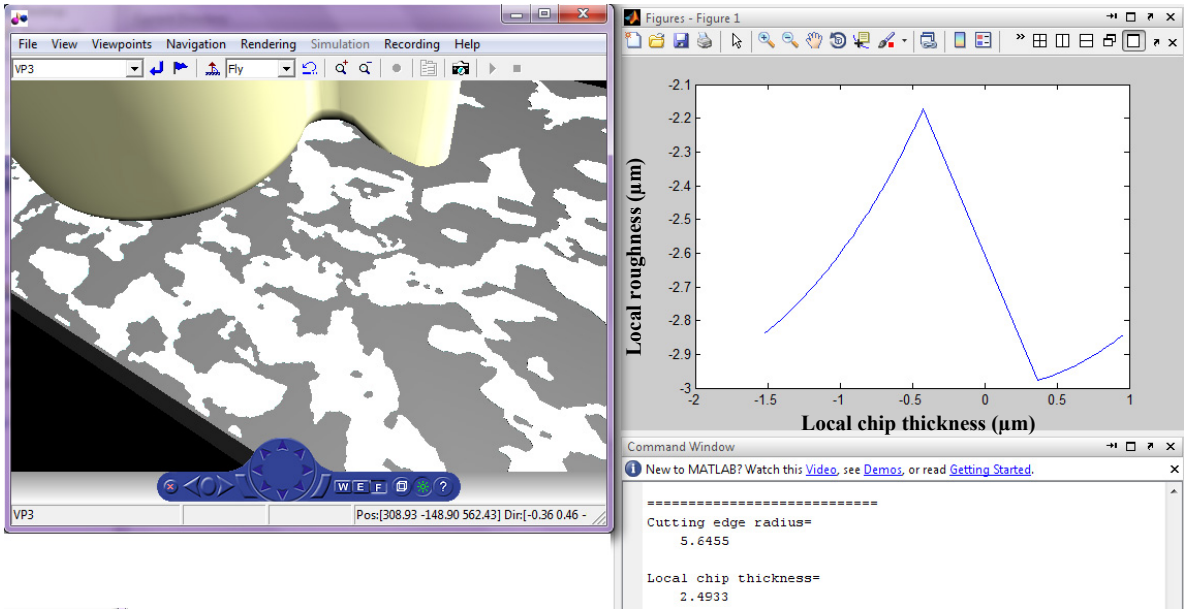

Fig. 6.11: Virtual micro-endmilling simulation: mix of cutting and ploughing of the machined surface.

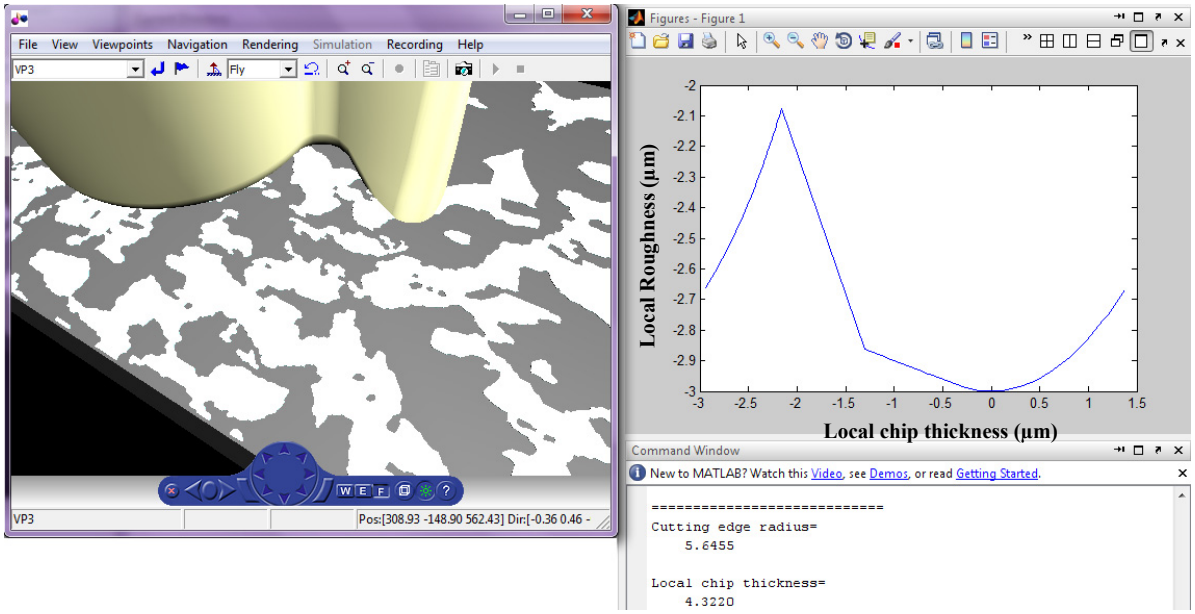

Fig. 6.12: Virtual micro-endmilling simulation: cutting is the dominant regime.

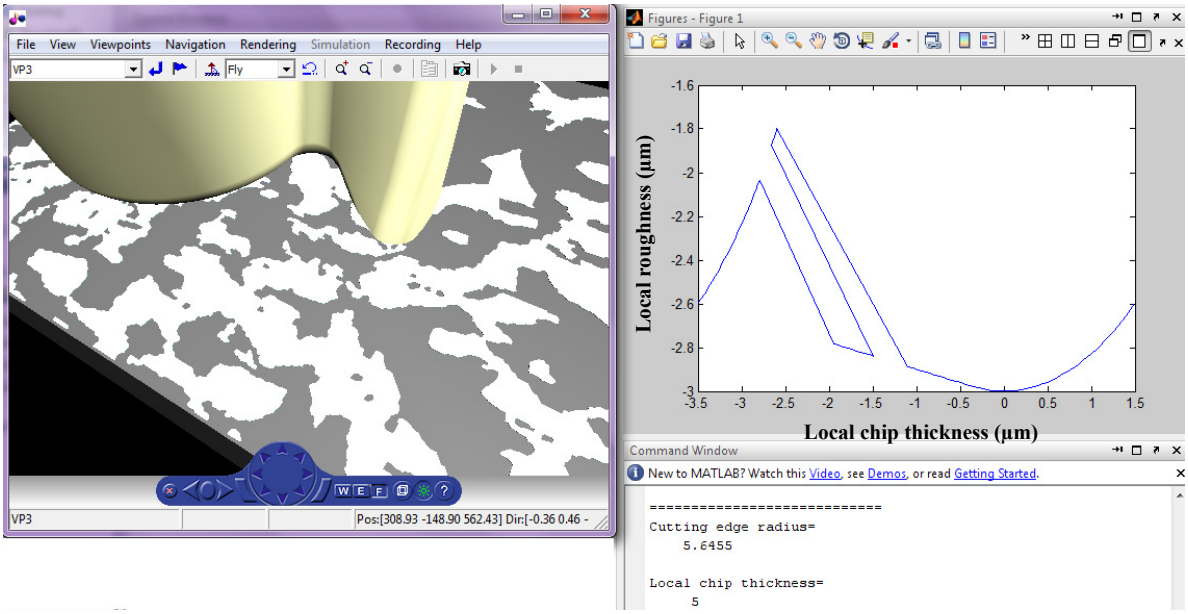

Fig. 6.13: Virtual micro-endmilling simulation: surfaces generated with micro-burr formation due to cutting and ploughing.

6.5 Summary

This chapter has presented a simulation-based study of the surface generation process in micro-endmilling of multi-phase materials. Initially, the generated roughnesses for AISI1040 and AISI8620 have been simulated for a wide range of cutting conditions. Then, a tool wear model has been incorporated into the surface generation model to improve its applicability. In particular, the adapted model allows accurate prediction of the generated roughness through detecting changes of the cutting tool geometries, due to wear, and thus enabling the realistic values of these geometries to be considered.

In addition, the AISI1040 workpiece has been heat-treated to achieve different morphological microstructures. Then, applying the detailed model of surface roughness to the captured microstructures has enabled using the model to compare the machinability of these modified microstructures in terms of the achievable roughness. Subsequently, the simulation results have been utilised to optimise the cutting process and identify processing windows, cutting conditions, which can reduce the resulting roughness while extending the tool life.

Furthermore, 3D models of the processed microstructure and cutting tool have been created to build a virtual reality environment using Matlab Virtual Reality toolbox. Using the developed surface roughness model, the proposed virtual model has been utilised to simulate the surface generation process and tool wear evaluation when processing multi-phase materials at micro-scale. The proposed model provides a tractable means to extend the understanding and improve the knowledge of the micro-

endmilling process. Especially, the model can be used to perform machining trials virtually without consuming energy and raw materials.

CHAPTER 7

CONCLUSION

This chapter summarises the main contributions and the conclusions reached in this work. It also provides suggestions for future work.

7.1 Contributions

This research addressed the influence of workpiece microstructure on the micro-endmilling process. In particular, the effects of material microstructure on matters such as cutting regime, tool wear and surface roughness were examined. These investigations were utilised to optimise the cutting process for the best possible performance. The contributions of this work include:

Effects of material microstructure on the micro-endmilling of Cu99.9E

a. ***Addressing the relationship between the workpiece microstructure in terms of grain size and the minimum chip thickness and the resulting roughness***. A thorough investigation of the effects of material microstructure in terms of grain size on the micro-milling process has been carried out, especially on cutting conditions and the resulting surface quality. In particular, an experimental study was conducted to investigate the machining response of two workpieces with different material microstructures. One workpiece was in "as received" CG Cu99.9E with an average grain size of 30 μm and the

other was in UFG Cu99.9E with an average grain size of 200 nm, produced by Equal-Channel Angular Pressing (ECAP).

b. ***Developing of an evaluation method that offers a comparative assessment of the modified microstructures and enables initial prediction of the minimum chip thickness.*** An AFM-based method to assess the homogeneity of the material microstructure was proposed. The method involved calculating the coefficient of friction of the individual grains inside the workpiece material which enables initial prediction of the minimum chip thickness. Estimated values of the minimum chip thickness are necessary to have normal cutting, before entering the transitional regimes associated with intermittent cutting and ploughing.

Modelling the material microstructure effects in μ-endmilling of multi-phase materials

c. ***Constructing a new deterministic model to simulate the surface generation process considering the machined microstructure during micro-milling together with an experimental study to validate it.*** A deterministic surface generation model of micro-endmilling has been developed especially to simulate the surface generation process associated with the machining of multi-phase materials. It takes into account the effects of the feed rate as the most important cutting parameters affecting the material machining response but also the cutting tool geometry, in particular the cutting edge radius, the cutter corner radius and the end cutting edge angle. In addition, as the workpiece cannot be considered anymore homogeneous at this scale of material removal, a special attention is paid to its microstructure. The model takes into account any variations of the minimum

chip thickness when moving from one phase to another by feeding maps of the material metallurgical microstructure into the model. Such maps are created by employing image processing techniques to process micrographs of the material microstructure and thus to convert them into planer maps of points that represent the coordinates of each pixel with the third binary number giving information about the phase at each point on the map. After that, an experimental study was conducted on two different dual-phase steel samples to validate the proposed model.

Tool wear in μ-endmilling: Material microstructure effect, modelling and experimental validation

d. ***Proposing a new approach and experimental setups for characterising and monitoring tool wear at micro-scale, and thus enabling examining and modelling the influence of material microstructure on tool wear in micro-endmilling of single and multi-phase steel.*** Various factors affecting the tool wear in micro-endmilling were examined and discussed. Special attention was given to the effects of the material microstructure on tool wear. The average values of cutting edge radius and tool flute profile were used to assess the tool wear. A new experimental setup was proposed to determine these two tool parameters, and then series of experiments on pearlite and ferrite steel were conducted to investigate the effects of their distinctive properties on the tool wear. The factors that affect the accuracy of the flute profile measurements were also discussed. Then, two regression models were created based on the experimental data in order to estimate the increase of the cutting edge radius of pearlite and ferrite steels independently. The aim was by combining them to be able to predict the tool wear when machining dual-phase steel workpieces predominantly composed from these two phases with different ratios. To

demonstrate the applicability of this generic method and at the same time to validate the models, the proposed approach was evaluated in two different experimental studies under different conditions.

Simulation-based study of the μ-endmilling process

e. ***Conducting a simulation-based study of the surface generation process in micro-endmilling of multi-phase materials***. The generated roughnesses when machining AISI 1040 and AISI 8620 at micro-scale have been simulated for a wide range of cutting conditions. Then, a tool wear model has been incorporated into the surface generation model to improve its applicability. In particular, the adapted model allows accurate prediction of the generated roughness through detecting changes of the cutting tool geometries, due to wear, and thus enabling the realistic values of these geometries to be considered.

f. ***Optimising the cutting process for the best possible performance.*** The results of conducted simulation trials have been utilised to optimise the cutting process and identify processing windows, cutting conditions, which can reduce the resulting roughness while extending the tool life.

g. ***Creating a virtual micro-milling environment that implements the developed surface generation and tool wear models.*** 3D models of the processed microstructure and cutting tool have been created to build a virtual reality environment using the Matlab Virtual Reality toolbox. The proposed virtual model has been developed to simulate the surface

generation process and tool wear evaluation when processing multi-phase materials at micro-scale.

7.2 Conclusions

The following conclusions can be drawn based on the work in the area of material microstructure effects on cutting regime, tool wear and surface generation in the micro-endmilling process:

Effects of material microstructure on the micro-endmilling of Cu99.9E

The investigation has shown that through refinement of the microstructure it is possible significantly to improve the specific cutting conditions in micro-milling. This can lead to a reduction in surface roughness and surface defects which are highly dependent on material homogeneity. In particular, the following conclusions can be drawn from this investigation:

- The calculated average minimum chip thickness was 0.397 μm with standard deviation (σ) = 0.039 for UFG Cu99.9E and 0.468 μm with standard deviation (σ) = 0.094 for CG Cu99.9E while the normalised minimum chip thickness was 0.156 for UFG Cu and 0.192 for CG Cu. This means that the cutting process started earlier in the case of the UFG Cu sample than for the CG workpiece, and thus a better surface quality would be expected after machining.

- Also, due to the significant variations in the minimum chip thickness over the scan area for the CG sample, the cutting process would be unstable and would result in

highly fragmented chips and defects in the machined surfaces. Conversely, the high homogeneity of the UFG Cu samples results in much less variation in the coefficient of friction and hence in the minimum chip thickness over the scanned area. Therefore the cutting process would be expected to be more stable and the defects on the machined surfaces to decrease.

- For both materials, CG and UFG Cu99.9E, a better surface quality was achieved at high cutting speeds and at feed rates 2-3 times the calculated minimum chip thickness. However, a significantly lower surface roughness was achieved at all cutting speeds and feed rates for UFG Cu99.9E compared to the CG material; the best result for the UFG material was Ra=0.037, while for the CG material it was Ra=0.057. This constituted a 35% reduction in surface roughness due to the UFG structure.

- For CG Cu99.9E, the micro-milled surface hardness achieved was 105 HV and remained constant down to a feed rate of 1 μm/tooth. It started to increase rapidly as the feed rate decreased further. This indicates an increase in work hardening induced at rates below 1 μm/tooth, and suggests changes in the cutting conditions from normal cutting to ploughing at very low feed rates. For UFG Cu99.9E, the constant level of hardness increased to 125 HV, which was 19% higher than for CG Cu99.9E. The hardness increased at feed rates of 0.75 μm/tooth and below, which indicates once more changes in the cutting conditions. Again, this shift in the feed rate below which the process behaviour changed from cutting to ploughing could also be attributed to the refined microstructure and homogeneity of UFG Cu99.9E.

- The cutting conditions under which the measurements of the coefficient of friction were conducted are different from the real cutting conditions. However, this method is proposed only to assess the modified microstructures. In particular, this method can be used as a comparative evaluation tool, for example, to assess the improvement in the homogeneity of the modified microstructure which should be associated with a reduced minimum chip thickness. On the other hand, to be generally applicable to any material, further experimental study is required to calibrate the prediction of the minimum chip thickness. In particular, the difference between scanning and machining conditions has to be examined.

Modelling the material microstructure effects in μ-endmilling of multi-phase materials

- The proposed planar map of microstructure has proven its feasibility to model the effect of multi-phase microstructure in the surface generation of the floor. However, the third dimension, depth of each phase, has to be incorporated into the microstructure map in order to be utilised for the surface generation of the side wall.

- The proposed surface generation model was experimentally validated by machining two different samples of dual-phase steel. In particular, slotting tests were performed on AISI 1040 and AISI 8620 samples under a range of chip-loads, especially feed rates ranging from 5 down to 0.6 μm per flute, and thus to assess the effect of their microstructure on the generated surface. The study showed a good agreement between the experimental and simulation results, with an average error of 14.5% and 17.4% for the AISI 1040 and AISI 8620 samples, respectively.

- Based on these results, it can be concluded that the model can be used both to predict the surface quality after micro-milling multi-phase materials under various machining conditions, and also as a tool to optimise the micro-milling process. Only at very low feed rates, the error is much higher, and thus the model cannot be applied at such cutting regimes. However, it is worth stressing that they are not suitable anyway for most practical applications taking into account the available cutters' geometries, especially the manufacturing constraints in producing tools with very small cutting edge radiuses.

- Another important feature of the model is that it allows the micro-burr formation at the phase boundaries to be taken into account in assessing the resulting surface roughness.

- Comparing the results obtained for both materials, AISI 1040 and AISI 8620, there are clear evidences of significant influence of the material microstructure on the achieved surface quality. This conclusion can be easily drawn based on the differences between the roughness measured on the AISI 8620 and AISI 1040samples that was achieved under the same cutting conditions and relatively similar cutter geometries.

- The best surface reflects the trade-offs between the kinematic parameters and the minimum chip thickness effects. Also, one can argue that the critical range of the feed rates is where the value of the feed is in the vicinity of the cutting edge radius. The best roughness values were achieved in this range, and also noticeable variations of the roughness can be easily seen, which indicates the importance of optimising machining parameters.

- The differences between the simulation and experimental results can be explained with the idealised cutting conditions used in the simplified model. Another reason for the difference between the simulation and experimental is the different cutting mechanisms that take place such as rubbing and burnishing at very low feed rate and have been considered by the model. Also, measurement uncertainties associated with the use of the scanning white light interferometer and moving of the cutter over prominent burrs left after the previous cutting passes are considered additional cause of these differences.

- Finally, the results of this research show clearly that special attention should be paid to the selection of the workpiece material, especially multi-phase ones, as well as the cutting conditions for their processing at micro-scale.

Tool wear in μ-endmilling: Material microstructure effect, modelling and experimental validation

- Inverse relationships between the exhibited wear, in case of pearlite, and the applied feed rates and speeds were identified which are contrary to those at macro-scale machining. Therefore, careful selection of the cutting parameters should be considered.

- In contrast for ferrite, there is a small variation of increase in the cutting edge radius when the results for the two different settings of the cutting speed and the feed rate are compared. In addition, the linear increase of the tool wear is much more pronounced.

- A higher tool wear was observed when machining ferrite than pearlite under the same cutting conditions. This phenomenon is explained with differences in mechanical properties of these two phases.

- To demonstrate the applicability and at the same time to validate them, the models have been tested at two different levels and under different conditions. There was a good agreement between the estimated tool wear and the experimental results. In particular, the average error was 14.7% and 17.5% for AISI 1040 and AISI 8620, respectively, when the machining was conducted with 800 μm cutters and 20% and 19% when processing AISI 1040 with 600 μm and 400 μm tools.

- Studying the experimental results obtained for both materials, it is not difficult to notice the higher tool wear resulting from the machining of the AISI 8620 workpiece in comparison with the AISI 1040 one under the same cutting conditions. This was expected and was attributed mostly to the higher percentage of ferrite in the AISI 8620 microstructure. Hence, it can be concluded that the influence of the material microstructure on the tools' wear is significant and by accounting for this models can be created to predict the tool wear when machining dual-phase materials.

- The differences between the predictions and experimental results were attributed to the limited number of experiments conducted on single-phase steels' samples independently. In addition, there were two other factors contributing to the observed discrepancies. In particular, the resulting tool wear was measured manually, and hence there was some uncertainty in performing this operation, and also it was not taken into account the engagement of the tools with more than one phase at the time.

- Finally, it should be noted that the tool wear models created by applying this approach could be easily refined to account for any new experimental data and thus to improve their prediction capabilities.

Simulation-based study of the µ-endmilling process

- The roughnesses obtained reflect different responses of the material microstructure to the machining process. So, the increase of roughness in the case of the AISI 8620 sample, average of 7% higher than AISI 1040, can be attributed to the higher percentage of ferrite phase present in the microstructure with its higher minimum chip thickness than the pearlite one.

- The increase of roughness with the volume of removed material can easily be seen. This can be explained by the increase of the cutter edge radius due to tool wear occurred after removing certain volumes of machined material. As a result, such an increase leads to more ploughing rather than cutting and in turn higher surface. Also, due to the increase of cutting edge radius, the range of feed rates at which the minimum chip thickness dominating the machining regime increases and the range at which the process kinematics lead the process decreases.

- Higher surface roughnesses are produced in the case of AISI 8620 when compared with those for AISI 1040. However, the differences between generated roughnesses in both materials increase with the amount of material removed. This relationship is

mainly attributed to the increase of the influence of the microstructure due to the increase of the minimum chip thickness effect.

- It can be concluded that the strategy of micro-milling a part should be adapted based on the total material to be removed and the required surface roughness. In particular, the applied feed rate could be increase after removing certain volume of materials in order to keep the resultant roughness at the aimed value.

- In the case of multi-phase materials, the limited reduction of grain size of the present phases could not improve the resulting roughness. In contrast, it could increase the resulting roughness due to the increase of the grain boundaries associated with more burr formation. This conclusion can be drawn based on the achievable roughness for both normalised and full-annealed AISI 1040 under the same cutting conditions. However, to avoid the heterogeneity of the microstructure, the reduction has to be large enough to result in small grain sizes when compared with the chip-load.

- The grid of results would help to select different inputs parameters, rather than those optimised by the algorithm. There would be less uncertainty risk. However, higher roughnesses might be expected.

- The proposed model provides a tractable means to extend the understanding and improve knowledge of the micro-endmilling process through performing machining trials virtually without consuming energy and raw materials. Especially, the model simulates virtually the influence of the microstructure on the cutting process and elucidates the underlying mechanism of micro-burr formation at the phase boundaries along with counting their contributions to the total surface roughness.

Finally, it can be concluded that, the results of this research confirmed the initial hypothesis that the increase in achievable roughness in micro-scale machining in contrast to conventional machining of polycrystalline and multi-phase materials is due to the effect of workpiece microstructure. This effect is even more significant when machining multi-phase materials owing to the dominance of the micro-burr formation during the surface generation process at phase boundaries.

7.3 Recommendations for Future Work

Based on the work presented here, some areas of future research efforts have been identified as follows:

- Introducing new ultra-refining methods that offer different microstructures in order to optimise the material microstructure and validating them for a wide range of materials.

- Expanding Son's model for the minimum chip thickness by considering the effect of the cutting speed on the coefficient of friction. This would enable more accurate minimum chip thickness to be estimated**.**

- Improving the planar map of microstructure through considering the depth of the present phases in order to create 3D maps which can be utilised to model workpiece microstructures on the generated roughness for both floor and side wall surfaces.

- Developing force models that consider the effect of multi-phase microstructure based on the proposed 3D map of microstructure.

- Improving the developed experimental setup for assessing the tool wear in order to detect changes in the cutter corner radius and the end cutting edge angle of the tool in addition to the cutting edge radius. The detecting of such changes of the cutting tool geometry would give a comprehensive image of the tool during cutting and enabling more accurate prediction of the resulting roughness.

- Improving the proposed virtual model for the micro-endmilling process through increasing its feasibility to simulate the chipping and material forming process and thus to offer a detailed insight of the cutting process at micro-scale.

Appendix A –

Equal Channel Angular Pressing: Principles

As the large size of metal crystals (grains) is a possible factor affecting surface quality in micro-milling, it is natural to seek a way of reducing the grain size of a micromilled material. One possibility is to use a special treatment such as electro deposition, which however is slow and limited to certain metals, for example, nickel. Another method is based on nano powder metallurgy, but there are economic, technical and health issues surrounding the production and use of nano particles. The third way, which is explored here, relies on severe plastic deformation (SPD) of bulk metals (Valiev *et al.* 2000). SPD subdivides initially coarse grains, typically 100 μm in size, into submicrometer sized grains. Such refined materials are referred to as ultrafine-grained (UFG). SPD can convert all types of metals into UFG equivalents. There are many SPD processes being tried, but the most popular is equal-channel angular pressing (ECAP) (Segal 1995).

In the ECAP process, a round or square billet is forced through a sharply bent channel (Figure A.1). Since the cross section of the channel is constant, the only mode of plastic deformation is simple shear at the channel bend. After this process is repeated 2-3 times, the original coarse grains become subdivided by multiple shear bands into so-called sub-grains of sub-micrometer sizes. For even larger numbers of ECAP passes, the accumulated plastic strain increases the crystallographic mis-orientation of sub-grains to such an extent that they can be treated as entirely new grains. Multiple passes of the billet through an ECAP die provide the opportunity for rotation of the billet about its axis between these passes. This

enables the material shear plane at the channel bend to be altered at each pass, which leads to a more homogeneous material structure.

The material subjected to grain refinement was copper Cu99.9E. It was delivered in the form of a hot extruded 20 mm diameter bar. The first operation was cold forward extrusion to reduce the bar diameter from 20 mm to 13 mm. Next, billets of about 8x8x46 mm were cut out from the extruded bar and processed by ECAP 8 times.

The microstructure of the copper samples was investigated using optical microscopy (OM) and transmission electron microscopy (TEM). The OM observations of the forward extruded copper revealed a CG structure, with an estimated average grain size of 30 μm (Figure 3.1a). The microstructure of the initial 20 mm diameter copper bar was not investigated. However, it is believed that the average grain size would be of the same order as in the cold extruded bar. Figure 3.1b represents the OM image of the forward extruded and subsequently ECAPed copper. In this case it is impossible to distinguish individual grains, but it is clear that a substantial grain refinement took place. The grain size in this case was evaluated using TEM (Figure 3.1c). The average size of 200 nm indicates the case of an advanced UFG structure produced by ECAP.

Three tensile samples, with 2.5 mm diameter and gauge length of 7.5 mm, were machined from the extruded and ECAPed billets. Tensile testing was carried out at room temperature and at a low speed of 0.5 mm/min. On average, the 0.2% proof strength was established to be 400 MPa and the ultimate tensile strength 428 MPa. The total elongation at fracture was 15.6%. The initial material was not tested. However, data obtained from the literature for the annealed Cu99.9E bars indicate a value of 70 MPa for yield strength, 220MPa for ultimate

tensile strength and 55% for elongation. Table A.1 summarises these results for both states of the material.

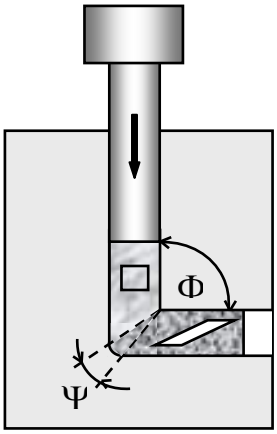

Fig. A.1: Principle of ECAP.

Table A.1 Mechanical properties of Cu99.9.

Cu99.9E	0.2% Proof strength; MPa	Ultimate tensile strength; MPa	Elongation to fracture; %
Initial	70	220	55
Extruded+ ECAPed	400	428	15.6

REFERENCES

ADE Phase Shift. URL: www.phase-shift.com, 2011, Last visited: 3 March 2011.

Altintas, Y., Brecher, C., Weck, M., and Witt, S., 2005, "Virtual Machine Tool," Annals of CIRP, 54 (2), pp. 651–674.

Altintas, Y., Merdol, D.S., 2007, "Virtual High Performance Milling," *Annals of CIRP, Manufacturing Technology* 55(1), pp. 81-84.

Altintas, Y. and Jin, X., 2011, "Mechanics of micro-milling with round edge tools," *Annals of CIRP, Manufacturing Technology*, 60(1), pp. 77-80.

Aramcharoen, A., Mativenga, P T., 2009, "Evaluation of critical parameters in micro machining of hardened tool steel," *International Journal of Nanomanufacturing* (IJNM). 3(1). pp 100-111. DOI: 10.1504/IJNM.2009.027053.

Arif, M., Rahman, M., and San, W., 2011, "Analytical model to determine the critical feed per edge for ductile–brittle transition in milling process of brittle materials," *International Journal of Machine Tools and Manufacture,* 51(3), pp. 170-181.

Arshad, H., Mahayuddin, R.Z., Haron, C.H.C. and Hassan, R., 2008, "Flank Wear Simulation of a Virtual End Milling Process," *European Journal of Scientific Research (EJSR),* 24(1), pp. 148-156.

Bhushan, B., 2005, "Nananotribology and nanomechanics: An introduction," Online book, URL: http://books.google.co.uk/books?id=Pi_gTu9gnvYC, Last visited: 3 March 2011.

Biermann, D. and Kahnis, P., 2010, "Analysis and simulation of size effects in micromilling," PRODUCTION ENGINEERING, 4 (1), pp. 25-34. DOI: 10.1007/s11740-009-0201-1.

Bissacco G., Hansen H.N. and De Chiffre L., 2006, "Size effects on surface generation in micromilling of hardened tool steel," Annals of the CIRP, 55 (1), pp. 593-596.

Chae, J., Park, S.S. and Freiheit, T., 2006, "Investigation of Micro-cutting operations," *Int. Journal of Machine Tools and Manufacture,* 46 (3-4), pp. 313-332.

Dhanorker, A., and Özel, T., 2008, "Meso/micro scale milling for micro-manufacturing," *Int. J. of Mechatronics and Manufacturing Systems,* 1(1), pp. 23-42.

Dirk, B., and Philip, K., 2010, "Analysis and simulation of size effects in micromilling" Prod. Eng. Res. Devel. 4:25–34 DOI 10.1007/s11740-009-0201-1.

Dornfeld, D., Min, S., and Yakeuchi, Y., 2006, "Recent advances in mechanical micromachining," *Annals of the CIRP,* 55 (2), pp. 745-768.

Ehmann, K.F., 2007, "A synopsis of U.S. micro-manufacturing research and development activities and trends," *Proceedings of the Int. Conf. on Multi-Material Micro Manufacture conference (4M),* Borovets, Bulgaria, pp. 7-13.

Elkaseer A.M., Virtual Model of the Micro-milling Process Consider workpiece Material Microstructure, Proceedings of the first annual meeting for the Egyptian scholars in UK and Ireland, London, UK, Oct. 2009,

Elkaseer A.M., Popov K.B., Negm M., Dimov S.S. and Minev R. "Material Microstructure Effect-Based Simulation Model for the Surface Generation Process in Micro-milling." proceedings of ICOMM/4M, Madison, Wisconsin, USA. Apr. 2010, 19-24.

Elkaseer A.M., Dimov S.S., Popov K.B., Minev R.. "Material Microstructure Effect-Based Investigation of Tool Wear in Micro-endmilling of Multi-phase Materials." Proceedings of 4M/ ICOMM, Oyonnax, France, Nov. 2010, 188-191.

Ferry, W. and Altintas, Y., 2008, "Virtual Five Axis Milling of Impellers, Part – II: Feedrate Optimisation of Five Axis Milling," *Trans. ASME, J. Manufac. Sc. and Eng.* 130, pp. 0110013-1:13.

Ferry, W. and Altintas, Y., 2008, "Virtual Five Axis Milling of Impellers, Part – I: Mechanics of Five Axis Milling," *Trans. ASME, J. Manufac. Sc. and Eng.,* 130, pp. 011005-1:11.

Filiz, S., Conley, C., Wasserman, M., and Ozdoganlar, B., 2007, "An experimental investigation of micromachinability of copper 101 using tungsten carbide micro-endmills," *Int. J. of Machine Tools and Manufacturing,* 47, pp. 1088–1100.

Furukawa, Y, and Moronuki, N., 1988, "Effect of material properties on ultra precise cutting processes," *Annals of the CIRP,* 37 (1), pp. 113-116.

Geißdörfer, S., Rosochowski, A., Olejnik, L., and Engel, U., 2008, "Micro-extrusion of an ultrafine grained copper can," *Proceedings of the Int. Conf. on Multi-Material Micro Manufacture (4M),* Cardiff, United Kingdom, pp. 191-194.

Jina, X., and Altintas, Y., 2011, "Prediction of micro-milling forces with finite element method," *Journal of Materials Processing Technology*, Accepted manuscript.

Gillespie L.K., 1979, "Deburring precision miniature parts," *Prec. Eng.* 1 (4), 189–198.

Gillibrand, D., 1979, "Micro-defects on machined carbon steel surfaces," *Tribology Int.,* 12 (4), pp. 165–169.

Goo, C., Menard, M., Huynh, L.H., Papadopoulos, C., Park, S.S., and Jun, M.B.G., 2010, "Micromachining of Polymer Composites Reinforced with Single-Walled Carbon

Nanotubes," *Proceedings of Int. Conf. on Micro-Manufacturing (ICOMM),* Madison, WI, USA, pp. 417-422.

Gowri, S., Kumar, P., Vijayaraj, R., Balan, A.S.S., 2007, "Micromachining: technology for the future," *Int. J. of Materials and Structural Integrity,* 1(1/2/3), pp. 161-179.

Grum J., Kisin M., 2003, "Influence of microstructure on surface integrity in turning-part 2: the influence of a microstructure of the workpiece material on cutting forces," *International Journal of Machine Tools and Manufacture.* 43 () 1545–1551.

Ikawa N., S. Shimada and H. Tanaka (1992), "Minimum Thickness of Cut in Micromachining," Nanotechnology 3:6-9.

Jun, M., Devor, R.E., Kapoor, S.G., and Englert, F., 2008, "Experimental investigation of machinability and tool wear in micro-endmilling," Trans of NAMRI/SME, 36, pp. 201-208.

Kata, N., and Ozdoganlar, B., 2010, "Machining Force and Surface Finish Variation across Grains during Orthogonal Micromachining of Aluminum," *Proceedings of Int. Conf. on Micro-Manufacturing (ICOMM),* Madison, WI, USA, pp. 133-137.

Kern Machine Tools, Inc. URL: http://www.kernmachine.com, 2011, Last visited: 3 March 2011.

Kim, C.J., Bono, M., and Ni, J., 2002, "Experimental analysis of chip formation in micro-milling," *Transactions of NAMRI/SME,* 30, 247–254.

Kirkup, L., and Frenkel, B., 2006, "An Introduction to Uncertainty in Measurement," Cambridge: Cambridge University Press.

Lai, X.M., Li, H.T., Li, C.F., 2008, "Modelling and analysis of micro scale milling considering size effect, micro cutter edge radius and minimum chip thickness," *Int J Mach Tools Manuf ,* 48, pp. 1–14.

Lee K., Dornfeld D.A., 2002, 2An Experimental Study of Burr Formation in Micro Milling Aluminum and Copper," *Technical Paper—Society of Manufacturing Engineers,* MR(MR02-202), pp. 1–8.

Lee W.B., Cheung C.F., To S., 1999, "Materials induced vibration in ultraprecision machining," Journal of Materials Processing Technology, 89-90, pp. 318–325.

Lee W.B., Cheung C.F., To S., 2002, "A micro plasticity analysis of microcutting force variation in ultra-precision diamond turning," *Journal of Manufacturing Science and Engineering*, 124 (2), pp. 170–177.

Li, H., Lai, X., Li, C., Feng, H. and Ni, J., 2008, Modelling and experimental analysis of the effects of tool wear, minimum chip thickness and micro tool geometry on the surface roughness in micro-end-milling. J. Micromech. Microeng, 18(2), 025006.

Lia, P., Aristimunob, P., Arrazolab, P., Hoogstratec, A.M., Oosterlingc, J.A.J., Langena, H.H., and Schmidta R.H., 2008, "A study of factors affecting the performance of micro square endmills in milling of hardened tool steels," *Proceeding of 4M, Cardiff, UK*, pp. 221-224.

Liu, K., 2005, "Process modelling of micro-cutting including strain gradient effect," PhD Thesis, George W. Woodruff School of Mechanical Engineering Georgia, Institute of Technology, USA.

Liu, K., and Melkote, S N., 2006, "Effect of plastic side flow on surface roughness in micro-turning process," *Int. J. of Machine Tools and Manufacturing,* 46(14), pp. 1778-1785.

Liu, X., Devor, R.E., and Kapoor, S.G., 2007, "Model-based analysis of the surface generation in microendmilling-Part I: Model development," *ASME J. Manuf. Sci. Eng.,* 129, pp. 453-460.

Liu, X., Devor, R.E., and Kapoor, S.G., 2007, "Model-based analysis of the surface generation in microendmilling-Part II: Experimental Validation and Analysis," *ASME J. Manuf. Sci. Eng.,* 129, pp. 461-469.

Liu, X., DeVor, R.E., Kapoor, S.G. and Ehman, K.F., 2004, "The mechanics of machining at the micro scale: assessment of the current state of the science," *ASME J. Manuf. Sci. Eng.,* 126, pp. 666–678.

Liu, X., Devor, R.E., Kapoor, S.G. and Ehmann, K.F., 2004, "The Mechanics of Machining at the Microscale: Assessment of the Current State of the Science." *ASME J. of Manufacturing Science and Engineering,* 126 (4), pp. 666-678.

Liu, X., Devore, R.E, Kapoor, S.G. 2006, "An analytical model for the prediction of minimum chip thickness in micromachining," *ASME J. of Manufacturing Science and Engineering,* 128, pp. 474-481.

Lucca D., Rohrer R., Komanduri R., 1991, "Energy dissipation in the ultra-precision machining of copper," *Annals of CIRP*, 40(1), pp. 69-72.

Malekian, M., Park, S., and Jun, B.G., 2009, "Tool wear monitoring of micro-milling operations," *Journal of Materials Processing Technology,* 209(10), pp.4903-4914.

Marinov V., 2000, “A Generic Virtual Machining Process,” *Proceedings of the 3rd World Congress on Intelligent Manufacturing Processes & Systems*, June 28-30, Cambridge, USA, pp. 203-208.

Mathworks: website: http://www.mathworks.com/help/toolbox/optim/ug/fmincon.html, 2011, Last visited 3 March 2011.

Merchant, M., E., 1944, "Basic Mechanics of the Cutting Process", *ASME Journal of Applied Mechanics*, 11, pp.168-175.

Merdol, D., Altintas, Y., 2008, “Virtual Cutting and Optimisation of Three Axis Milling Processes”, Int. J. machine Tools and Manufacture, 48 (10), pp. 1063-1071.

Merdol, D.S. and Altintas, Y., 2008, “Virtual Simulation and Optimisation of Milling Operations: Part I –Optimisation, Feed Rate Scheduling”, *Trans. ASME, J. Manufac. Sc. and Eng.,* 130, pp. 051005.

Merdol, D.S. and Altintas, Y., 2008, Virtual Simulation and Optimisation of Milling Operations: Part I – Process Simulation”, *Trans. ASME, J. Manufac. Sc. and Eng.,* 130, pp. 051004.

Mian A., Driver N. and Mativenga P.T., 2010, "A comparative study of material phase effects on micro-machinability of multiphase materials," *International Journal of Advanced Manufacturing Technology,* 50(1-4), pp. 163-174. DOI: 10.1007/s00170-009-2506-9.

Mian, A., and Mativenga, P.T., 2009, "Micromachining of coarse grained multi-phase material". *Proceedings of the I MechE Part B J. of Engineering Manufacture,* 223 (4), pp. 377-385. DOI: 10.1243/09544054JEM1185.

Mian, A., Driver, N. and Mativenga, P.T., 2009, "Micromachining of coarse grained multi-phase material". Proceedings of the Institution of Mechanical Engineers - Part B: Journal of Engineering Manufacture, 223(4), pp. 377-385. DOI: 10.1243/09544054JEM1185.

Mian, A., Driver, N., and Mativenga, P. T., 2010, "A comparative study of material phase effects on micro-machinability of multiphase materials". *Int. J. of Advanced Manufacturing Technology,* 50(1-4), pp. 163-174. DOI: 10.1007/s00170-009-2506-9.

Miao, J. C., Chen, G. L., Lai, X. M., Li, H. T., and Li, C. F., 2007, "Review of Dynamic Issues in Micro-End-Milling," *Int. J. Adv. Manuf. Technol.,* 31, pp. 897–904.

Min S., Dornfeld D., Inasaki I., Ohmori H., Lee D., Deichmueller D., Yasuda T. and Niwa K. 2006, "Variation in Machinability of Single Crystal Materials in Micromachining," *Annals of the CIRP,* 55 (1), pp. 103-106.

Mintegi, E., 2007, “MICROM: a revolutionary monitoring system to detect tool breakage and collisions, enhance machine cycles and introduce a new probing concept in micro-milling,” PhD thesis, Mondragon University, Spain.

Moriwaki T., Sugimura N., Luan S., 1993, “Combined stress material flow and heat analysis of orthogonal micromachining of copper,” *Annals of CIRP,* 42 (1), pp. 75-78.

Ng, C., Melkote, S., Rahman, M., and Kumar, A., 2006, “Experimental study of micro- and nano-scale cutting of aluminum 7075-T6,” *Int. J. of Machine Tools and Manufacture,* 46, pp. 929–936.

Özel, T. and Karpat, Y., 2005, “Predictive Modeling of Surface Roughness and Tool Wear in Hard Turning Using Regression and Neural Networks,” *Int. J. of Machine Tools and Manufacture,* 45, pp. 467-479.

Özel, T., Thepsonthi, T., Ulutan, D., and Kaftanoğlu, B., 2011, “Experiments and finite element simulations on micro-milling of Ti–6Al–4V alloy with uncoated and CBN coated micro-tools,” *Annals of CIRP, Manufacturing Technology,* 60(1), pp. 85-88.

Palanisamy, P. and Shanmugasundaram, S., 2008, “Modelling of tool wear and surface roughness in hard turning using regression and artificial neural network,” *Int. J. of Machining and Machinability of Materials,* 4(1), pp.76-94.

Park Systems Corp., URL: www.parkafm.com, 2011, Last visited: 26 December 2010.

Pham, D.T., and Karaboga, D., "Intelligent Optimisation Techniques: Genetic Algorithms, Tabu Search, Simulated Annealing and Neural Networks," Springer-Verlag New York, Inc. Secaucus, NJ, USA, 1998 ISBN: 1852330287.

Pham, D.T., Dimov, S.S., Popov, K.B., Elkaseer, A.M.A., 2008, "Effects of microstructure on surface roughness and burr formation in micro-milling: A review," *Proceedings of 3rd Virtual Int. Conf. on Innovative Production Machines and Systems (IPROMS),* pp. 270-275.

Pham D.T., Elkaseer A.M., Popov K.P., Dimov S.S., Olejnik L. and Rosochowski A. "Micro-milling of Coarse-Grained and Ultrafine-Grained Cu99.9E: Effects of Material Microstructure on Machining Conditions and Surface Quality." *Proceedings of 4M/ ICOMM,* Karlsruhe, Germany. Sept. 2009, 241-244.

Pham, D.T., Elkaseer, A.M.A., Popov, K.B., Dimov, S.S., Olejnik, L., and Rosochowski, A., 2009, "An experimental and statistical study of the factors affecting surface roughness in the micromilling process," *Proc. of IPROMS,* pp. 143-148.

Popov, K. , Dimov, S. , Ivanov, A. , Pham, D. T. and Gandarias, E., 2010, "New tool-workpiece setting up technology for micro-milling," *Int. J. of Adv. Manufacturing Technology,* Springer, 47, pp. 21–27.

Popov, K.B., Dimov, S.S., Pham, D.T., Minev, R.M., Rosochowski, A., and Olejnik, L., 2006, "Micro-milling: material microstructure effects," *Proceedings of the I MechE Part B J. of Engineering Manufacture,* 220, pp. 1807-1813.

Presz, W. and Rosochowski, A., 2006, "The influence of grain size on quality of microformed components," *Proceedings of the 9th ESAFORM Conf. on Material Forming,* Glasgow, UK, pp. 587-590.

Rahman, M., Kumar, S., Prakash, J., 2001, "Micro milling of pure copper," Journal of Materials Processing Technology, 116(1), pp. 39-43.

Rosochowski, A., Olejnik, L., Roginski, S., and Richert, M., 2007, "Micro-EDM of UFG aluminium," *Proceedings of the Int. Conf. on Multi-Material Micro Manufacture (4M),* Borovets, Bulgaria, pp. 203-206.

Rosochowski, A., Presz, W., Olejnik, L., and Richert, M., 2007, "Micro-extrusion of ultra-fine grained aluminium," *Int. J. Advanced Manufacturing Technology,* 33, pp. 137-146.

Schmitz T., Davies M., Kennedy M., 2002, "Tool point frequency response prediction for high-speed machining by RCSA," *ASME Journal of Manufacturing Science and Engineering*, 123, pp. 700-707.

Schneider, G., and Cmfge Jr., 2002, "Cutting Tool Applications," ISBN: 0615121918Segal, V.M., 1995, "Materials processing by simple shear," *Materials Science and Engineering*, A197, pp. 157-164.

Shaw M., 1995, “Precision finishing,” *Annals of CIRP,* 44 (1), pp. 343-348.

Simoneau, A., Ng, E. and Elbestawi, M.A., 2006, “Surface defects during microcutting.” *Int. J. of Machine Tools and Manufacturing,* 46, pp. 1378–1387.

Simoneau, E.Ng, and Elbestawi, M.A., 2006, “Chip formation during microscale cutting of a medium carbon steel,” *Int. J. Mach. Tools & Mfg*, 46, pp. 467–481.

Simoneau, E.Ng, and Elbestawi, M.A., 2006, “Surface defects during microcutting. *Int. J. Mach. Tools & Mfg*, 46, pp. 1378–1387.

Simoneau, E.Ng, and Elbestawi, M.A., 2006, “The effect of microstructure on chip formation and surface defects in microscale, mesoscale, and macroscale cutting of steel,” *Annals of the CIRP,* 55 (1), pp. 97-102.

Simoneau, E.Ng, and Elbestawi, M.A., 2006, “The effect of microstructure on chip formation and surface defects in microscale, mesoscale, and macroscale cutting of steel,” *Annals of the CIRP,* 55 (1), pp. 97-102.

Simoneau, E.Ng, and Elbestawi, M.A., 2007, “Grain size and orientation effects when microcutting AISI 1045 steel,” *Annals of the CIRP,* 65 (1), pp. 57- 60.

Simoneau, E.Ng, and Elbestawi, M.A., 2007, "Modeling the effects of microstructure in metal cutting," *Int. J. Mach. Tools & Mfg*, 47, pp. 368–375.

Smith W. F., Hashemi J., 2006, "Foundations of Materials Science and Engineering (4th ed.)," McGraw-Hill, ISBN 0-07-295358-6.

Son, S.M., Lim, H.S., and Ahn, J.H., 2005, "Effects of friction coefficient on the minmum cutting thickness in micro cutting," *Int. J. Machine Tools and Manufacturing,* 45, pp. 529-535.

Taniguchi, N., (ed), 1996, "Nanotechnology: Integrated Processing Systems for Ultra-precision and Ultra-fine Products," *Oxford University Press,* ISBN 0 19 8562837.

Tansel, I.N. and Rodriguez, O., 1992, Automated monitoring of microdrilling operations, Trans. of NAMRI/SME, pp. 205–210.

Tansel, I.N., 1994, Identification of the prefailure phase in microdrilling operations with multiple sensors, Int. J. of Machine Tools & Manufacturing 34(3), pp. 351–364.

Tansel, I.N., Arkana, T.T. , Baoa, W.Y. , Mahendrakara, N., Shislerb, B., D. Smithb and McCoolb, M., 2000, "Tool wear estimation in micro-machining.: Part I: tool usage–cutting

force relationship," *International Journal of Machine Tools and Manufacture,* 40(4), pp.599-608.

Tansel, I.N., Trujillo, M., Nedbouyan, A., Velez, C., Bao, W.-Y., Arkan, T.T. and Tansel, B., 1998, "Micro-end-milling-III. Wear estimation and tool breakage detection using acoustic emission signals," *Int. J. of Machine Tools & Manufacturing,* 38(12), pp. 1449–1466.

Tonshoff H., 1988, "Developments and trends in monitoring and control of ma-chining processes," *Annals of CIRP*, 37(2), pp. 61-622.

Uhlmann, E., Piltz, S., and Schauer, K., 2005, "Micro milling of sintered tungsten–copper composite materials," *J. of Materials Processing Technology,* 167, pp. 402–407.

Uriarte, L., Azcárate, S., Herrero, A., Lopez de Lacalle, L.N., and Lamikiz, A, 2008, "Mechanistic modelling of the micro end milling operation," *Proceedings of the I MechE Part B J. of Engineering Manufacture,* 222 (1), pp. 23-33.

Valiev, R.Z., Islamgaliev, R.K., and Alexandrov, I.V. 2000, "Bulk nanostructured materials from severe plastic deformation" *Progress in Materials Science,* 45, pp. 103-189.

Vogler, M., Kapoor, S. and Devor, R., 2004, "On the modeling and analysis of machining performance in microendmiling, Part 1: Surface generation," *ASME J. of Manufacturing Science and Engineering,* 126, pp. 685–694.

Vogler, M., Kapoor, S., and Devor, R., 2004, "On the modeling and analysis of machining performance in microendmiling, part 2: cutting force prediction," *ASME J. Manuf. Sci. Eng.,* 126, pp. 695–705.

Vogler, M.P., Devor, R.E. and Kapoor, S.G., 2003, "Microstructure-level force prediction model for micro-milling of multi-phase materials," ASME J. Manuf. Sci. Eng., 125, pp. 202–209.

Vogler, M.P., Devor, R.E. and Kapoor, S.G., 2003, "Microstructure-level force prediction model for micro-milling of multi-phase materials," *ASME J. Manuf. Sci. Eng.,* **125**, pp. 202–209.

Wang, J., 2008, "Micromilling Mechanism Research and Realisation," PhD Thesis, Laboratoire de Genie Industriel et de Production Mecanique, Universite Paul Verlaine de Metz, France.

Wang, J., Gong, Y., Abba, G., Chen, K., Shi, J. and Cai, G., 2007, "Surface generation analysis in micro end milling considering the influences of grain," *Proceedings of Design, Test, Integration and Packaging for MEMS/MOEMS Conference*, Stresa, Italy.

Wang, W., Kweon, S.H., and Yang, S.H., 2005, "A study on roughness of the micro end milled surface produced by a miniatured machine tool," *J. of Materials Processing Technology,* 162-163, pp. 702-708.

Weule, H., Huntrup, V., and Tritschle, H., 2001, ''Micro-Cutting of Steel to Meet New Requirements in Miniaturisation,'' CIRP Ann., 50, pp. 61–64.

Yuan, Z. J., Zhou, M., and Dong, S., 1996, ''Effect of Diamond Tool Sharpness on Minimum Cutting Thickness and Cutting Surface Integrity in Ultraprecision Machining,'' *J. Mater. Process. Technol.,* 62, pp. 327–330.

Zhang, L., 2010, "Virtual Simulation and Optimisation for 5-Axis Milling Process," *J Advanced Materials Research,* 102-104, pp. 754-757.

Author's Biography

Ahmed Abdelrahman Elkaseer was born in El-mahala El-kobra, Egypt and grew up in Cairo. He received his bachelor's degree with honours in 2001 in Production Engineering from Faculty of Engineering, Helwan University. His Master's research was on the investigation of surface quality in hard turning. However, Prior to his viva test, he was awarded a scholarship from the Egyptian Government to study a PhD in the UK.

On July 2007, Ahmed enrolled in a doctoral program in Micro-machining at the Manufacturing Engineering Centre (MEC), Cardiff University, under the guidance of Professor D.T. Pham. His research concerns performing experimental, modelling and simulation-based study of the influence of material microstructure in the micro-milling process. His graduate study has led to several publications in the area of micro-machining process.

Ahmed met his wife, S.S. Ali, in Cairo 2002. Soon after they were happily married on 17 March 2003, They have gifted two lovely kids "Abd-Elrahman" and "Marium".

After graduation, Ahmed and his family will be moving to Cairo, Egypt where he has accepted a lecturer position in Ain-shams University.